DIGITAL ACCESS TO SCHOLARSHIP AT HARVARD
DASH.HARVARD.EDU

HARVARD LIBRARY

DDI2 inhibition promotes MHC class I antigen presentation and immune checkpoint blockade efficacy in cancers

Citation

Nguyen, Nhu Tran. 2023. DDI2 inhibition promotes MHC class I antigen presentation and immune checkpoint blockade efficacy in cancers. Doctoral dissertation, Harvard University Graduate School of Arts and Sciences.

Link

https://nrs.harvard.edu/URN-3:HUL.INSTREPOS:37375874

Terms of use

This article was downloaded from Harvard University's DASH repository, and is made available under the terms and conditions applicable to Other Posted Material (LAA), as set forth at
https://harvardwiki.atlassian.net/wiki/external/NGY5NDE4ZjgzNTc5NDQzMGIzZWZhMGFlOWI2M2EwYTg

Accessibility

https://accessibility.huit.harvard.edu/digital-accessibility-policy

Share Your Story

The Harvard community has made this article openly available.
Please share how this access benefits you. Submit a story

HARVARD UNIVERSITY
Graduate School of Arts and Sciences

DISSERTATION ACCEPTANCE CERTIFICATE

The undersigned, appointed by the

Division of Medical Sciences

in the subject of Biological and Biomedical Sciences

have examined a dissertation entitled

DDI2 inhibition promotes MHC class I antigen presentation and immune checkpoint blockade efficacy in cancers

presented by Nhu Tran Nguyen

candidate for the degree of Doctor of Philosophy and hereby certify that it is worthy of acceptance.

Signature: David M. Langenau (Apr 11, 2023 18:58 EDT)

Typed Name: Dr. David Langenau

Signature: Nir Hacohen (Apr 10, 2023 14:10 EDT)

Typed Name: Dr. Nir Hacohen

Signature: Scott Rodig (Apr 10, 2023 19:48 EDT)

Typed Name: Dr. Scott Rodig

Signature: Darrell Irvine (Apr 11, 2023 07:21 EDT)

Typed Name: Dr. Darrell Irvine

Date: April 10, 2023

DDI2 inhibition promotes MHC class I antigen presentation and immune checkpoint blockade efficacy in cancers

A dissertation presented

by

Nhu Tran Nguyen

to

The Division of Medical Sciences

in partial fulfillment of the requirements

for the degree of

Doctor of Philosophy

in the subject of

Biological and Biomedical Sciences

Harvard University

Cambridge, Massachusetts

April 2023

©2023 Nhu Tran Nguyen

All rights reserved.

Dissertation Advisor: Dr. David Fisher Nhu Tran Nguyen

DDI2 inhibition promotes MHC class I antigen presentation and immune checkpoint blockade efficacy in cancers

Abstracts

The landscape of cancer treatments has changed dramatically over the last ten years with the use of novel checkpoint blockade immunotherapy. Even though immune checkpoint inhibitors have produced favorable objective response rates clinically, many patients have developed either primary or acquired resistance. Downregulation of the Major Histocompatibility Complex class I (MHC-I), which is critical for host defense against foreign antigens, has been observed in non-responders to those inhibitors, highlighting the importance of MHC-I antigen presentation on tumors in response to checkpoint blockades. The cytosolic protein DNA Damage Inducible 1 homolog 2 (DDI2) delivers ubiquitylated substrates to proteasomes and also has retrovirus-related proteolytic activity. We report that DDI2 constitutively antagonizes antigen presentation on MHC-I complexes. Deleting *DDI2*, genetically inactivating *DDI2*'s ubiquitin-dependent protease activity, or pharmacologically inhibiting it by using the existing FDA-approved-human immunodeficiency virus (HIV)-1 protease inhibitor, nelfinavir, increased beta-2-microglobulin (B2M) levels, surface MHC-I complexes, and antigen presentation of cytosolic proteins in many cancer cell lines. Stimulation of antigen presentation occurs after antigenic peptides enter the endoplasmic reticulum (ER) but before MHC-I complexes reach the cell surface. DDI2 inhibition increases cytotoxic T cell activation *in vitro* and anti-PD-1 efficacy against melanoma and pancreatic murine tumor

models. Furthermore, *DDI2* expression inversely correlates with activated $CD8^+$ T-cell signatures in 80% of human solid tumors, suggesting a role for DDI2 in limiting MHC-I antigen presentation in humans. This ability of DDI2 inhibitors to enhance immune recognition and anti-PD-1 responses in mice strongly suggests that they can enhance the efficacy of immune checkpoint blockade in cancer therapy.

TABLE OF CONTENTS

Abstracts iii
List of figures vi
Acknowledgments vii

CHAPTER 1. INTRODUCTION 2
1.1. Immune checkpoint blockade therapy in cancers 2
1.1.1. Overview of cancer immunosurveillance 2
1.1.2. Immune checkpoint molecules and checkpoint blockade strategies 6
1.1.3. Current challenges of immune checkpoint blockade therapy in cancers 13
1.2. Downregulation of MHC-I confers resistance to immune checkpoint blockade 14
1.2.1. MHC-I complex and antigen presentation processing 14
1.2.2. Reduced MHC-I protein expression in tumors as a resistance mechanism to immune checkpoint blockade 16
1.3. Unique characteristics of the cytosolic DDI2 protease 18
1.4. Our hypothesis and findings 18

CHAPTER 2. DDI2 INHIBITION INCREASES B2M AND SURFACE MHC-I LEVELS IN MULTIPLE CANCERS 20
2.1. Inhibiting DDI2 increases B2M and surface MHC-I 21
2.2. Nelfinavir does not affect transcription or degradation of antigen precursors 28
2.3. Nelfinavir increases antigen presentation at a step within the ER 37

CHAPTER 3. DDI2 INHIBITION ENHANCES T CELL CYTOTOXICITY IN VITRO AND THE EFFICACY OF IMMUNE CHECKPOINT BLOCKADE IN VIVO 40
3.1. DDI2 inhibition in cancers enhances cytotoxicity of $CD8^+$ T cells 41
3.2. DDI2 inhibition by nelfinavir promotes anti-tumor immunity in mice 44
3.3. *DDI2* levels correlate inversely with activated CD8+ T cell signature mRNA 47

CHAPTER 4. CURRENT WORK IN PROGRESS AND FUTURE DIRECTIONS 60
4.1. Designing and screening for novel DDI2 inhibitors to enhance the efficacy of immune checkpoint blockade 61
4.1.1. Preliminary data 61
4.1.2. Future directions 64
4.2. Exploring the effects of DDI2 inhibitors as adjuvants in a vaccination setting 65

CHAPTER 5. DISCUSSION AND CONCLUSIONS 66

CHAPTER 6. MATERIALS AND METHODS 71

Bibliography 81

LIST OF FIGURES

Figure 1.1. Hallmarks of cancer with new additions
Figure 1.2. The cancer-immune cycle
Figure 1.3. Overview of mechanisms of CTLA-4 immune checkpoint pathway and effects of CTLA-4 blockade
Figure 1.4. Overview of mechanisms of PD-1 immune checkpoint pathway and effects of PD-1 blockade
Figure 1.5. The basic MHC-I antigen presentation pathway
Figure 2.1. Genetic or pharmacologic inhibition of DDI2 elevates levels of B2M and surface MHC-I
Figure 2.2. Nelfinavir increases total B2M and surface MHC-I protein levels in multiple human cancer cell lines
Figure 2.3. HIV-1 protease inhibitors inhibit DDI2 and enhance total B2M and MHC-I protein levels
Figure 2.4. Nelfinavir increases presentation of the antigenic peptide, SIINFEKL, at a step after it enters the ER and before it reaches the cell surface
Figure 2.5. Nelfinavir treatment increases the SIINFEKL peptide presentation on the cell surface from degradation of Venus-SIINFEKL
Figure 2.6. A diagram depicting different experimental precursors used here (Figure 2) to identify how DDI2 inhibition by nelfinavir (NF) affects the production of the antigenic peptide, SIINFEKL, its transport into the ER, and degradation of surface MHC-I-SIINFEKL complexes
Table 3.4. List of genes comprising (A) activated CD8+ T-cell immune signatures, (B) activated B-cell immune signatures, and (C) activated dendritic cell immune signatures as described previously
Table 3.5. *DDI2* levels correlate inversely with activated $CD8^+$ T cell mRNA signatures in many patient tumor types
Figure 3.6. *DDI2* levels correlate inversely with activated CD8+ T cell mRNA signatures in the great majority (80%) of patient solid tumor types
Figure 3.7. *DDI2* levels do not correlate with activated B cell mRNA signatures in multiple patient solid tumor types
Figure 3.8. *DDI2* levels do not correlate with activated dendritic cell mRNA signatures in multiple patient solid tumor types
Figure 4.1. The impact of thirty-six compounds at different concentrations on cell viability of human melanoma MEL624
Figure 4.2. Preliminary data from screening thirty-six compounds for induction of surface MHC-I and total B2M levels in MEL624
Figure 4.3. D1 compound inhibits DDI2

Acknowledgments

First and foremost, I would like to thank my dissertation advisor, Dr. David Fisher, for his remarkable support and guidance during my PhD training. Thanks to Dr. Fisher, I was able to get out of my comfort zone to pursue new skills and become more confident in articulating my ideas and data. His incredible scientific insights, perseverance, and commitment as a mentor have significantly contributed to my tremendous growth as a scientist. Dr. Fisher is one of my biggest inspirations to apply to medical school as the next step in my professional career. He has been highly supportive of my pursuit of medical education to become a physician-scientist.

I am extremely thankful to the research fellows in the Fisher laboratory, Dr. Inbal Rachmin and Dr. Jennifer Allouche, who have been the pioneers of my dissertation project. They have instilled confidence in me to continue the work on this fascinating project. Thank you Dr. Alfred Goldberg and Dr. Gallen Collins for being incredible collaborators. Their expertise and insights have really driven the project to exciting and significant breakthroughs. I am so grateful to various past and present members of the Fisher laboratory for all their support and advice. They have really become my second family and I cannot imagine graduate school without them.

I would like to thank Dr. David Langenau, Dr. Shawn Demehri, and Dr. Mo Motamedi for serving on my dissertation advisory committees and providing critical insights that helped to make this research project successful.

Finally, I would like to thank my grandmother, Lan Nguyen, and my parents, Son Nguyen and Van Tran for all your love, sacrifice, and support that they have always given me. Last but not least, I am thankful to have my husband, Derrick Tengco in my life, who has been a tremendous supporter and partner.

CHAPTER 1. INTRODUCTION

1.1. Immune checkpoint blockade therapy in cancers

1.1.1. Overview of cancer immunosurveillance

Cancer cells are characterized as having genetic/epigenetic alterations and defects in their regulatory circuits, leading to their abnormal cell development and homeostasis (reviewed in Hanahan, 2022; Hanahan & Weinberg, 2000). Increasingly emerging hallmarks of cancer through intensive research efforts indicate the complexity and diversity of underlying principles of tumor pathogenesis (reviewed in Hanahan, 2022) (Figure 1.1).

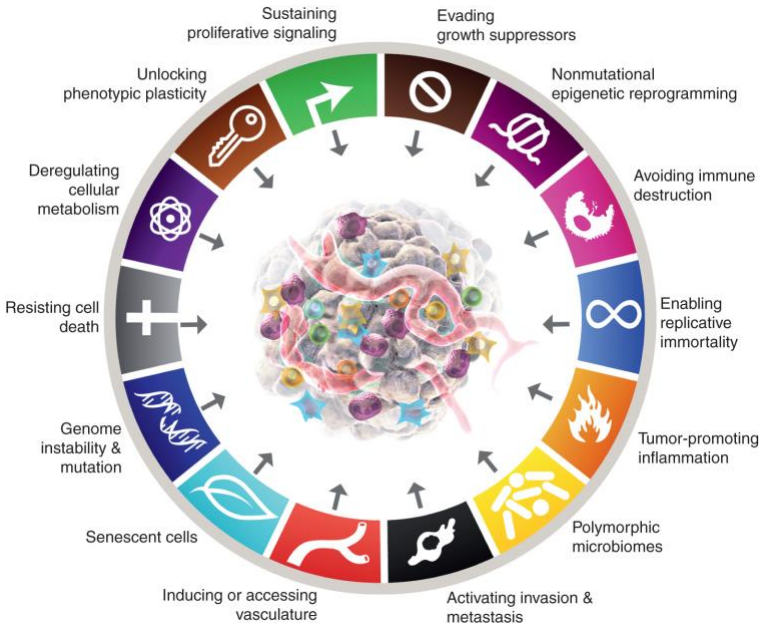

Figure 1.1. Hallmarks of cancer with new additions. The figure was reprinted from Hanahan, 2022.

One of the mechanisms of oncogenesis is the escape of cancer cells from the surveillance of the immune system. The concept of immunosurveillance in cancer is built upon the premise that cancer cells express antigens distinct from their normal cellular counterparts, either neoantigens or self-antigens. Cancer cells accumulate several mutations during tumor development to

produce mutated proteins not expressed in normal cells called neoantigens. In addition, tumor cells express self-antigens, which are also present in normal cells, but with aberrant expression or location. These antigens might elicit responses from the host's immune system, which perceives them as non-self (reviewed in Morad et al., 2021).

The idea of cancer immunosurveillance was first conceived in the nineteenth century with the invention of Coley's toxin by Dr. William Coley to treat his patients diagnosed with inoperable bone and self-tissue sarcoma. By injecting a combination of a heat-killed streptococcal organism and *Serratia marcescens* into patients, he observed shrinkage of malignant tumors, convincing him that a severe infection was required to regress cancer (Coley, 1898; Coley, 1991). Even though he and others throughout the twentieth century suggested the involvement of the immune system in eliminating cancer cells (Burnet, 1957; Ehrlich, 1909), their hypothesis remained controversial and unappreciated (reviewed in McCarthy, 2006; Rao et al., 2019). Not until the early 1990s did the understanding of tumor surveillance become more validated. Several studies showed that immune effectors, such as interferon-γ (IFN-γ) and perforin, were significant to antitumor immunity using mouse models. Moreover, deficiency in these effectors led to susceptibility to tumor engraftment and proliferation in these mice (Dighe et al., 1994; Smyth et al., 2000; Street et al., 2001). Tumors grew slower in immunocompetent mice (more immunogenic), compared to those in immunodeficient mice (Shankaran et al., 2001; Svane et al., 1997). In parallel with animal studies, there was an increased risk of cancer development in immunosuppressive organ transplant patients (Birkeland et al., 1995; Penn, 1993). Altogether, these data show that tumors develop differently in the presence of the immune system, confirming its protective role against cancer cells. They also indicate that the immune

system can create selective pressure that makes tumor cells undergo a dynamic and complex immunoediting process to survive and proliferate.

The immunoediting hypothesis states that in the presence of the immune system, cancer development occurs in three phases: elimination, equilibrium, and escape. During the elimination phase, different immune cell populations and effectors from both innate and adaptive immunity cooperate to recognize and destroy nascent transformed cells, preventing them from becoming malignant and clinically detectable. If the immune system completely clears tumor cells, the elimination step constitutes the whole immunoediting process. However, tumor cells capable of surviving through the elimination step enter the equilibrium phase with the immune system, which limits their net growth and holds them in a functional dormancy state, primarily by adaptive immunity. At some point, the constant pressure from the immune system and the genetic instability of cancer cells can select for cell populations with reduced immunogenicity that can evade immune surveillance and destruction. These less immunogenic tumor cell populations might go through various immunoediting mechanisms to enter the escape phase, where the immune system fails to control tumor growth, causing clinically apparent disease (reviewed in Dunn et al., 2002; Mittal et al., 2014; Schreiber et al., 2011).

An antitumor immune response efficient at eliminating cancer cells must go through a series of steps that are properly initiated, repeated, and amplified. This series of stepwise events refers to as the cancer-immune cycle (Figure 1.2). 1) Neoantigens are produced during tumor development and released from dead cancer cells. Dendritic cells capture these neoantigens and move to the nearest draining lymph node. 2) Dendritic cells present acquired antigens through major histocompatibility class I (MHC-I) and MHC-II to T cells. 3) Upon recognizing cancer-specific antigens (priming), effector T cells are activated (activation). 4) The activated T

lymphocytes express certain cell adhesion molecules and chemokine receptors required for trafficking and infiltrating into the tumor. Then, they leave the draining lymph node to enter the bloodstream and travel to the tumor tissue. 5) Those T cells infiltrate into the tumor, and 6) recognize cancer cells through the engagement of their T cell receptors (TCRs) and antigens presented on MHC-I molecules on cancer cells. 7) Finally, those cancer cells are killed by cytotoxic T cells ($CD8^+$ T cells) through either granule-exocytosis mediated by perforin and granzymes or apoptosis induced by Fas ligand/Fas receptor pathway (reviewed in Chen & Mellman, 2013; Kim & Cho, 2022; Raskov et al., 2021).

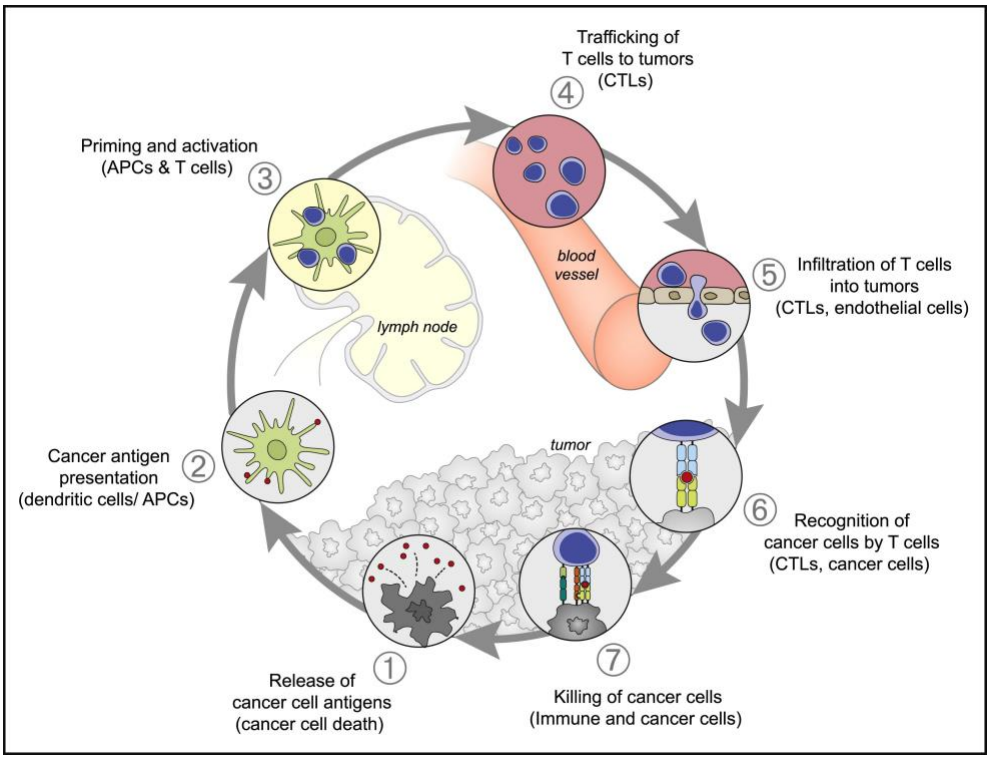

Figure 1.2. The cancer-immune cycle. The cancer-immunity cycle is described as seven major steps, starting from releasing cancer cell antigens from cancer cell death and ending with killing cancer cells by activated cytotoxic T lymphocytes. Each step is described with primary cell types

involved in parentheses and the location of the activity listed. The figure was reprinted from Chen & Mellman, 2013.

1.1.2. Immune checkpoint molecules and checkpoint blockade strategies

Under normal physiological conditions, an overactivated $CD8^+$ T cell response can lead to autoimmunity, causing irreversible damage to the host's tissue. In order to dampen the immune response to prevent overactivation, there are a variety of immune checkpoint molecules that act as inhibitory receptors on the surface of different immune cells (reviewed in Morad et al., 2021; Raskov et al., 2021). Interestingly, cancer cells can utilize these immune checkpoint pathways to suppress the antitumor immune response, benefitting their tumor development. Two prominent immune checkpoint molecules garnering considerable attention are cytotoxic T lymphocyte antigen-4 (CTLA-4/CD152) and programmed death-1 (PD-1/CD279).

For T cells to be fully activated, upon the binding of the TCR to the antigen-MHC complex, an independent costimulatory signal is required, which is the interaction between the CD28 receptor on T cells and its two ligands, CD80/B7.1 and CD86/B7.2 highly expressed on professional antigen-presenting cells, such as mature dendritic cells, macrophages, and activated B cells (June et al., 1990; Shahinian et al., 1993; Viola & Lanzavecchia, 1996). CD28 costimulation is fundamental to T cell activation and sensitivity; it prevents T cell anergy and promotes cytokine production and lymphocyte proliferation (Harding et al., 1992). CTLA-4 and CD28 are homologous glycoproteins in the immunoglobulin superfamily (Brunet et al., 1987). Even though the CTLA-4 receptor on T cells binds to identical ligands as CD28, it binds with a much higher affinity (Linsley et al., 1994) and exerts inhibitory effects on T cell activation (Krummel & Allison, 1995). An earlier study by the Sharpe group also showed that CTLA-4-

deficient mice had hyperactivated T cells and quickly developed lymphoproliferative disease with multiorgan lymphocytic infiltration and lethal tissue damage (Tivol et al., 1995). CTLA-4 mitigates $CD4^+$ T cell activation while boosting the activity of regulatory T cells, causing an immunosuppressive phenotype through a variety of mechanisms (Guntermann & Alexander, 2002; Hou et al., 2015; Kong et al., 2014; Paterson et al., 2015; Qureshi et al., 2012) (Figure 1.3a). Based on these observations, strategies to inhibit or antagonize the CTLA-4 signaling pathway can serve as promising options to enhance the antitumor immune response. First *in vivo* administration of CTLA-4 antibodies led to a long-lasting immune response against cancer cells, resulting in the rejection of tumors (Leach et al., 1996). Even though complete ablation of CTLA-4 was shown to induce significant autoimmunity (Tivol et al., 1995), inhibition of CTLA-4 using antibodies did not lead to a detrimental autoimmune response in mice (Leach et al., 1996). From the preclinical studies, several clinical trials have been initiated on patients to evaluate the therapeutic effects of humanized CTLA-4 antibodies, including Ipilimumab and Tremelimumab. A landmark trial in 2010 (Hodi et al., 2010) and others (Hodi et al., 2003; Ribas et al., 2005; Robert et al., 2011) led to the approval of Ipilimumab in 2011 for the treatment of advanced melanoma by the US Food and Drug Administration (FDA). In a pooled analysis of overall survival (OS) data of multiple studies from advanced melanoma patients receiving Ipilimumab, the median OS was 11.4 months, and the OS curve plateaued at year 3, when the survival rates ranged from 20% to 26% (Schadendorf et al., 2015) (Figure 1.3b). Even though Ipilimumab has shown durable responses in melanoma patients, it has been associated with inflammatory side effects called immune-related adverse events (irAEs) in about 60% of patients (Hodi et al., 2010). CTLA-4 antibodies were also explored in other solid tumors, though with more modest responses observed in patients (reviewed in Baumeister et al., 2016). In 2022, the

FDA-approved Trimelimumab in combination with other therapies for treating unresectable hepatocellular carcinoma and metastatic non-small cell lung cancer (Keam, 2023).

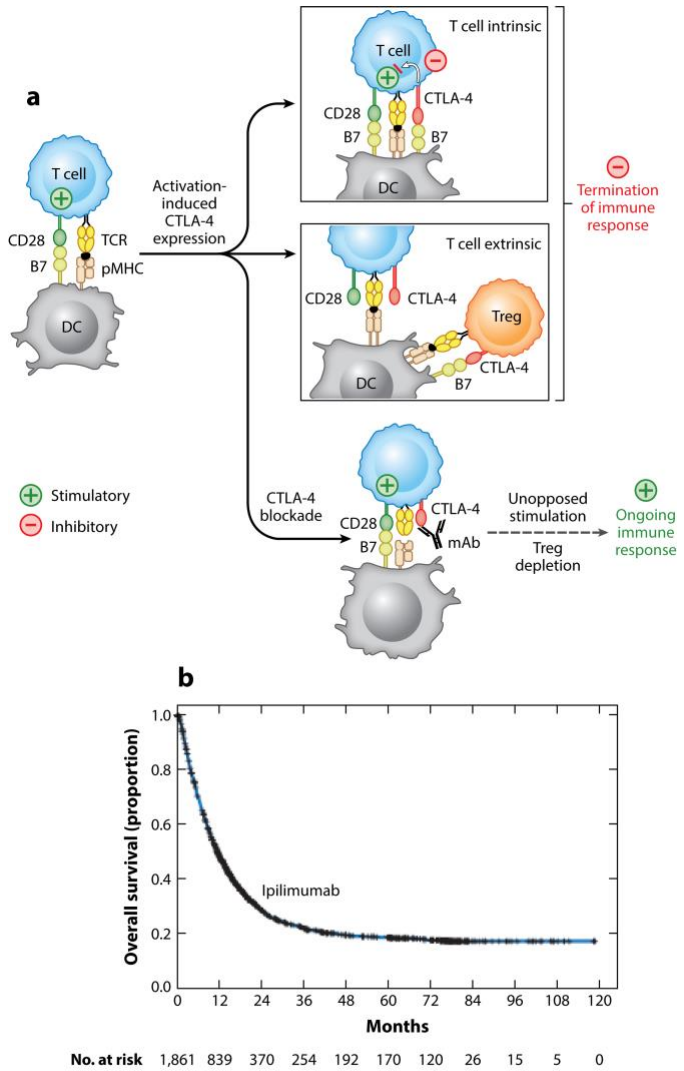

Baumeister SH, et al. 2016.
Annu. Rev. Immunol. 34:539–73

Figure 1.3. Overview of mechanisms of CTLA-4 immune checkpoint pathway and effects of CTLA-4 blockade. (a) CTLA-4 expression is induced upon T cell activated. Through T cell-intrinsic pathway, CTLA-4 receptor on T cell surface outcompetes with CD28 receptor for their shared ligands, B7.1 and B7.2 to reduce TCR and CD28 signaling. In T cell-extrinsic fashion,

CTLA-4 expressed on one T cell may inhibit activation of other T cells by decreasing the expression of ligands B7.1 and B7.2 on antigen-presenting cells, leading to reduced availability for CD28 engagement. Blocking CTLA-4 by a monoclonal antibody prevents the interaction of CTLA-4 and its ligands and may deplete regulatory T cells, allowing CD28 signaling to promote an immune response. **(b)** A meta-analysis of advanced melanoma patients receiving Ipilimumab, who were followed up for 3 to 10 years, showed approximately 20% overall long-term survival (Schadendorf et al., 2015). The figure was reprinted from Baumeister et al., 2016.

The second immune checkpoint molecule, PD-1 (Figure 1.4), bears the name because of its initial description as a receptor that induced cell death of an activated T cell hybridoma (Ishida et al., 1992). However, subsequent studies showed that PD-1 did not activate the caspase or programmed cell death pathways; instead, it is a negative regulator to counteract the T cell activation (reviewed in Ishida, 2020). PD-1 is a type I transmembrane protein consisting of an immunoglobulin superfamily domain, a ~20 amino acid stalk, a transmembrane domain, and an intracellular domain containing an immunoreceptor tyrosine-based inhibitory motif (ITIM) and an immunoreceptor tyrosine-based switch motif (ITSM). PD-1 can be expressed on T cells and other cell types, including but not limited to B cells, natural killer cells, activated monocytes, and dendritic cells (reviewed in Keir et al., 2008). Interestingly, it is not readily expressed on resting T cells but induced upon T cell activation signals (Nishimura et al., 1996). PD-1 receptor binds specifically to two ligands, programmed death-ligand 1 (PD-L1)/CD274/B7-H1 and PD-L2/CD273/B7-DC. These two ligands have different expression patterns. PD-L1 is expressed on both hematopoietic (T cells, natural killer cells, dendritic cells, macrophages, B cells, and bone marrow-derived mast cells) and non-hematopoietic cells (e.g. endothelial cells, epithelial cells,

keratinocytes), while PD-L2 expression is restricted to mainly hematopoietic cells. In addition to PD-1 as their receptor, PD-L1 and PD-L2 have their second distinct binding partner: PD-L1 binds to B7.1 and PD-L2 binds to Repulsive Guidance Molecule b (RGMb), delivering additional inhibitory signals to T cell activity (reviewed in Sharpe & Pauken, 2018).

Upon engagement of PD-L1 or PD-L2 to PD-1 receptor, tyrosine residues in the intracellular domain of PD-1 are phosphorylated to recruit tyrosine phosphatase SHP-2, leading to attenuated phosphorylation of TCR signaling molecules and TCR downstream stimulation, reduced T cell activation and cytokine production, and enhanced T cell exhaustion (Figure 1.4a). PD-1 pathway can work through a remarkable number of mechanisms to act as a gatekeeper in the adaptive immune system. To name a few, PD-1 can inhibit phosphatidylinositol 3-kinase activity (Parry et al., 2005) to diminish Akt activation and decrease expression of the transcription factors required for effector cell functions (Kao et al., 2011). In addition, PD-1 pathway has been demonstrated to stimulate proteins that impair T cell proliferation and cytokine production (Quigley et al., 2010), promote antiapoptotic gene expression while reducing proapoptotic gene expression (Gibbons et al., 2012), or inhibit TCR-mediated positive selection to shape T cell repertoire (Keir et al., 2005). PD-1 acts on not only secondary lymphoid organs but also non-lymphoid tissues, including tumors, making it a unique and central negative regulator of the adaptive immune response spanning from the initial T cell priming and differentiation to after activated T cells migrate to the effector sites (reviewed in Pauken et al., 2021). Active investigations are ongoing to understand the role of the PD-1 pathway on other non-T cell populations, such as innate lymphoid cells or natural killer cells.

In the tumor microenvironment, PD-L1 and PD-L2 expression, to a lesser extent, have been identified in a wide variety of solid tumors, including but not limited to melanoma, breast,

lung, ovarian, bladder, stomach, and liver cancer (Brown et al., 2003; Hamanishi et al., 2007; Inman et al., 2007; Nakanishi et al., 2007; Strome et al., 2003; Wu et al., 2006). Moreover, PD-L1 expression strongly correlates with unfavorable prognosis in several cancer types, suggesting that high PD-L1 levels on tumors may facilitate cancer development and invasion into deeper tissue (reviewed in Baumeister et al., 2016). PD-1 is expressed more frequently on tumor-specific tumor-infiltrating lymphocytes (TILs), contributing to tumor immunosuppression phenotype (Blank et al., 2003). Thus, the PD-1 immune checkpoint pathway has been demonstrated as a major mechanism of tumor immune evasion and its perturbation is an appealing strategy for cancer therapeutic implications. Studies in mice showed that PD-1 blockade by either a genetic approach or a monoclonal antibody augments the antitumor immune response through increasing cytotoxicity and cytokine production (Hirano et al., 2005; Iwai et al., 2005; Latchman et al., 2004). Because of higher expression levels of PD-1 on TILs and its ligands on tumor cells, inhibition of PD-1 pathway might result in less toxicity from autoimmunity compared to anti-CTLA-4 (Morad et al., 2021). These observations have led to the development of antibodies against PD-1 (Nivolumab and Pembrolizumab) and PD-L1 (Atezolizumab, Avelumab, and Durvalumab), which have been proven to induce effective and potent antitumor responses in clinical trials. In 2014, PD-1 antibodies were first approved by the FDA for advanced or metastatic melanoma. Since then, these antibodies have been approved as the treatment for over 20 different types of cancer, including non-small cell lung cancer, head and neck cancer, Hodgkin lymphoma, cervical cancer, and triple-negative breast cancer (Vaddepally et al., 2020). Response rates range from 13% to 69% with common solid tumors in the 20-30% overall response rate range (Pauken et al., 2021). Even though the rates of irAEs are

more limited than CTLA-4 blockade, PD-1 inhibitors still result in higher toxicity in patients than in preclinical models (Hirano et al., 2005).

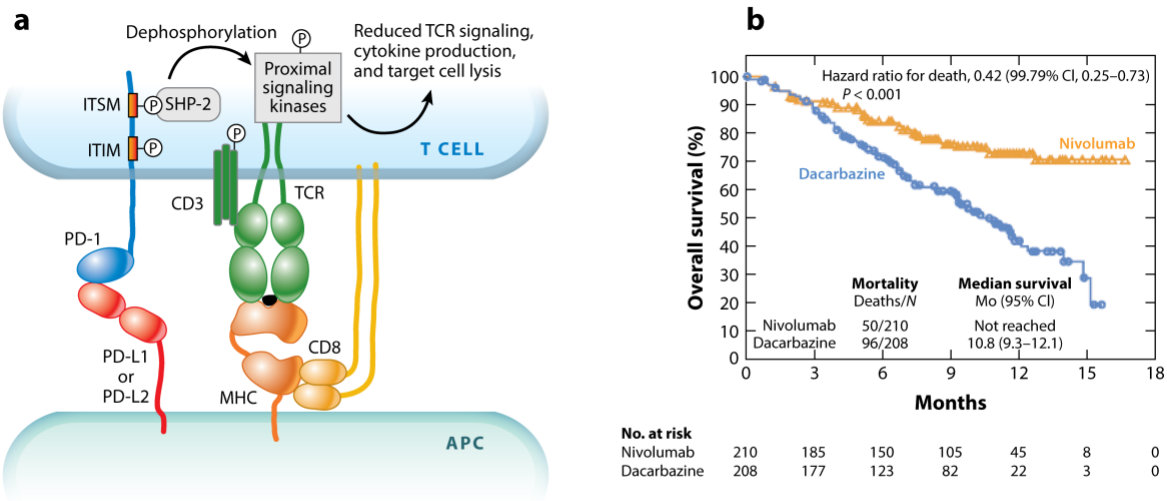

Baumeister SH, et al. 2016.
Annu. Rev. Immunol. 34:539–73

Figure 1.4. Overview of mechanisms of PD-1 immune checkpoint pathway and effects of PD-1 blockade. (a) PD-1 is inducibly expressed on T cell surface upon T cell activation signals, while its ligands PD-L1 and PD-L1 are expressed on antigen-presenting cells or tumor cells. Engagement of PD-L1 or PD-L2 with PD-1 receptor results in phosphorylation of tyrosine residues on the intracellular domain of PD-1 receptor, recruiting the tyrosine phosphatase SHP-2. As a result, phosphorylation of downstream TCR signaling molecules is reduced, limiting T cell effector functions. **(b)** In a study conducted by Robert et al., the treatment of PD-1 antibody, Nivolumab, was associated with significantly improved overall survival and progression-free survival, compared to the chemotherapy agent, dacarbazine, in previously untreated metastatic melanoma patients without a BRAF mutation (Robert et al., 2015). The figure was reprinted from Baumeister et al., 2016.

1.1.3. Current challenges of immune checkpoint blockade therapy in cancers

Discovery of cancer immunosurveillance and the development of immune checkpoint inhibitors have become one of the most significant breakthroughs that drastically change the landscape of cancer therapy. Despite the remarkable clinical successes of immune checkpoint inhibitors, there are several challenges remaining. In cancer types with low immunogenicity such as glioblastoma, a lack of response to checkpoint blockade has been observed. Even with cancers in which immune checkpoint inhibitors have proven promising clinical efficacy like melanoma, the resulting objective and durable response has only been limited to a subset of patients. Several patients do not respond to the treatment in the first place (primary resistance) or eventually relapse after an initial response (acquired resistance) (Barrueto et al., 2020; Morad et al., 2021; Sharma et al., 2017). Consequently, significant efforts have been made to decipher resistance mechanisms to immune checkpoint blockade with the goal of improving its clinical benefits. Two major categories of factors contributing to immune evasion and resistance to checkpoint inhibitors are patient-intrinsic and -extrinsic factors. Patient-intrinsic factors are divided into multiple sub-categories: patient systemic factors (age, sex, human leukocyte antigen (HLA) genotype, and genetic polymorphisms), tumor-intrinsic, and tumor microenvironment factors. Patient-extrinsic factors are environmental influences (also known as the exposome) that can impact responses to cancer therapy. Among those listed, characteristics intrinsic to the tumors themselves, including mutational landscape, antigen presentation, IFN-γ signaling, and immune-evasive oncogenic signaling pathways, are major determinants of response and resistance to immune checkpoint blockade in various cancer types. One of the most common strategies of malignant cells to evade cytotoxic T cell recognition and killing is to decrease antigen

presentation by reducing expression of MHC-I molecules on the cell surface. Therefore, identifying ways to increase MHC-I presentation should promote $CD8^+$ T cell recognition of cancers and may also enhance the efficacy of immune checkpoint blockade with antibodies targeting PD-1 or CTLA-4 (reviewed in Kalbasi & Ribas, 2020).

1.2. Downregulation of MHC-I confers resistance to immune checkpoint blockade

1.2.1. MHC-I complex and antigen presentation processing

Most nucleated cells present intracellular peptides through the MHC-I heterodimers on the cell surface to inform the immune system of their health status. MHC-I molecules are encoded by several genes and are classified into highly polymorphic classical MHC-I (HLA-A, -B, and -C) and less polymorphic non-classical MHC-I (HLA-E, -F, and -G). For the purpose of simplification, hereinafter, I refer to classical MHC-I as MHC-I. Structurally, the MHC-I complex is composed of the HLA heavy chain, which contains the peptide binding fold, and the β2-microglobulin (B2M) light chain (reviewed in Thomas & Tampé, 2019). The nucleotide-binding domain and leucine-rich repeat-containing family, caspase recruitment domain-containing 5 (NLRC5) has been demonstrated to be the master transcriptional regulator of MHC-I genes (Meissner et al., 2010). Upon the binding of IFN-γ, a known inducer of MHC-I genes, to its receptor on the cell surface, the janus kinase/signal transducer and activator of transcription 1 (JAK/STAT1)-dependent pathway is activated, leading to the translocation of NLRC5 into the nucleus and its association with other proteins to form the transcriptional complex called the class I transactivator (CITA) enhanceosome to induce MHC-I gene expression (reviewed in Cho et al., 2021). Studies showed that *Nlrc5*$^{-/-}$ mice have decreased MHC-I expression, impairing $CD8^+$ T cell cytotoxicity (Lupfer et al., 2017; Staehli et al., 2012).

After translation, MHC-I components are assembled in the ER, partially folded, and stabilized by ER-associated chaperone proteins, including calreticulin, ERp57 (also known as PDIA3), protein disulphide isomerase (PDI), and the dedicated chaperone tapasin (reviewed in Neefjes et al., 2011). Calreticulin is a lectin that binds to N-glycosylated MHC-I molecules, allowing a strong interaction of MHC-I and tapasin (Wearsch et al., 2011). The third component of the MHC-I complex that determines its stability is the 8-10 residue antigenic peptides that bind deeply into the peptide-binding grove on MHC-I. These peptides are generated during the continuous degradation of cell proteins, primarily by the ubiquitin-proteasome pathway (Rock et al., 1994). Although most proteasome products are rapidly hydrolyzed to amino acids in the cytosol, a small fraction of the generated peptides are translocated by the transporter associated with antigen processing (TAP) into the endoplasmic reticulum (ER) lumen. MHC-I together with TAP, tapasin, calreticulin, and ERp57 are called the peptide-loading complex (PLC), which catalyzes the peptide association with MHC-I heavy chain and B2M molecules (reviewed in Tanaka, 2009; Thomas & Tampé, 2019). If a peptide tightly binds to the groove in an MHC-I molecule, the MHC-I complex is released from its chaperones, and then transported through the ER and the Golgi apparatus to the cell surface for antigen presentation. Contrarily, when peptides and MHC-I complex fail to associate with each other in the ER, they are transported back into the cytosol for degradation through a process called ER-associated degradation (ERAD) (Hughes et al., 1997; Koopmann et al., 2000) (Figure 1.5).

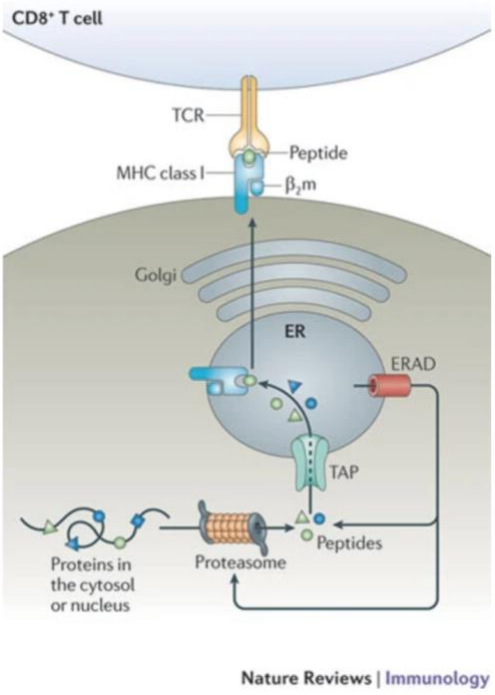

Figure 1.5. The basic MHC-I antigen presentation pathway. The presentation of antigenic peptides on MHC-I complexes consists of multiple reactions. First, proteins in the cytosol or the nucleus are degraded by the proteasome. The generated peptides are translocated into the endoplasmic reticulum (ER) lumen via the transporter associated with antigen processing (TAP) and assembled onto the grove of MHC-I molecules, which comprise of a polymorphic heavy chain and a light chain called β2-microglobulin (B2M). The peptide-MHC complexes are then translocated from the ER to the Golgi and plasma membrane to present the antigen to $CD8^+$ T cells through T cell receptor (TCR). ERAD: ER-associated antigen degradation. The figure was reprinted from Neefjes et al., 2011.

1.2.2. Reduced MHC-I protein expression in tumors as a resistance mechanism to immune checkpoint blockade

Due to their abundant genetic rearrangements, frequent mutations, and tendency to express normally rare proteins (e.g. gp100 in melanoma), protein turnover in cancer cells generates an unusual array of antigenic peptides ("neoantigens"). However, cancers often evade T Cell recognition by decreasing MHC-I protein expression. There are three lines of evidence for the clinical importance of MHC-I loss. First, MHC-I positively correlates with TILs found in tumors, indicating the importance of MHC-I to antitumor T cell response. Second, loss of MHC-I is associated with a worse prognosis in various cancer types, including melanoma, glioblastoma, bladder, breast, and other cancers. Third, loss in MHC-I levels leads to resistance to immune checkpoint inhibitors. Defects in the MHC-I antigen presentation pathway can occur in many stages: transcription, pre/post-translation, or due to alterations in signaling pathways and extrinsic stimuli from the tumor microenvironment (reviewed in Dhatchinamoorthy et al., 2021).

Among components in the MHC-I antigen processing machinery, B2M is required for the proper folding and function of the overall peptide-MHC-I complex. Evidently, B2M expression has been found to be associated with response to immune checkpoint blockade in cancers. In 2016, in a study analyzing biopsy samples from four metastatic melanoma patients who developed acquired resistance to the PD-1 monoclonal antibody, Pembrolizumab, one patient had a truncating mutation in the *B2M* gene from the relapse tumor, resulting in loss of surface MHC-I protein expression compared to the baseline tumor and adjacent stroma cells (normal cells) (Zaretsky et al., 2016). In a larger cohort of seventeen metastatic melanoma patients treated with immune checkpoint inhibitors, 29.4% of patients with progressing disease had frameshift mutations or loss of heterozygosity in the *B2M* gene (Sade-Feldman et al., 2017). Reduction or complete loss of surface MHC-I protein expression in 43% cases of melanoma patients (through transcriptional downregulation of *HLA-I* or *B2M*) led to primary resistance to anti-CTLA-4 (Rodig et al., 2018).

Therefore, identifying ways to increase MHC-I presentation should promote $CD8^+$ T cell recognition of cancers and may also enhance the efficacy of immune checkpoint blockade with antibodies targeting PD-1 or CTLA-4 (Angell et al., 2014; S. S. Gu et al., 2021; Luo et al., 2018; Manguso et al., 2017; Yamamoto et al., 2020).

1.3. Unique characteristics of the cytosolic DDI2 protease

DDI2 has several unique features. 1) Although it contains a domain similar to those in retroviral proteases, it shows endoproteolytic activity only against ubiquitylated proteins (Dirac-Svejstrup et al., 2020; Sha & Goldberg, 2016; Yip et al., 2020). 2) Its only known physiological substrates are the ER membrane-bound precursors to transcription factors, Nrf1/NFE2L1/TCF11 and Nrf3/NFE2L3, whose cleavage by DDI2 upon proteasome inhibition allows them to enter the nucleus and increase transcription of proteasomal genes (Chowdhury et al., 2017; Fassmannová et al., 2020; Koizumi et al., 2016). 3) DDI2 also functions as a "shuttling factor" that binds ubiquitylated proteins and delivers them to the 26S proteasome using its Ubiquitin-like (Ubl) domain (Collins et al., 2022). 4) Inhibition or mutation of DDI2's proteolytic activity with nelfinavir allosterically disrupts its ability to function as a shuttling factor (Collins et al., 2022).

1.4. Our hypothesis and findings

While studying novel factors modulating protein expression in melanomas, we observed an unanticipated property of nelfinavir, an FDA-approved inhibitor of HIV-1 protease: an ability to increase protein levels of B2M in multiple tumor types. The present studies were undertaken to identify the cellular mediator of nelfinavir, examine its influence on MHC-I antigen presentation,

and determine whether it or related compounds may help promote anti-tumor cytotoxic T-cell responses.

Nelfinavir was developed as a specific inhibitor of the HIV-1 protease required for retroviral maturation (Longer et al., 1995). However, recent studies (Collins et al., 2022; Y. Gu et al., 2020) have identified a widely expressed mammalian target of nelfinavir, DDI2, which is one of five human proteins containing a protease domain similar to that in HIV. Here, we report an unrecognized role for DDI2 protease in restricting antigen presentation by MHC-I. We show here that although DDI2 is a cytosolic enzyme, it normally limits the processing of MHC-I complexes after they are in the ER, and that genetic or pharmacological inhibition of DDI2 increases surface MHC-I levels and antigen presentation in many types of cancer cell lines. Moreover, this increase in MHC-I presentation enhances the sensitivity of cancer cells to cytotoxic T cells and to immune checkpoint inhibitors *in vivo*.

CHAPTER 2. DDI2 INHIBITION INCREASES B2M AND SURFACE MHC-I LEVELS IN MULTIPLE CANCERS

This chapter is adapted from the manuscript (in preparation for submission):

Nhu T. Nguyen[*], Galen Andrew Collins[*], Inbal Rachmin[*], Jennifer Allouche[*], Sachiko T. Homma, Abdulla Al Emran, Shanivi Srikonda, Max von Franque, Shailbala Singh, Chuan Yan, Kristina Todorova, Tal H. Erlich, Yi Sun, Hongyan Xie, Abigail Scharf, Oriah Jeselsohn, Christopher Ott, Anna Mandinova, Russell Jenkins, David Langenau, F. Stephen Hodi, Cassian Yee, Alfred L. Goldberg[#] and David E. Fisher[#]. DDI2 inhibition promotes MHC-I antigen presentation and tumor immunotherapy.

*Contributed equally

#Contributed equally (corresponding authors)

2.1. Inhibiting DDI2 increases B2M and surface MHC-I

During studies of protein expression in MEL624 cells, we unexpectedly observed that treatment with 10 μM nelfinavir for 1-3 days increased the cellular content of B2M 2-3 fold (Figure 2.1A). A similar increase in B2M with nelfinavir was seen in the pancreatic ductal adenocarcinoma (PDAC) KP4 and colon carcinoma HCT 116 cell lines (Figure 2.1A), and in twelve other cancer cell lines (Figure 2.2A-D). We then tested if nelfinavir not only raised B2M content but also increased MHC-I molecules on the cell surface. In MEL624, KP4, and HCT116 cells, nelfinavir at 10 μM increased surface MHC-I (*i.e.,* HLA-A, B, C) molecules (Figure 2.1B). A similar approximately 1.5 to 2.5-fold increase in surface MHC-I levels upon nelfinavir treatment occurred in other melanoma cell lines tested (Figure 2.2E).

Because the shuttling factor DDI2 has a retroviral protease domain with structural homology to HIV protease and is inhibited by nelfinavir (Collins et al., 2022), we tested whether DDI2 may mediate the effects of nelfinavir on B2M levels by generating CRISPR knockouts of

DDI2. We observed that the deletion of *DDI2* in MEL624 and KP4 by itself increased B2M levels and prevented any further increase in B2M by nelfinavir (Figure 2.1A). In addition, using a CRISPR-engineered version of HCT116 (DDI2 D252N) that inactivated DDI2's proteolytic active site (Koizumi et al., 2016), we found that the loss of its protease activity also increased the levels of B2M and prevented any further stimulation by nelfinavir (Figure 2.1A). Deletion of *DDI2* or mutation of its protease active site on its own increased surface MHC-I levels and significantly blunted the increase in surface MHC-I upon nelfinavir treatment (Figure 2.1B). Thus, genetic or pharmacologic inhibition of the DDI2 protease also promotes surface MHC-I expression.

We then tested whether re-expressing DDI2 in the *DDI2*-deficient HAP1 cells could restore the nelfinavir response. Transfection of wildtype (WT) DDI2 reduced B2M levels and restored the stimulation by nelfinavir (Figure 2.1C). However, no effect was seen upon transfection of a DDI2 mutant lacking its Ubl domain, which is essential for DDI2 binding to ubiquitin and to proteasomes (Collins et al., 2022; Collins & Goldberg, 2020). This requirement for the Ubl domain is consistent with the prior finding that DDI2 exhibits proteolytic activity only against ubiquitylated proteins (Dirac-Svejstrup et al., 2020; Sha & Goldberg, 2016; Yip et al., 2020). Thus, genetic or pharmacologic inhibition of DDI2's protease activity promotes expression of B2M and the appearance of MHC-I complexes on the cell surface.

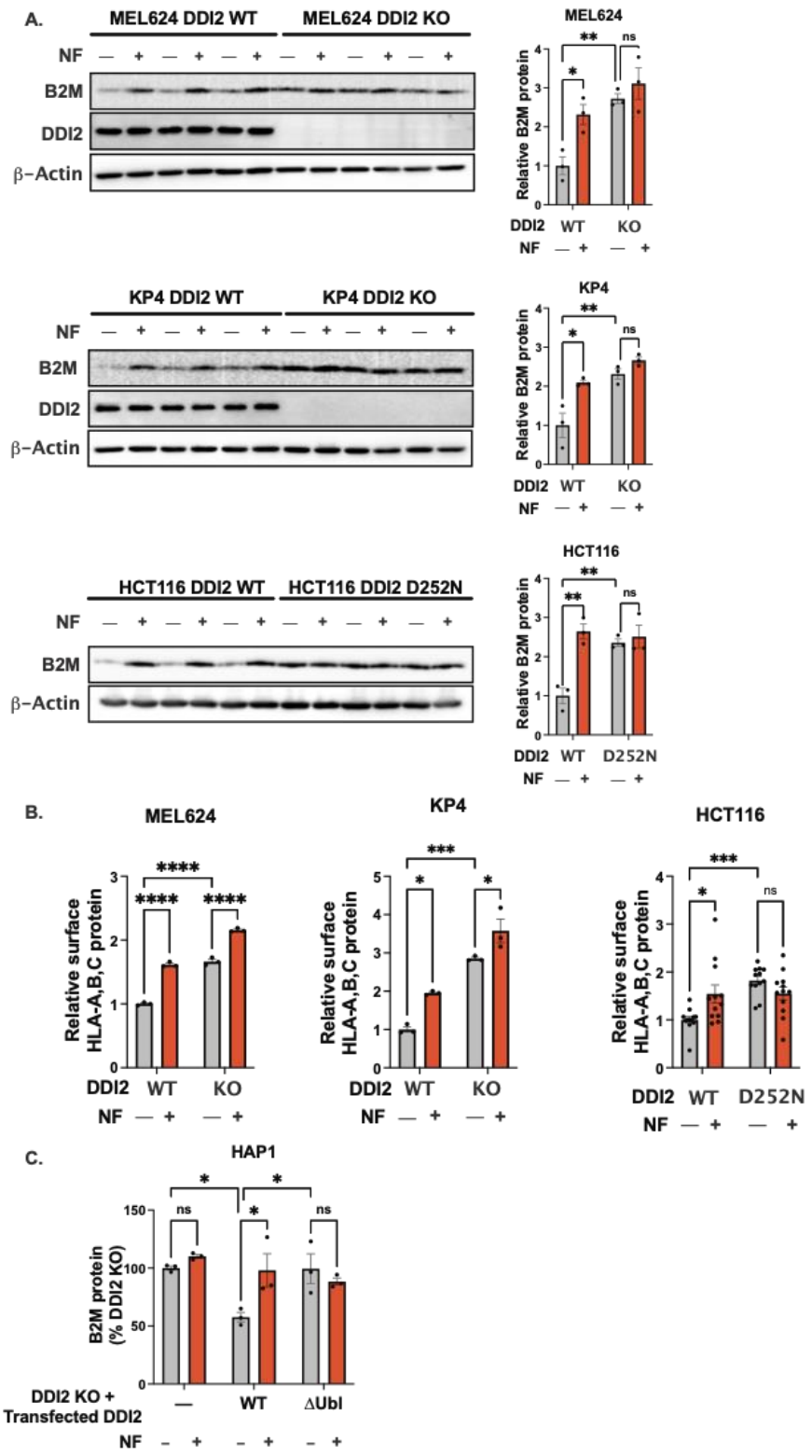

Figure 2.1. Genetic or pharmacologic inhibition of DDI2 elevates levels of B2M and surface MHC-I. (A) Representative immunoblots of B2M, DDI2, and β-actin in human melanoma

Figure 2.1. (Continued)

MEL624 *DDI2*$^{+/+}$ (DDI2 WT) and *DDI2*$^{-/-}$ (DDI2 KO), pancreatic ductal adenocarcinoma (PDAC) KP4 DDI2 WT and DDI2 KO and colon cancer HCT116 DDI2 WT and DDI2 D252N mutant treated with nelfinavir (NF) (10 μM) or DMSO (left panels) with quantification of B2M protein expression normalized to β-actin and from DDI2 WT treated with DMSO control (right panels); n = 3. **(B)** Flow cytometry-based quantification of surface HLA-A,B,C protein expression of melanoma MEL624 DDI2 WT and DDI2 KO, PDAC KP4 DDI2 WT and DDI2 KO, and colon cancer HCT116 DDI2 WT and DDI2 D252N mutant treated NF (10 μM) or DMSO; at least n = 3. **(C)** Quantification of immunoblots for B2M normalized to GAPDH in HAP1 DDI2 KO cells transfected with FLAG-tagged DDI2 WT, FLAG-tagged DDI2 without the N-terminal Ubl domain (ΔUbl), or empty vector (—) for 48 hours followed by 24 hours of treatment with NF (10 μM) or DMSO; n = 3. All data are expressed as mean ± s.e.m. and analyzed using two-way ANOVA with Tukey's post hoc test. * $p < 0.05$, ** $p < 0.01$, *** $p < 0.001$, **** $p < 0.0001$, ns indicates not statistically significant.

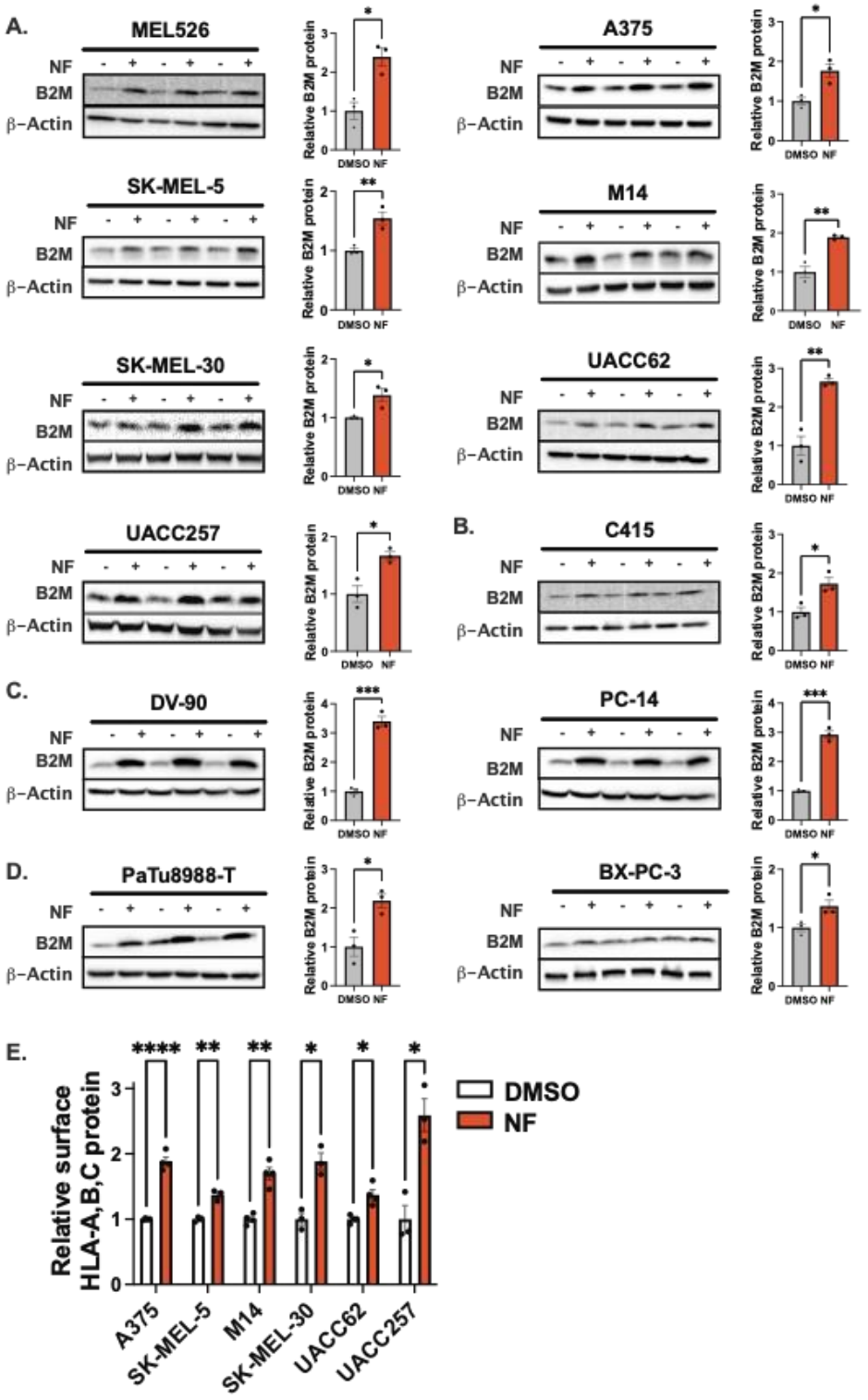

Figure 2.2. Nelfinavir increases total B2M and surface MHC-I protein levels in multiple human cancer cell lines. (A-D) Total B2M protein levels of **(A)** melanoma cell lines, **(B)** a low-

Figure 2.2. (Continued)

B2M, early-passage melanoma cell line, **(C)** lung cancer lines, and **(D)** pancreatic adenocarcinoma lines after treatment with nelfinavir (NF) at 10 μM; n = 3. The left panels show representative immunoblots, and the right panels show quantification of B2M protein expression normalized to β-actin and DMSO. **(E)** Flow cytometry-based quantification of surface HLA-A,B,C protein expression of melanoma cell lines after treatment of NF at 10 μM, at least n = 3. All data are expressed as mean ± s.e.m. For **(A-D)**, data are analyzed using unpaired, two-tailed t-tests. For **(E)**, data are analyzed using multiple unpaired t-tests with the Holm-Šídák method. * $p < 0.05$, ** $p < 0.01$, *** $p < 0.001$, **** $p < 0.0001$.

Nelfinavir at 10 μM gave the largest effects in the melanoma cells, and surprisingly higher concentrations reduced this stimulation (Figure 2.3A). Similar effects to those of nelfinavir were observed with another HIV protease inhibitor, tipranavir (Brower et al., 2008; De Clercq, 2009), which increased both MHC-I and B2M levels in A375 cells (Figure 2.3B). However, several other retroviral protease inhibitors (atazanavir, ritonavir, indinavir, and lopinavir) (Brower et al., 2008; De Clercq, 2009) did not significantly raise MHC-I and B2M levels (Figure 2.3B). To learn if these divergent effects are due to differences in their abilities to inhibit DDI2, we tested whether these agents could reduce the protease activity of purified DDI2. Like nelfinavir, tipranavir at 50 μM inhibited the cleavage of a ubiquitylated fluorescent protein (Collins et al., 2022; Yip et al., 2020) (Figure 2.3B). By contrast, the HIV protease inhibitors that did not increase MHC-I and B2M significantly in cells, did not inhibit DDI2's enzymatic activity (Figure 2.3B). In fact, the relative abilities of these different agents to raise B2M and MHC-I levels in cells was proportional to their capacity to inhibit purified DDI2.

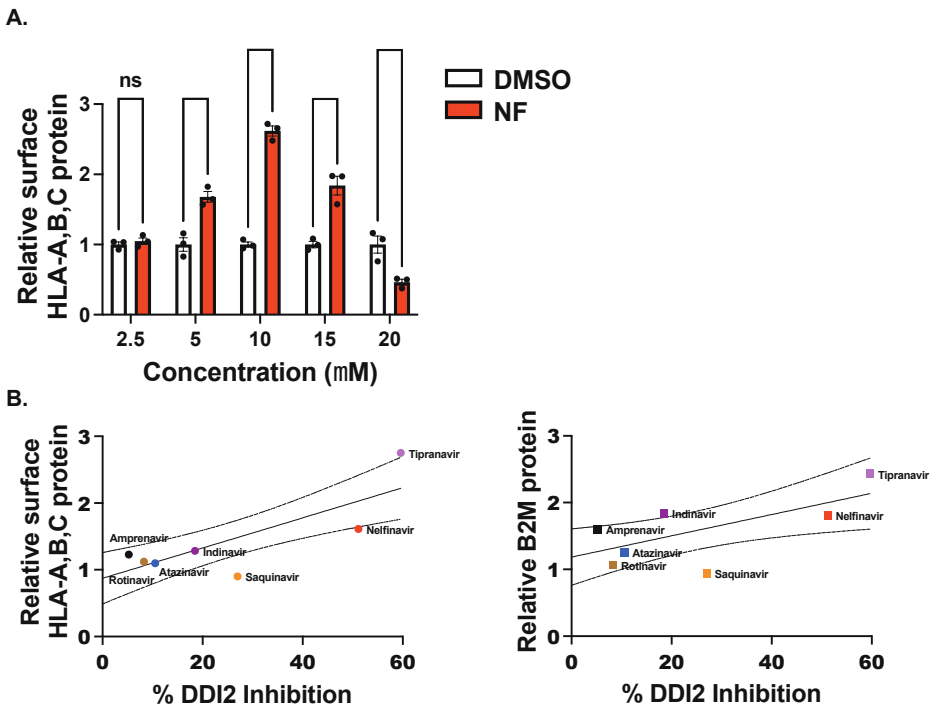

	Amprenavir	Rotinavir	Atazinavir	Indinavir	Saquinavir	Nelfinavir	Tipranavir
% DDI2 inhibition	5	8	11	18	27	51	60

Figure 2.3. **HIV-1 protease inhibitors inhibit DDI2 and enhance total B2M and MHC-I protein levels. (A)** Dose-response of nelfinavir (NF) in enhancing surface HLA-A, B, C protein expression in human melanoma cell line MEL624 treated for 72 hours with 10 μM NF or the vehicle DMSO; n = 3. Data are mean ± s.e.m. and analyzed using two-way ANOVA with Šídák's post-test. *** $p < 0.001$, **** $p < 0.0001$, ns indicates not statistically significant. **(B)** Correlation between the ability of different HIV-1 protease inhibitors to reduce DDI2 activity at 10 μM and their effects on levels of surface MHC-I complexes (left panel) or B2M (right panel) relative to the levels with vehicle control. To determine the degree of inhibition of purified DDI2 by different HIV-1 protease inhibitors (50 μM), we monitored the production of a short, fluorescent cleavage product of 150 nM Ub(n)NeR-sf-GFP by 150 nM DDI2, as described (Yip et al., 2020). To evaluate their effects on B2M or surface MHC-I molecules, human melanoma A375 cell line was treated with the HIV-1 protease inhibitors or vehicle DMSO at 10 μM for 24

Figure 2.3. (Continued)

hours. Relative B2M protein levels were determined by immunoblotting and normalized to GAPDH and DMSO. Relative surface HLA-A, B, C protein levels were quantified using flow cytometry and normalized to DMSO. Dashed lines represent 95 % confidence intervals of the linear regression.

2.2. Nelfinavir does not affect transcription or degradation of antigen precursors

To test how DDI2 inhibition can increase antigen presentation, we used the ovalbumin-derived antigenic peptide SIINFEKL, which binds to the mouse MHC H2 Kb class I complex and is specifically recognized by the 25-D1.16 antibody (Porgador et al., 1997). HEK293 cells with the H2 Kb gene integrated into the genome were transfected with the fluorescent antigenic precursor protein, Venus-SIINFEKL. We next employed a brief pulse of citric acid (pH 3) to strip preexistent surface MHC-I molecules from the surface (Sugawara et al., 1987) to achieve greater sensitivity in detecting any increase in antigen presentation by nelfinavir. By 18 hours after acid stripping, these cells had recovered about 100% of their initial levels of SIINFEKL antigen on surface MHC-I molecules (Figure 2.4A). However, the cells treated with nelfinavir presented at least 2-fold more SIINFEKL peptide on MHC-I molecules as measured with the 25-D1.16 antibody. This stimulation by nelfinavir of SIINFEKL presentation was evident by 14 hours (Figure 2.5) after the stripping and increased further during the subsequent two days (Figure 2.4A).

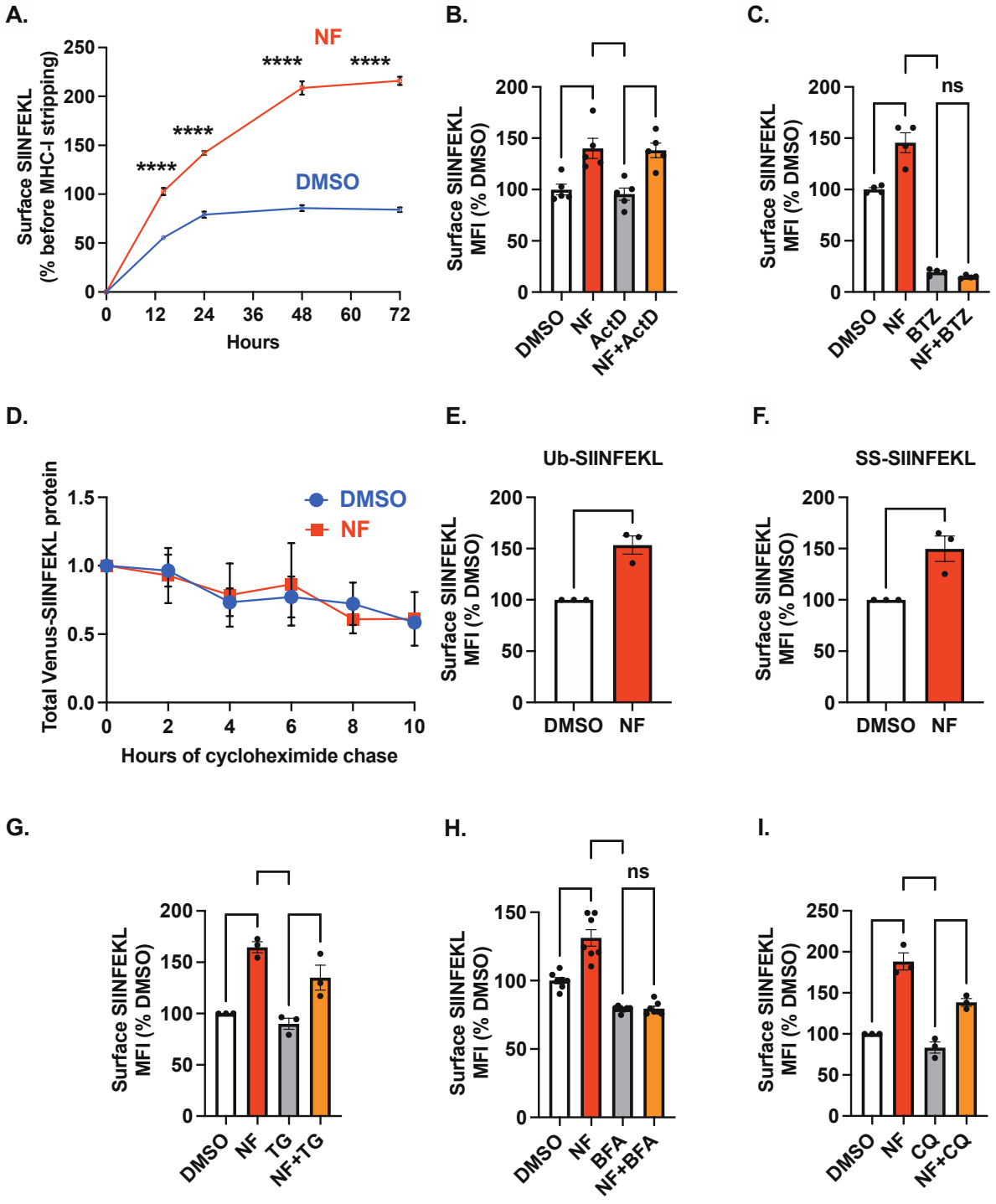

Figure 2.4. Nelfinavir increases presentation of the antigenic peptide, SIINFEKL, at a step after it enters the ER and before it reaches the cell surface. (A) Nelfinavir (NF) treatment increases the SIINFEKL peptide presentation on the cell surface from degradation of Venus-

Figure 2.4. (Continued)

SIINFEKL. The geometric mean fluorescent intensity (MFI) of the MHC-I-SIINFEKL complex was normalized to the levels of this complex before acid stripping (10 μM NF treatment or vehicle control); n = 4. **(B)** Preventing transcription by Actinomycin D (ActD) does not reduce the stimulation of SIINFEKL presentation by NF. MFI of surface MHC-I-SIINFEKL produced from Venus-SIINFEKL, relative to the vehicle control, after 10 hours of treatment (10 μM NF, 1 μg/mL ActD); n = 5. **(C)** Proteasome function is necessary to generate the SIINFEKL peptide from Venus-SIINFEKL even when cells were treated with NF. MFI of surface MHC-I-SIINFEKL, relative to the vehicle control, after 16 hours of treatment (10 μM NF, 0.5 μM bortezomib (BTZ)); n = 4. **(D)** NF treatment did not increase the degradation of Venus-SIINFEKL. Venus protein was measured by immunoblotting hours after adding 50 μg/mL cycloheximide; n = 4. **(E)** NF increases SIINFEKL presentation even if proteasome production of peptides is bypassed. MFI of surface MHC-I-SIINFEKL from N-terminal ubiquitin-fusion of SIINFEKL peptide, relative to the vehicle control, after 9 hours of treatment (10 μM NF); n = 3. **(F)** NF increases SIINFEKL presentation even if SIINFEKL is directly delivered to the ER through signal peptidase. MFI of surface MHC-I-SIINFEKL from N-terminal signal sequence (SS)-tagged SIINFEKL, relative to the vehicle control, after 9 hours of treatment (10 μM NF); n = 3. **(G)** Raising ER chaperones by treatment with thapsigargin (TG) did not increase the presentation of SIINFEKL. MFI of surface MHC-I-SIINFEKL from Venus-SIINFEKL, relative to the vehicle control, after 16 hours of treatment (10 μM NF, 0.25 μM TG); n = 3. **(H)** The increased presentation of SIINFEKL by nelfinavir does not occur by stabilization of surface MHC-I-peptide complexes. MFI of surface MHC-I-SIINFEKL from Venus-SIINFEKL, relative to the vehicle control, after 9 hours of treatment (10 μM NF, 5 μg/mL Brefeldin A (BFA)); n = 7.

Figure 2.4. (Continued)

(I) Inhibition of lysosomal function by chloroquine (CQ) treatment partially reduces the stimulation of SIINFEKL presentation by NF from Venus-SIINFEKL. MFI of surface MHC-I-SIINFEKL from Venus-SIINFEKL, relative to the vehicle control, after 18 hours of treatment (10 μM NF, 10 μM CQ); n = 3. All data are expressed as mean ± s.e.m. For **(A)** and **(D)**, data are analyzed using two-way ANOVA with Šídák's post-test. For **(B)**, **(C)**, **(G)**, **(H)**, and **(I)** data are analyzed by ordinary one-way ANOVA with Tukey's post hoc test. For **(E)** and **(F)**, data are analyzed using unpaired, two-tailed t-tests. * $p < 0.05$, ** $p < 0.01$, *** $p < 0.001$, **** $p < 0.0001$, ns indicates not statistically significant.

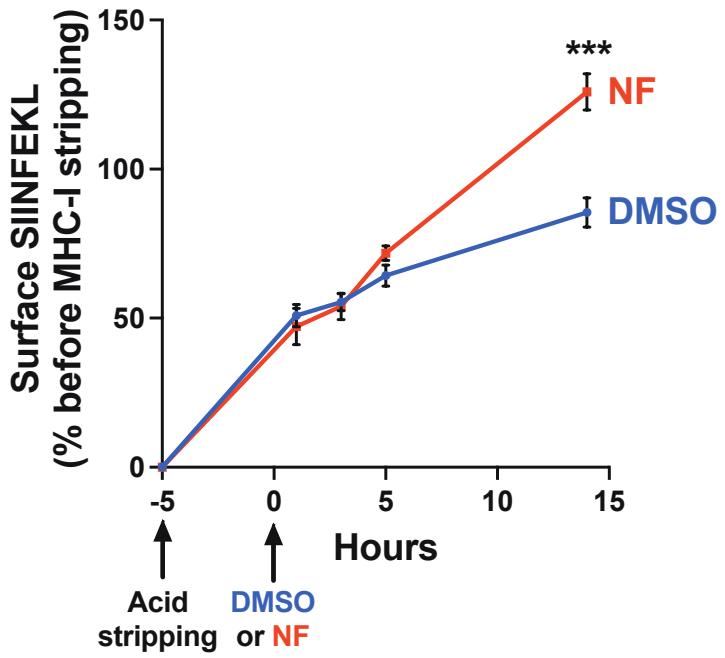

Figure 2.5. Nelfinavir treatment increases the SIINFEKL peptide presentation on the cell surface from degradation of Venus-SIINFEKL. The geometric mean fluorescent intensity (MFI) of the MHC-I-SIINFEKL complex was normalized to the levels of this complex before

Figure 2.5. (Continued)

acid stripping (10 μM NF treatment or vehicle control); n = 6. Data are mean ± s.e.m. and analyzed using two-way ANOVA with Šídák's post-test. *** $p < 0.001$.

Further studies attempted to determine how inhibition of DDI2 enhances the presentation of SIINFEKL (Figure 2.6). Because DDI2 is known to activate two transcription factors (Chowdhury et al., 2017; Sha & Goldberg, 2016), we tested whether the increase in SIINFEKL presentation with nelfinavir depends on new gene expression. Unlike IFN-γ, which increases the mRNAs for *B2M* and *HLA-A, B, C* genes (Heron et al., 1978), nelfinavir treatment did not increase levels of these transcripts (Figure 2.7A). Also, nelfinavir by itself did not induce the expression of IFN-γ (Figure 2.7B). Furthermore, when total transcription was blocked with Actinomycin D, nelfinavir still promoted SIINFEKL presentation from Venus-SIINFEKL (Figure 2.4B). Thus, nelfinavir does not require gene transcription to increase antigen presentation. The primary source of peptides for MHC-I assembly is the ubiquitin-proteasome pathway (Rock et al., 1994), which generates the SIINFEKL peptide from Venus-SIINFEKL by 26S proteasomes in the cytosol (Figure 2.6). As expected, blocking this pathway with the proteasome inhibitor bortezomib markedly reduced SIINFEKL presentation and prevented the stimulation by nelfinavir (Figure 2.4C). Because DDI2 helps deliver ubiquitylated proteins to 26S proteasomes for degradation (Collins et al., 2022), we tested whether nelfinavir enhanced the breakdown of the precursor protein Venus-SIINFEKL, which would generate more antigenic peptides that could be loaded onto MHC-I molecules. Venus-SIINFEKL has been reported to be a relatively stable protein and accordingly, there was only limited degradation of Venus-SIINFEKL after cells were incubated with cycloheximide to block protein synthesis (Figure

2.4D). More importantly, nelfinavir treatment did not significantly increase the degradation of Venus-SIINFEKL (Figure 2.4D). Thus, although the effects of nelfinavir require proteasome-mediated production of antigenic peptides, it does not increase antigen presentation by enhancing proteasomal degradation of precursor proteins.

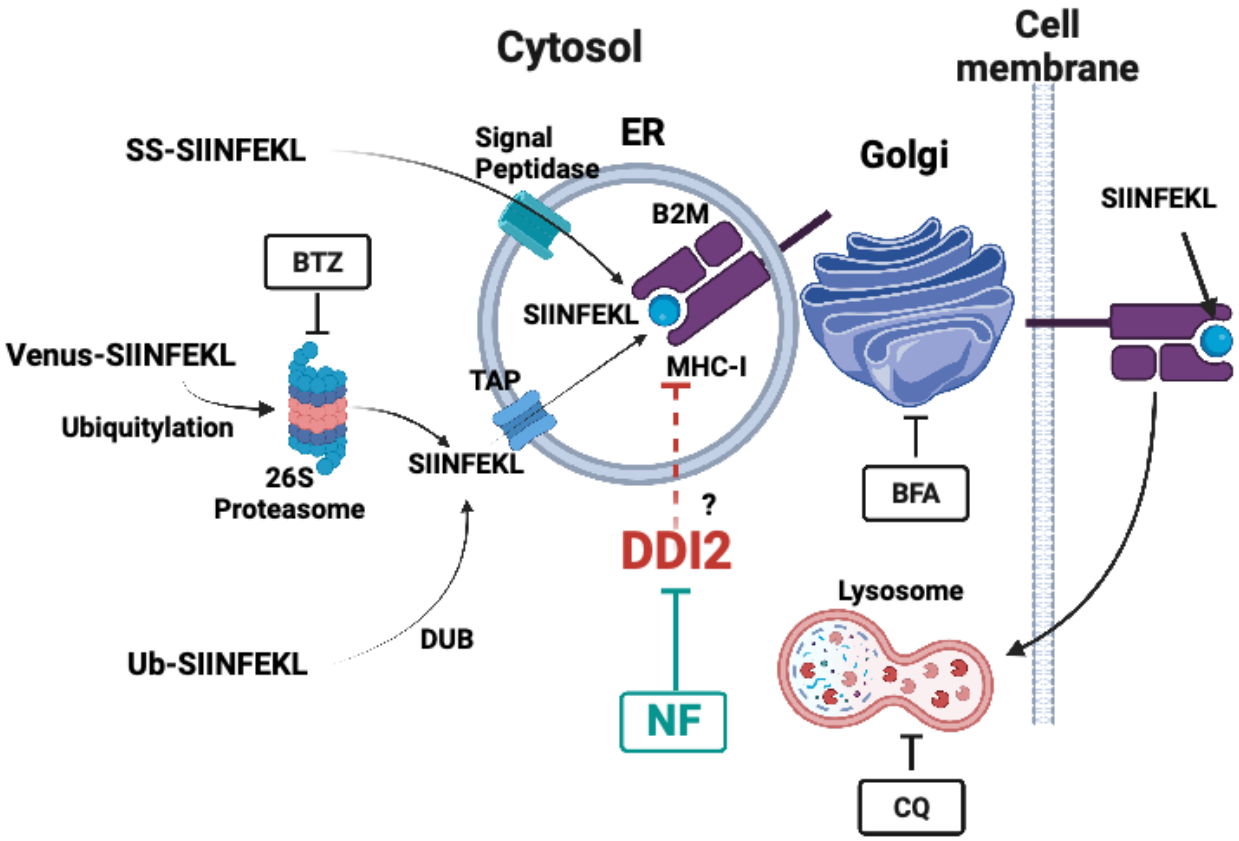

Figure 2.6. A diagram depicting different experimental precursors used here (Figure 2) to identify how DDI2 inhibition by nelfinavir (NF) affects the production of the antigenic peptide, SIINFEKL, its transport into the ER, and degradation of surface MHC-I-SIINFEKL complexes. SS-SIINFEKL is the precursor SIINKFEKL fused to a signal sequence, which is cleaved by the signal peptidase and directs its transport into the ER. Ub-SIINFEKL is the precursor SIINFEKL fused to ubiquitin's C-terminus. DUB represents a cytosolic de-

Figure 2.6. (Continued)

ubiquitylating enzyme. The ubiquitination reaction directs venus-SIINFEKL to the proteasome which releases the SIINKFEKL during the degradation of the precursor protein Venus-SIINFEKL. The SIINFEKL then is translocated into the ER through the TAP transporter. Bortezomib (BTZ) inhibits the proteasome. Brefeldin A (BFA) inhibits transport through the Golgi apparatus, and chloroquine (CQ) inhibits the acidification of endosomes and lysosomes, disrupting autophagy. The diagram was generated by BioRender.

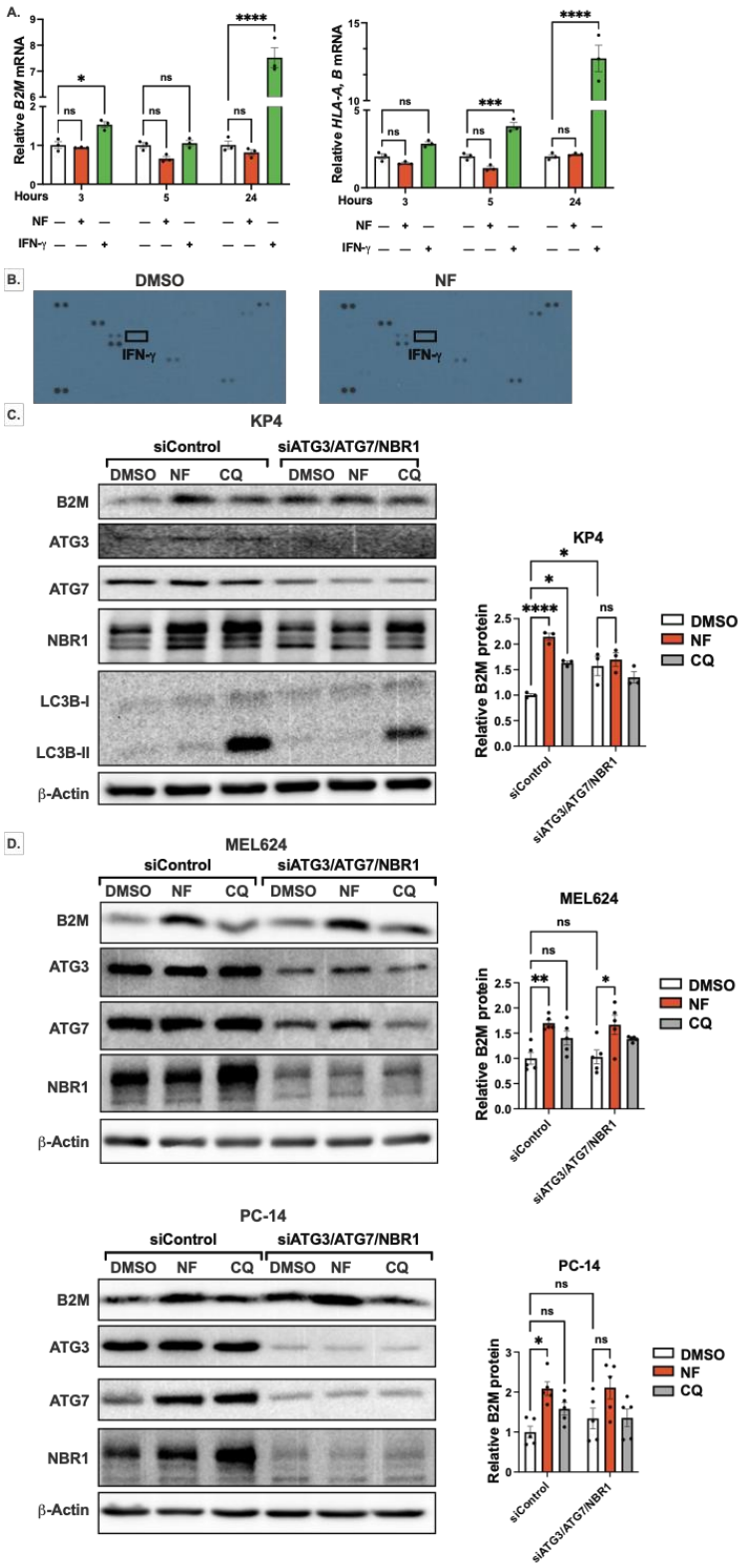

Figure 2.7. DDI2 inhibition does not increase B2M levels by enhancing transcription, induction of IFN-γ interferon, or inhibiting autophagy. **(A)** Nelfinavir (NF) does not induce

Figure 2.7. (Continued)

B2M mRNA expression (left panel) or HLA-A, B mRNA expression (right panel) determined by qRT-PCR in triplicates. **(B)** NF does not induce IFN-γ production. The experiments were performed by the Human XL Cytokine Array. A375 was treated with DMSO (left panel) and NF (10 μM) (right panel) for 24 hours. **(C-D)** Immunoblotting of proteins from human **(C)** pancreatic cell line KP4, **(D)** melanoma cell line MEL624 and lung adenocarcinoma cell line PC-14 that were transfected with either siControl or siRNAs against autophagy genes Atg3/Atg7/Nrb1 (1:1:1 ratio) for 24 hours before being treated with DMSO, NF (10 μM), or chloroquine (CQ) (10 μM) for an additional 24 hours. The left panels show the immunoblots and the right panels show the quantification of relative B2M protein expression normalized to β-actin and siControl/DMSO. All data are expressed as mean ± s.e.m. For **(A)**, data are analyzed using two-way ANOVA with Dunnett's post-test. For **(C)** and **(D)**, data are analyzed using two-way ANOVA with Tukey's post hoc test. * $p < 0.05$, ** $p < 0.01$, *** $p < 0.001$, **** $p < 0.0001$.

This conclusion was strongly supported in experiments where we bypassed antigenic peptide production by proteasomes and generated SIINFEKL in the cytosol by expressing SIINFEKL fused to ubiquitin's C-terminus (Ub-SIINFEKL). Deubiquitylating enzymes rapidly remove this ubiquitin moiety, producing free SIINFEKL in the cytosol (Fruci et al., 2003), which can serve as the precursor for the surface MHC-I complex. Nelfinavir still increased the presentation on the cell surface of SIINFEKL derived from Ub-SIINFEKL (Figure 2.4E), and thus it must stimulate a step after the antigenic peptides are produced.

2.3. Nelfinavir increases antigen presentation at a step within the ER

Like proteasome-derived peptides, the SIINFEKL derived from Ub-SIINFEKL requires the TAP1/2 complex on the ER membrane for transport into the ER and loading onto the MHC-I complex (Thomas & Tampé, 2019). To test if nelfinavir promotes the TAP-dependent step or the subsequent fate of the transported peptides, we expressed SIINFEKL fused to a signal sequence, SS-SIINFEKL, which directs its transport into the ER. As the signal peptidase complex delivers the SS-SIINFEKL into the ER (Hearn et al., 2009), the signal sequence is removed by the signal peptidase (Blobel & Dobberstein, 1975). Nelfinavir still enhanced the presentation on surface MHC-I of SIINFEKL after it had been delivered into the ER lumen (Figure 2.4F).

Nelfinavir and the inhibition of DDI2 have been reported to induce ER stress (Gills et al., 2007) and the unfolded protein response (UPR), which leads to the production of ER chaperones (*i.e.,* calnexin, calreticulin, and BiP), which help catalyze the assembly of the MHC-I complex by the antigen peptide-loading complex (Thomas & Tampé, 2019). We, therefore, tested if triggering the ER stress response and the resulting rise in ER chaperones might promote MHC-I presentation. The addition of thapsigargin, which induces ER stress by inhibiting the Ca^{2+} ATPases, did not increase SIINFEKL presentation and even seemed to reduce the stimulation by nelfinavir (Figure 2.4G). Furthermore, because the ER chaperones are induced in the UPR through gene transcription, and Actinomycin D did not blunt the effects of nelfinavir (Figure 2.4B), the induction of the UPR cannot explain nelfinavir's stimulation of antigen presentation.

Surface proteins like MHC-I molecules are continually being cleared by the endosomal-lysosomal pathway (Naslavsky et al., 2004). To test whether nelfinavir enhances the stability of surface MHC-I peptide complexes, we used Brefeldin A, which blocks the delivery of MHC-I molecules from the ER through the Golgi to the cell surface (Misumi et al., 1986). (In this

experiment, we did not strip MHC-I surface molecules with a brief acid wash as in previous experiments with SIINFEKL). Brefeldin A treatment slightly lowered surface MHC-I molecules within 9 hours and completely blocked the increase in MHC-I by nelfinavir (Figure 2.4H). However, in the brefeldin A-treated cells, nelfinavir did not stabilize MHC-I molecules already on the cell surface. Thus, nelfinavir stimulates antigen presentation not by increasing the production of peptides in the cytosol or by enhancing the stability of MHC-I-peptide complexes on the cell surface, but by stimulating a step in the ER (or perhaps the Golgi apparatus) after the loading of peptides onto the MHC-I molecules and before delivery of the complex to the surface membrane.

Recently, however, the degradation of surface MHC-I molecules was reported to restrict antigen presentation in PDAC cells, and the authors observed that the abundance of peptide-MHC-I complexes on the cell surface is determined by their rate of degradation in lysosomes (Yamamoto et al., 2020). We, therefore, tested further whether nelfinavir might increase surface MHC-I molecules by inhibiting lysosomal function, similar to the use of chloroquine, which was reported to enhance antigen presentation in PDAC cells (Yamamoto et al., 2020). Chloroquine treatment of HEK293 cells increased SIINFEKL presentation modestly, but much less than was seen with nelfinavir. Furthermore, the effects of nelfinavir in enhancing antigen presentation appeared to be blunted by chloroquine, suggesting separate pathways for these two compounds (Figure 2.4I). In PDAC KP4 cells, the increase in B2M levels with chloroquine was similar to that observed with nelfinavir (Figure 2.7C). Furthermore, knocking down the key autophagy genes – ATG3, ATG7, and NBR1 – with siRNA increased B2M to a similar extent as nelfinavir treatment (Figure 2.7C). However, when melanoma MEL624 cells or lung adenocarcinoma PC-14 cells were treated with chloroquine or when key autophagy genes (ATG3, ATG7, and NBR1)

were knocked down, the resulting increases in B2M levels were lower than upon nelfinavir treatment (Figure 2.7D). These observations confirm that peptides generated by lysosomal proteolysis are not important precursors of the increase in antigenic peptides by nelfinavir. More importantly, they indicate the existence of two distinct pathways affecting surface MHC-I complexes: the endosomal-lysosomal pathway, which is independent of DDI2 and seems particularly important in PDAC cells (Yamamoto et al., 2020), and a DDI2-dependent process probably present in all antigen-presenting cells, which restrains the delivery of the peptide-loaded complexes to the cell surface.

CHAPTER 3. DDI2 INHIBITION ENHANCES T CELL CYTOTOXICITY *IN VITRO* AND THE EFFICACY OF IMMUNE CHECKPOINT BLOCKADE *IN VIVO*

This chapter is adapted from the manuscript (in preparation for submission):

Nhu T. Nguyen*, Galen Andrew Collins*, Inbal Rachmin*, Jennifer Allouche*, Sachiko T. Homma, Abdulla Al Emran, Shanivi Srikonda, Max von Franque, Shailbala Singh, Chuan Yan, Kristina Todorova, Tal H. Erlich, Yi Sun, Hongyan Xie, Abigail Scharf, Oriah Jeselsohn, Christopher Ott, Anna Mandinova, Russell Jenkins, David Langenau, F. Stephen Hodi, Cassian Yee, Alfred L. Goldberg# and David E. Fisher# . DDI2 inhibition promotes MHC-I antigen presentation and tumor immunotherapy.

*Contributed equally

#Contributed equally (corresponding authors)

3.1. DDI2 inhibition in cancers enhances cytotoxicity of CD8$^+$ T cells

Further studies tested whether the increase in antigen presentation on MHC-I could trigger greater activation of CD8$^+$ T cells, as suggested by prior studies (Burr et al., 2019; Dhatchinamoorthy et al., 2021; Yamamoto et al., 2020) We pre-treated three human melanoma cell lines with nelfinavir or the vehicle DMSO for 72 hours prior to incubation with HLA-A2-restricted CD8$^+$ T cells specific for melanocyte antigen, gp100 (Yee et al., 2002). Nelfinavir treatment enhanced CD8$^+$ T cell activation in all three cell lines as measured by IFN-γ production (Figure 3.1A). Similarly, when we incubated pancreatic adenocarcinoma cells (BX-PC-3) with nelfinavir and then exposed them to CD8$^+$ T cells specific for the Vestigial-like 1 antigen expressed in many pancreatic tumors (Bradley et al., 2020), increased IFN-γ secretion was observed (Figure 3.1B). Also, upon incubation of two different *DDI2* knockout clones of MEL624 with gp100-specific CD8$^+$ T cells, IFN-γ production was significantly increased (Figure 3.1C). Thus, the loss of DDI2 activity in the cancer cells enhanced T cell activation.

These findings would predict that nelfinavir treatment should enhance the susceptibility of the cancer cells to killing by the cytotoxic T cells. Cytotoxicity, as assayed by the percentage of cells undergoing apoptosis (caspase activation), was markedly increased in melanoma lines A375 and MEL624 after treatment with nelfinavir for 3 days (Figure 3.1D). These *in vitro* studies together indicate that increased antigen presentation by DDI2 inhibition promotes $CD8^+$ T-lymphocyte activation and killing of cancer cells.

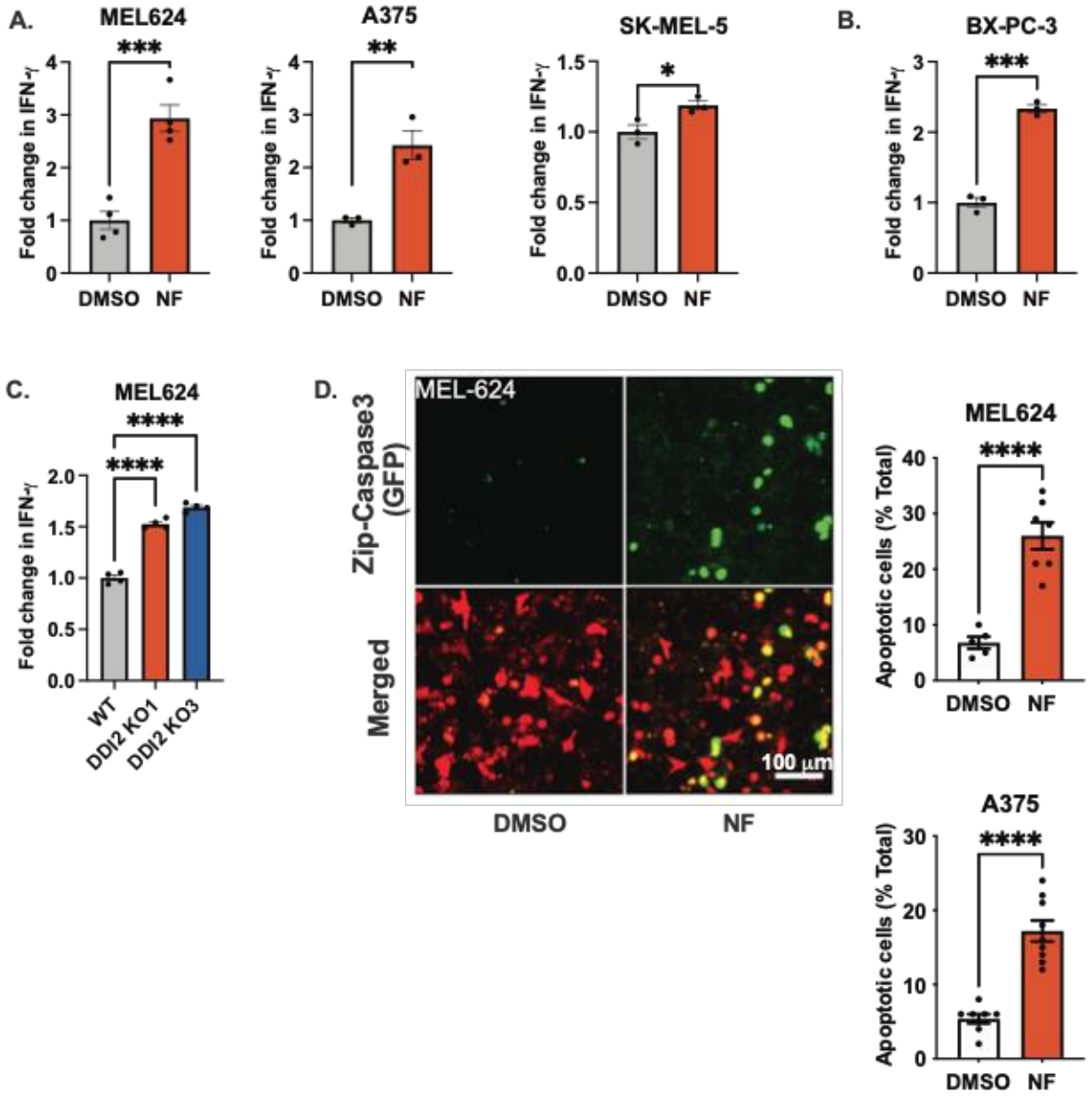

Figure 3.1. DDI2 inhibition increases the activation of CD8$^+$ T cells *in vitro*. (A) IFN-γ secretion by human gp-100 CD8$^+$ T cells after incubation with nelfinavir (NF)-treated relative to DMSO-treated melanoma cell lines A375, MEL624, and SK-MEL-5; at least n = 3. **(B)** IFN-γ secretion by human VGLL-1 CD8$^+$ T cells after incubation NF-treated relative to DMSO-treated human pancreatic cancer cell line BX-PC-3; n = 3. **(C)** IFN-γ secretion by human gp-100 CD8$^+$ T cells after incubation with melanoma MEL624 DDI2 WT or 2 different clones of *DDI2*$^{-/-}$

Figure 3.1. (Continued)

(DDI2 KO1 and DDI2 KO3), normalized to DDI2 WT; n = 4. **(D)** Representation of confocal image of melanoma cell line MEL624 transfected with GFP-tdTomato-Zip-Caspase3 plasmid treated with 10 μM NF or DMSO, followed by incubation with gp-100 $CD8^+$ T cells. Melanoma cells are red, apoptotic melanoma cells are green, and merged images are yellow; scale bar 100 μm. The graph shows the quantification of the percentage of apoptotic melanoma cells (GFP^+) from the total transfected melanoma cells MEL624 or A375 ($tdTomato^+$) with NF treatment relative to DMSO control treatment; scale bar 100 μm. All data are expressed as mean ± s.e.m. For **(A)**, **(B)**, and **(D)**, data are analyzed using unpaired, two-tailed t-tests. For **(C)**, data are analyzed using ordinary one-way ANOVA with Dunnett's post-test. * $p < 0.05$, ** $p < 0.01$, *** $p < 0.001$, **** $p < 0.0001$.

3.2. DDI2 inhibition by nelfinavir promotes anti-tumor immunity in mice

To determine if inhibition of DDI2 might also enhance anti-tumor immunity *in vivo*, we studied PDAC KPC and melanoma UV3 cell lines, two transplantable syngeneic murine tumors that also showed induction of B2M *in vitro* (Figure 3.2A). The KPC or UV3 cells were inoculated subcutaneously into C57BL/6 mice, which were immediately administered nelfinavir or vehicle daily for 21 days. When the transplanted tumors reached 50-100 cubic millimeters (around 7 days), the animals were then injected intraperitoneally with three doses of anti-PD-1 monoclonal antibody or isotype-matched control antibody (Figure 3.3A). By itself, the nelfinavir treatment increased the levels of B2M (Figure 3.3B) and the presence of invading $CD8^+$ T-lymphocytes in both types of tumors (Figure 3.3C). With both cancer lines, the mice treated with the combination of nelfinavir and anti-PD-1 showed decreased tumor mass and significantly

increased survival relative to those receiving only the immune checkpoint inhibitor (Figure 3.2B, Figure 3.3D-E). By itself, nelfinavir treatment had no effect on survival but appeared to slightly reduce tumor growth rates (as had been reported previously for small-cell lung cancers) (Kawabata et al., 2021). Importantly, *B2M*-deleted UV3 melanoma cells, which we generated via CRISPR/Cas9, were refractory to the combined nelfinavir and anti-PD-1 treatments (Figure 3.2B, Figure 3.3E), confirming that antigen presentation on MHC-I was necessary for the enhanced tumor rejection.

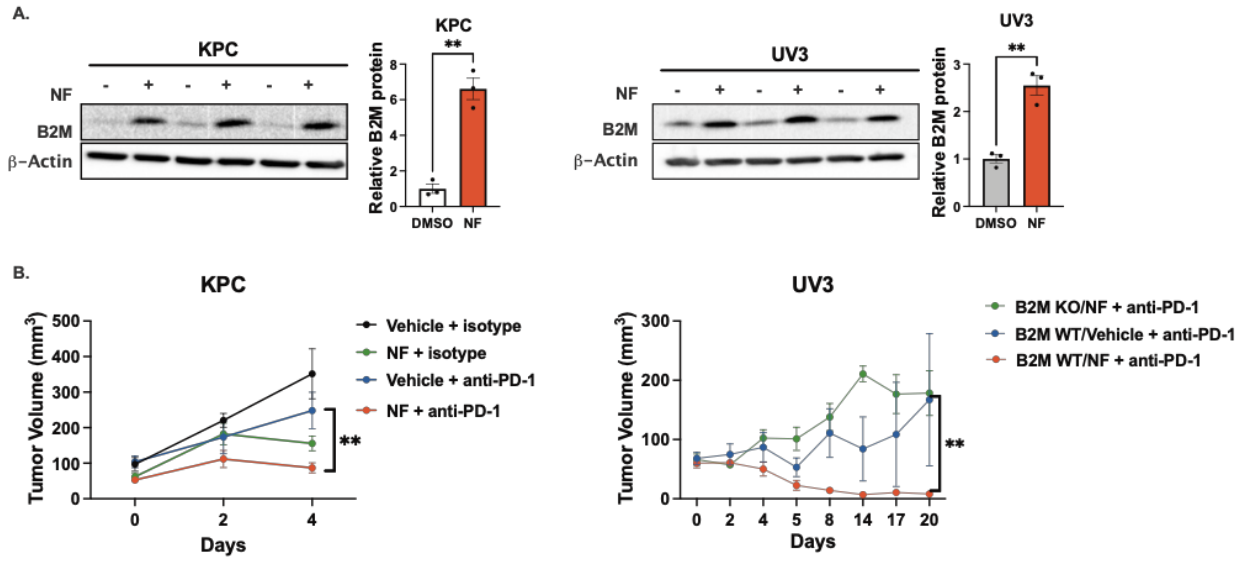

Figure 3.2. Nelfinavir treatment enhances the anti-tumor effects of anti-PD-1 antibodies in implantable mouse tumor models. (A) Murine pancreatic ductal adenocarcinoma cell line KPC and melanoma UV3 with 10 mM nelfinavir (NF) treatment or DMSO control *in vitro*. The left panels show representative immunoblots, and the right panels show quantification of B2M protein expression normalized to b-actin and DMSO; n = 3. Data are mean ± s.e.m. and analyzed using unpaired, two-tailed t-tests. **(B)** The left panel shows average tumor growth of C57BL/6

Figure 3.2. (Continued)

mice inoculated with pancreatic cancer KPC cells and treated with vehicle + isotype-matched antibody, vehicle + anti-PD-1, NF + isotype-matched antibody, or NF + anti-PD-1; n = 6. The right panel shows the average tumor growth of C57BL/6 mice inoculated with melanoma UV3 cells, which were either with *B2m*$^{+/+}$(B2M WT) or *B2m*$^{-/-}$ (B2M KO), treated with vehicle + anti-PD-1 or NF + anti-PD-1; at least n = 7. Data are mean ± s.e.m. and analyzed using two-way ANOVA with Tukey's post hoc test. ** $p < 0.01$, *** $p < 0.001$.

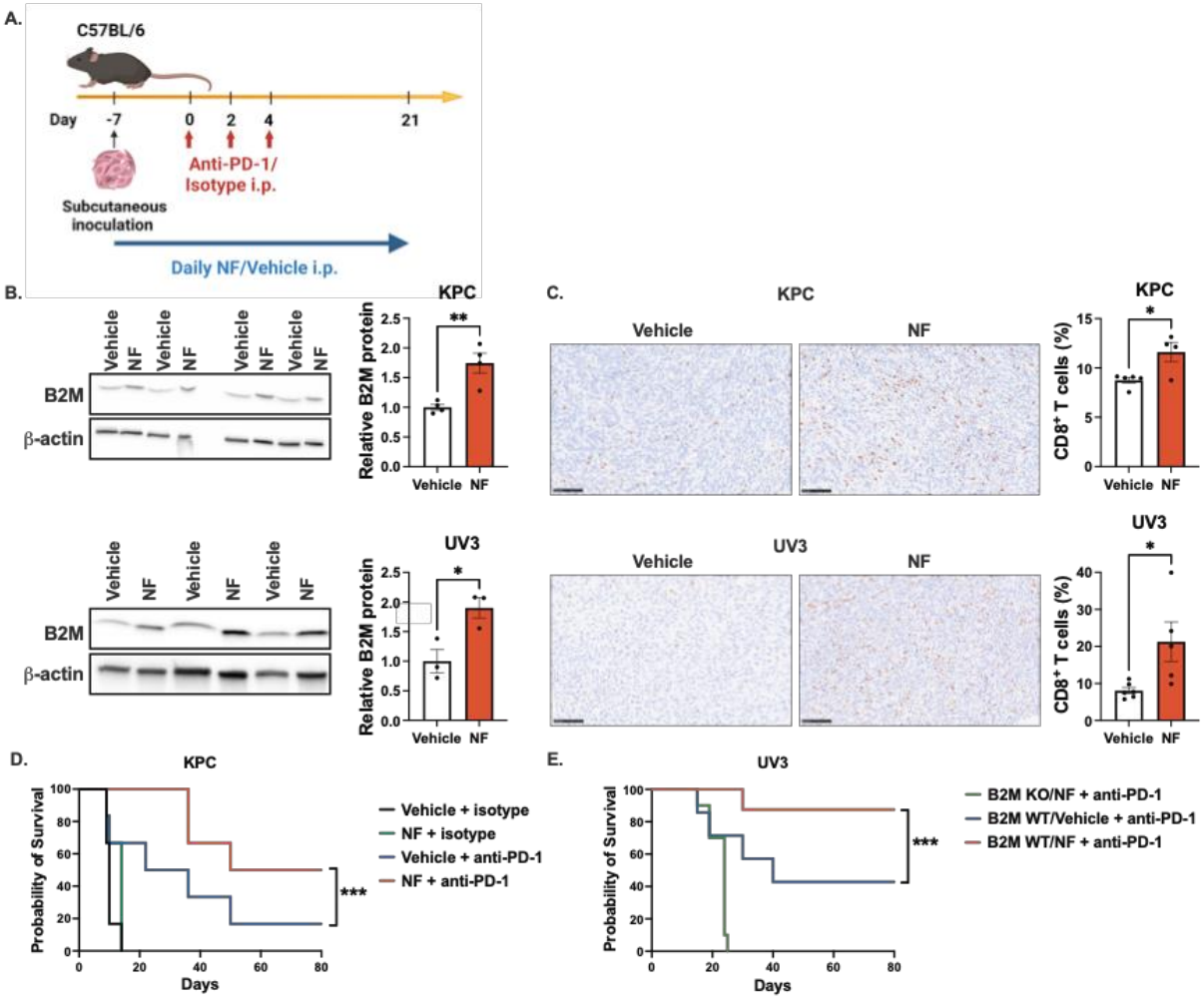

Figure 3.3. Nelfinavir promotes the anti-tumor effects of anti-PD-1 treatment. (A) Schematic representation for the treatment in C57BL/6 mice following subcutaneous inoculation with murine cancer cells. Nelfinavir (NF) and anti-PD-1 antibody were administered intraperitoneally at 100 mg/kg and 10 mg/kg, respectively. **(B)** Immunoblots with quantification of B2M protein expression from KPC tumors (top panel; n = 4) or UV3 tumors (bottom panel; n = 3) harvested from mice treated with NF or vehicle. Quantifications of B2M levels are normalized to β-actin and vehicle. **(C)** Immunohistology stain for KPC (top panel) or UV3 (bottom panel) tumor-infiltrating $CD8^+$ lymphocytes from tumors harvested from mice treated with NF or vehicle; at least n = 4, scale car 100 μm. **(D)** Survival of C57BL/6 mice inoculated

Figure 3.3. (Continued)

with pancreatic cancer KPC cells and treated with vehicle + isotype-matched antibody, NF + isotype-matched antibody, vehicle + anti-PD-1, and NF + anti-PD-1; n = 6. **(E)** Survival of C57BL/6 mice inoculated with melanoma UV3 cells (B2M WT or B2M KO) and treated with vehicle + anti-PD-1 and NF + anti-PD-1; at least n = 7. All data are expressed as mean ± s.e.m. For **(B)** and **(C)**, data are analyzed using unpaired, two-tailed t-tests. For **(D)** and **(E)**, data are analyzed using log-rank tests. * $p < 0.05$, ** $p < 0.01$, *** $p < 0.001$.

3.3. *DDI2* levels correlate inversely with activated $CD8^+$ T cell signature mRNA

To test if these findings *in vitro* and in mouse models are relevant to human cancers, we hypothesized that as an antagonist of MHC-I antigen presentation, *DDI2* levels might inversely correlate with tumor T-cell infiltration. We analyzed mRNA expression levels in tumor samples from a large number of patients bearing thirty different solid cancers (The Cancer Genome Atlas) (Ru et al., 2019). Activated $CD8^+$ T-cell-related gene signatures (Table 3.4A) were examined as previously described (Charoentong et al., 2017). In 24 out of a total of 30 solid tumor types, the presence of activated $CD8^+$ T signatures correlated inversely with the levels of *DDI2* expression (most often with $p < 0.0001$) (Table 3.5, Figure 3.6). Among these 24 are many of the most common human malignancies. Activated B cell signatures (Figure 3.7, Table 3.4 B) and activated dendritic cell signatures (Figure 3.8, Table 3.4C) showed no consistent correlations with *DDI2* levels in the same 30 cancer types. The inverse correlations between activated $CD8^+$ T cell signatures and *DDI2* expression are consistent with the hypothesis that in a large fraction of human tumors, DDI2 activity may limit immune rejection, presumably by reducing antigen presentation.

Table 3.4. List of genes comprising (A) activated CD8$^+$ T-cell immune signatures, (B) activated B-cell immune signatures, and (C) activated dendritic cell immune signatures as described previously (Charoentong et al., 2017).

A

Activated CD8$^+$ T-cell immune gene signature
ADRM1
AHSA1
C1GALT1C1
CCT6B
CD37
CD3D
CD3E
CD3G
CD69
CD8A
CETN3
CSE1L
GEMIN6
GNLY
GPT2
GZMA
GZMH
GZMK
IL2RB
LCK
MPZL1
NKG7
PIK3IP1
PTRH2
TIMM13
ZAP70

B

Activated B-cell immune gene signature
ADAM28
CD180
CD79B
BLK
CD19
MS4A1
TNFRSF17
IGHM
GNG7
MICAL3
SPIB
HLA-DOB
IGKC
PNOC
FCRL2
BACH2
CR2
TCL1A
AKNA
ARHGAP25
CCL21
CD27
CD38
CLEC17A
CLEC9A
CLECL1

C

Activated dendritic cell immune gene signature
ABCD1
C1QC
CAPG
CCL3L3
CD207
CD302
ATP5B
ATP5L
ATP6V1A
BCL2L1
C1QB
SNURF
SPCS3
CCNA1
CEACAM8
NOS2
SRA1
TNFRSF6B
TREM1
TREML1
RHOA
SLC25A37
TNFSF14
TREML4
VNN2
XPO6
CLEC4C
TNFAIP2
UBD

Table 3.5. *DDI2* levels correlate inversely with activated CD8$^+$ T cell mRNA signatures in many patient solid tumor types. For each tumor type, sample size (N), correlation coefficient (r) representing the relationship between *DDI2* levels and activated CD8$^+$ T-cell related gene signatures (Table 3.4A), and p-value are shown. All the results from a total of 30 tumor types in this table are based upon data generated by The Cancer Genome Atlas (TCGA) Research Network: https://www.cancer.gov/tcga. Correlation analyses were performed by spearman correlation coefficient and p values were calculated by two-tailed t-test.

Patient tumor type	Sample size (N)	Correlation coefficient (r)	p-value
Liver hepatocellular carcinoma (LIHC)	373	-0.449	<0.0001
Thyroid carcinoma (THCA)	509	-0.394	<0.0001
Adrenocortical carcinoma (ACC)	89	-0.393	0.0003
Prostate adenocarcinoma (PRAD)	498	-0.384	<0.0001
Uterine Carcinosarcoma (UCS)	57	-0.364	0.0054
Kidney renal clear cell carcinoma (KIRC)	534	-0.362	<0.0001
Kidney renal papillary cell carcinoma (KIRP)	291	-0.332	<0.0001
Bladder urothelial carcinoma (BLCA)	408	-0.329	<0.0001
Pheochromocytoma and Paraganglioma (PCPG)	184	-0.328	<0.0001
Glioblastoma multiforme (GBM)	166	-0.322	<0.0001
Cervical and endocervical cancers (CESC)	309	-0.309	<0.0001
Uterine corpus endometrial carcinoma (UCEC)	546	-0.305	<0.0001
Breast invasive carcinoma (BRCA)	1100	-0.302	<0.0001
Esophageal carcinoma (ESCA)	185	-0.297	<0.0001
Testicular germ cell tumors (TGCT)	156	-0.277	0.0005
Lower grade glioma (Brain) (LGG)	530	-0.266	<0.0001
Lung adenocarcinoma (LUAD)	517	-0.262	<0.0001
Lung squamous cell carcinoma (LUSC)	501	-0.261	<0.0001
Sarcoma (SARC)	266	-0.261	<0.0001
Rectum adenocarcinoma (READ)	167	-0.243	0.0016
Head and neck squamous cell carcinoma (HNSC)	522	-0.240	<0.0001
Stomach adenocarcinoma (STAD)	415	-0.214	<0.0001
Skin cutaneous melanoma (SKCM)	472	-0.202	<0.0001
Ovarian serous cystadenocarcinoma (OV)	307	-0.173	0.0024
Kidney chromophobe (KICH)	66	-0.217	0.0807
Colon adenocarcinoma (COAD)	459	-0.073	0.1201
Mesothelioma (MESO)	1100	-0.146	0.1772
Cholangiocarcinoma (CHOL)	36	-0.201	0.2397
Pancreatic adenocarcinoma (PAAD)	179	-0.034	0.6533
Uveal melanoma (UVM)	80	-0.009	0.9368

Figure 3.6. *DDI2* levels correlate inversely with activated CD8$^+$ T cell mRNA signatures in the great majority (80%) of patient solid tumor types. Scatter plots show the correlation between *DDI2* levels and activated CD8$^+$ T-cell-related gene signatures (Table 3.4A) of 30 patient solid tumor types (refer to Table 3.5). Correlation analyses given for each cancer type were performed using the spearman correlation coefficient and p values were calculated by two-tailed t-tests.

Figure 3.6. (Continued)

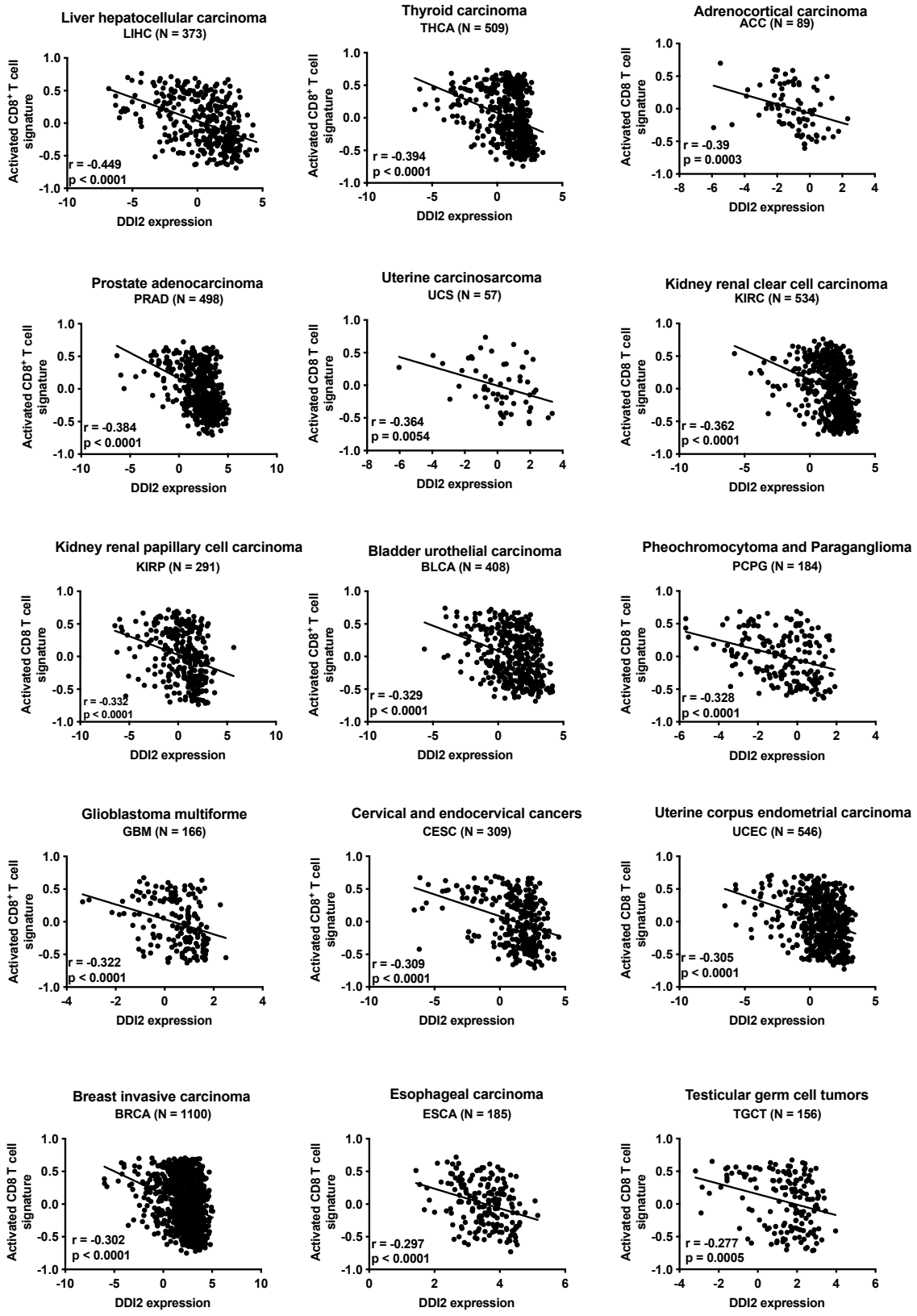

Figure 3.6. (Continued)

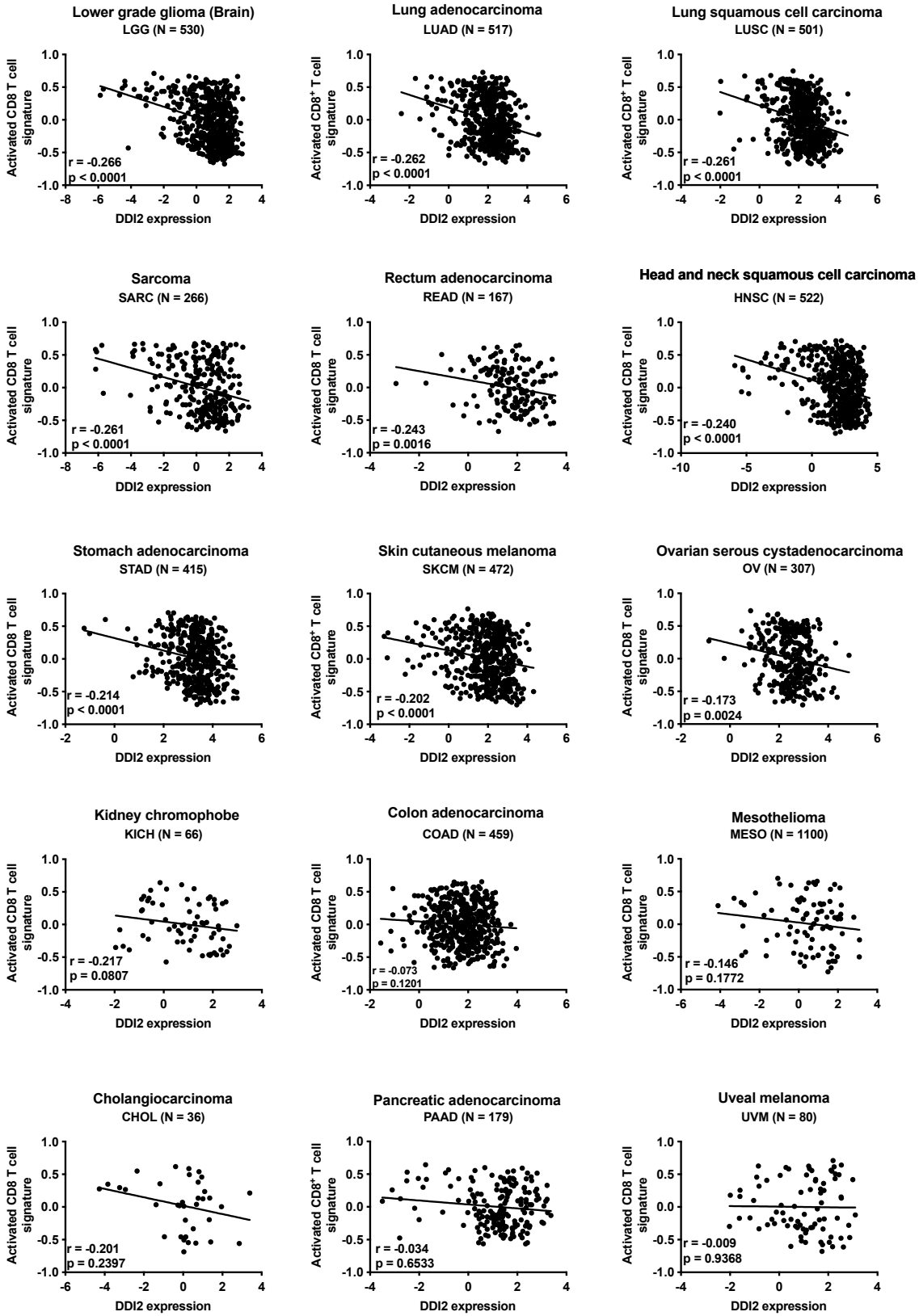

Figure 3.7. *DDI2* levels do not correlate with activated B cell mRNA signatures in multiple patient solid tumor types. Scatter plots show the relationship between *DDI2* levels and activated B-cell-related gene signatures (Table 3.4B) of 30 patient solid tumor types. Correlation analyses given for each cancer type were performed using the spearman correlation coefficient and p values were calculated by two-tailed t-tests.

Figure 3.7. (Continued)

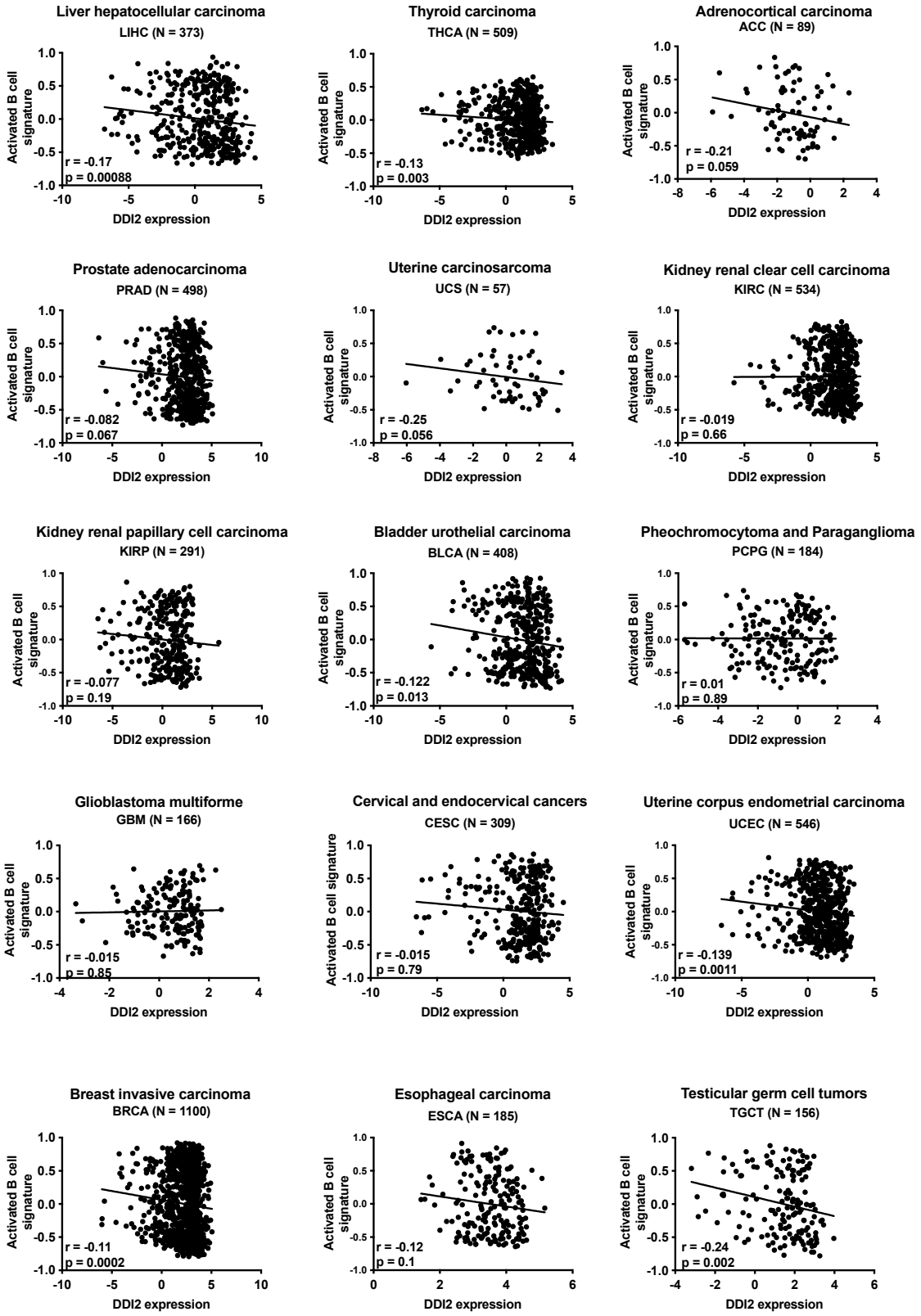

Figure 3.7. (Continued)

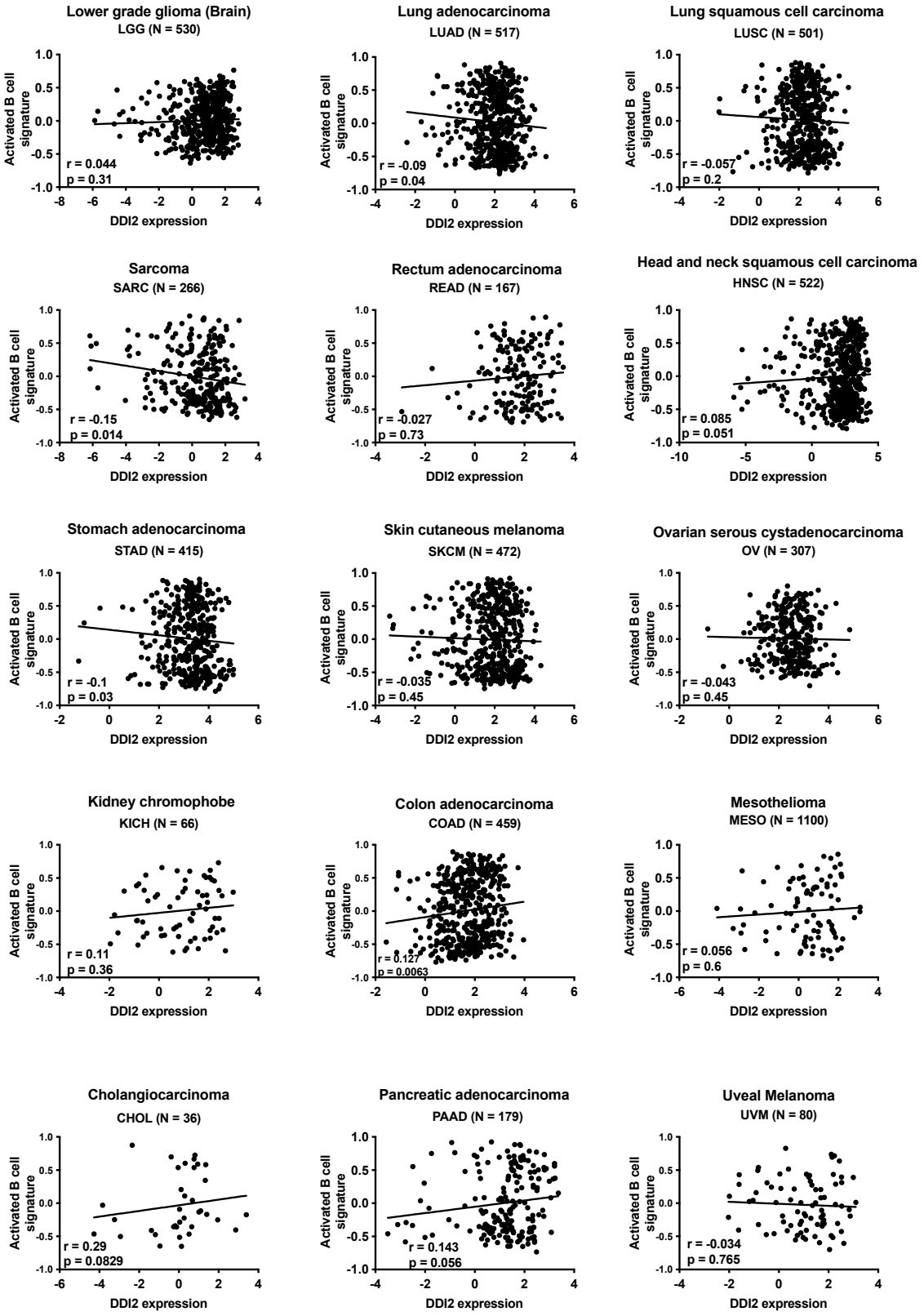

Figure 3.8. *DDI2* levels do not correlate with activated dendritic cell mRNA signatures in multiple patient solid tumor types. Scatter plots show the relationship between *DDI2* levels and activated dendritic cell-related gene signatures (Table 3.4C) of 30 patient solid tumor types. Correlation analyses given for each cancer type were performed using the spearman correlation coefficient and p values were calculated by two-tailed t-tests.

Figure 3.8. (Continued)

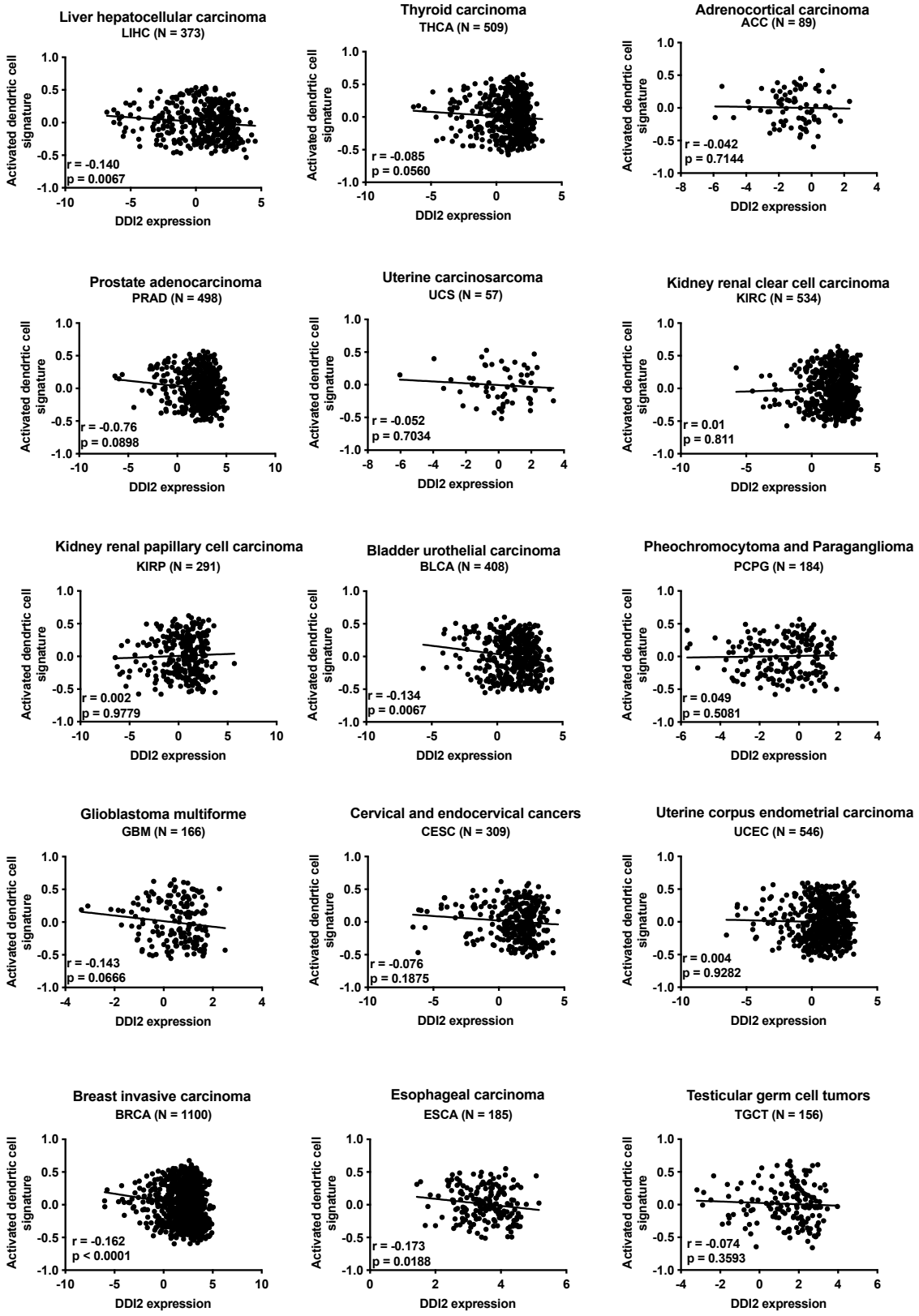

Figure 3.8. (Continued)

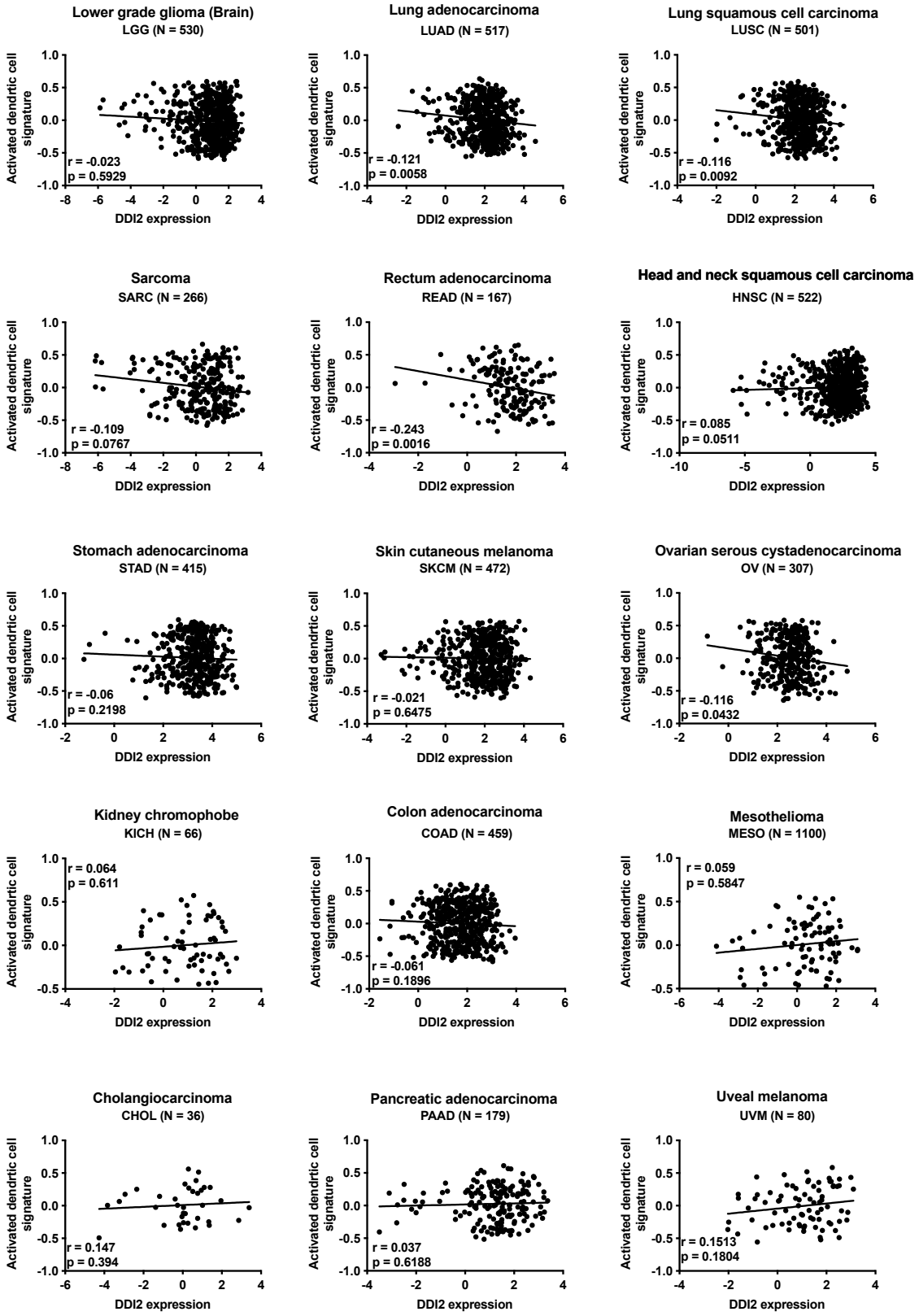

CHAPTER 4. CURRENT WORK IN PROGRESS AND FUTURE DIRECTIONS

4.1. Designing and screening for novel DDI2 inhibitors to enhance the efficacy of immune checkpoint blockade

4.1.1. Preliminary data

Nelfinavir and tipranavir, though approved drugs, were developed as inhibitors of the related HIV-1 protease and not DDI2. In particular, for nelfinavir, surface MHC-I levels begin to decrease at concentrations greater than 10 μM (Figure 2.3A), potentially due to its toxicity. These non-specific actions of nelfinavir at high concentrations can be viewed as undesirable, although they possibly contribute to tumor growth inhibition. These drugs' modest potency could pose a challenge in achieving active exposure clinically (Eke et al., 2019; Herforth et al., 2002; Marzolini et al., 2001). Therefore, developing more specific and potent inhibitors of DDI2 represents an attractive approach to enhance antigen presentation and immune checkpoint blockade therapy.

Our lab has collaborated with the Namchuk group at Harvard Medical School to seek potential replacements for nelfinavir and tipranavir as DDI2 inhibitors. By performing in silico strategies, Namchuk group designed thirty-six molecules as new candidate inhibitors against DDI2. We then performed an assay to assess their cell toxicity in the human melanoma cell line MEL624 after their incubation of 72 hours and at three different concentrations (10, 20, and 50 μM) (Figure 4.1). Among these compounds, A2, D1, and F3 led to a reduction in cell viability at 50 μM, while B5 was toxic at all tested concentrations. Next, we evaluated their ability to induce surface MHC-I and total B2M protein expression in MEL624 using nelfinavir as the positive control. From a pilot experiment, we selected five compounds that significantly induced surface MHC-I levels at any concentration tested (Figure 4.2A). Compound D1 also increased total B2M

protein expression 2-fold (Figure 4.2B) and showed comparable activity to nelfinavir in inhibiting DDI2 (Figure 4.3). Follow-up of other active analogs (e.g. A4) is ongoing.

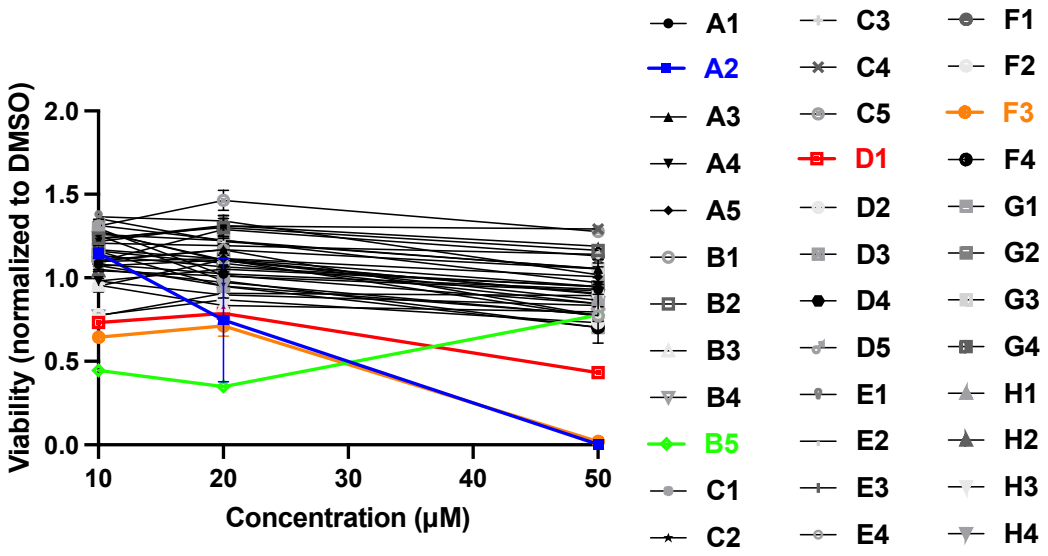

Figure 4.1. The impact of thirty-six compounds at different concentrations on cell viability of human melanoma MEL624. The cell line MEL624 was treated with thirty-six compounds (Table 4.1) at three concentrations: 10, 20, and 50 μM for 72 hours. Cell viability was determined using the CellTiter-Glo Cell Viability Assay, according to the manufacturer's instructions. Cell viability from the treatment groups was normalized to their DMSO control group at their matched concentration. Compounds in black have comparable cell viability to DMSO, while compounds in colors other than black decrease cell viability to some degree.

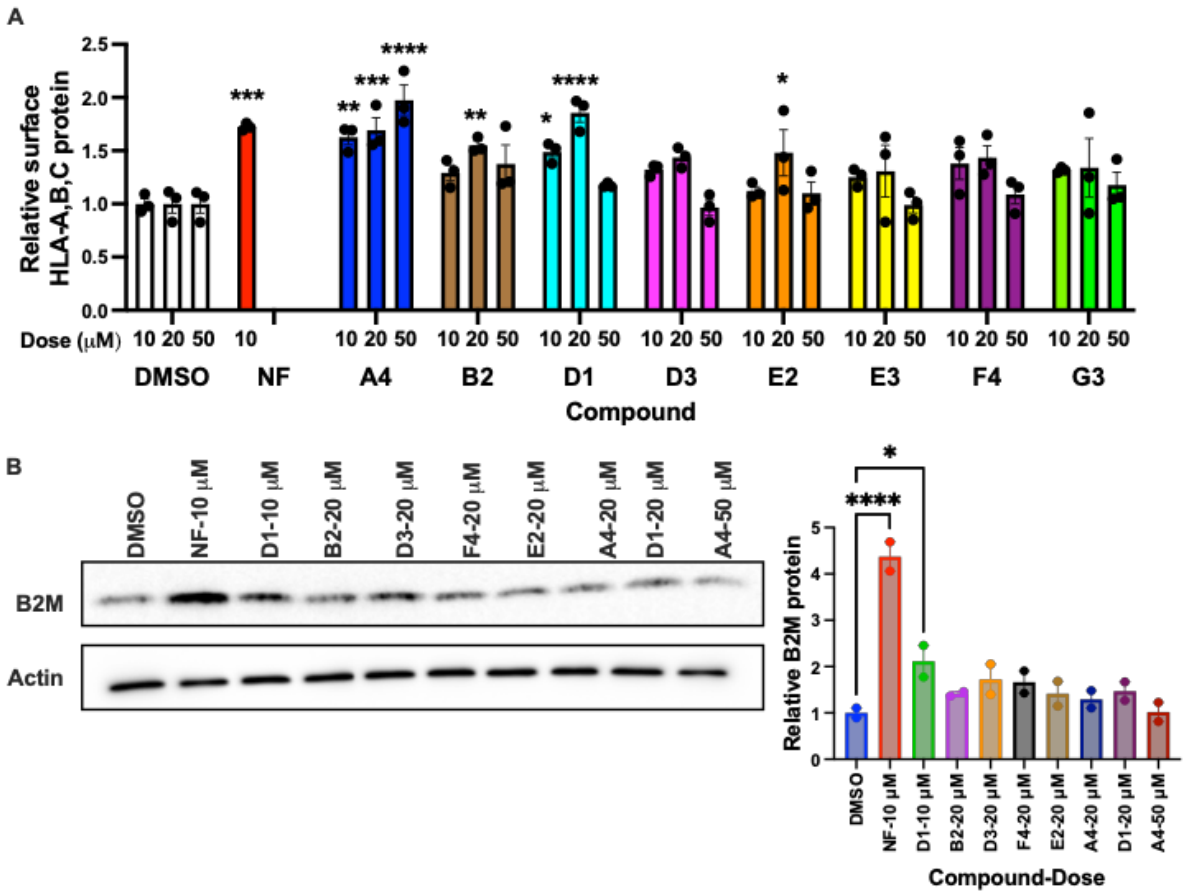

Figure 4.2. Preliminary data from screening thirty-six compounds for induction of surface MHC-I and total B2M levels in MEL624. (A) Flow cytometry-based quantification of surface HLA-A,B,C protein expression of the melanoma cell line MEL624 after treatment of nelfinavir (NF) or other compounds at indicated concentrations; n = 3. All data are expressed as mean ± s.e.m. and are analyzed using two-way ANOVA with Dunnett's method in comparison with the DMSO control group. **(B)** Total B2M protein levels of MEL624 after treatment with NF or other compounds at indicated concentrations; n = 3. The left panel shows a representative immunoblot, and the right panel shows quantification of B2M protein expression normalized to β-actin and DMSO. * $p < 0.05$, ** $p < 0.01$, *** $p < 0.001$, **** $p < 0.0001$.

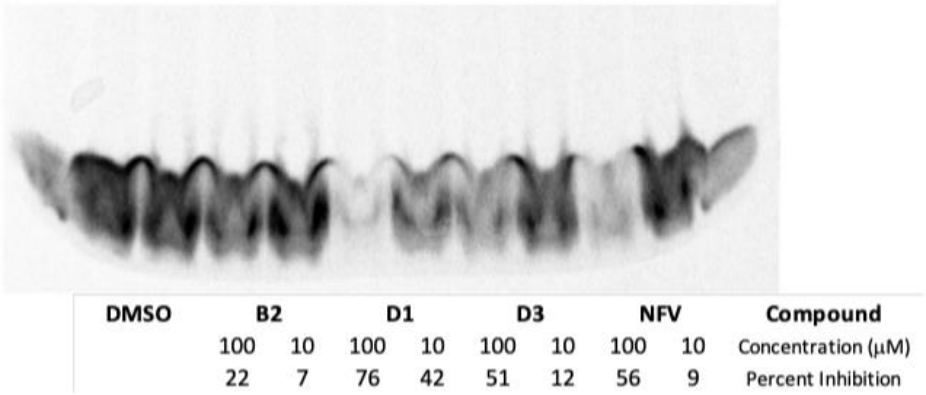

Figure 4.3. D1 compound inhibits DDI2. Representative data for the gel-based DDI2 inhibition assay as a two-point titration of DDI2 inhibition by nelfinavir (NFV) and novel compounds including D1. To determine the degree of inhibition of purified DDI2 of different compounds (10 or 100 μM), we monitored the production of a short, fluorescent cleavage product of 150 nM Ub(n)NeR-sf-GFP by 150 nM DDI2, as described (Yip et al., 2020). Percent inhibition was calculated as remaining signal intensity versus the DMSO control lanes.

4.1.2. Future directions

These preliminary data provide us with a lead molecule for further development to pharmacologically inhibit DDI2. We are in the process of optimizing the D1 compound's scaffold for improved potency and properties. Currently, we are screening an additional forty commercially available analogs of D1 using previously used assays to measure surface MHC-I, total B2M protein levels as well as DDI2 inhibition activity. In addition, we are planning to further verify the functionality of the increases in antigen presentation by utilizing the HEK293 system that expresses SIINFEKL-H2 Kb complex to quantify the induction of SIINFEKL antigen on the cell surface (as in Figure 2.4 for nelfinavir) upon the treatment of these novel compounds. Potential hits from these assays will eventually be tested *in vivo*, specifically in the

PDAC KPC and melanoma UV3 syngeneic murine xenograft models (as in Figure 3.3 for nelfinavir), to determine their efficacy in enhancing immune checkpoint blockade therapy.

4.2. Exploring the effects of DDI2 inhibitors as adjuvants in a vaccination setting

DDI2 inhibition can be beneficial when the increase in antigen presentation is required to elicit an effective immune response, such as in a vaccination setting. To test our hypothesis, we are optimizing a mouse model to characterize the immune response against a specific antigen in the absence or presence of nelfinavir. First, C57BL/6 mice were sensitized to the ovalbumin protein through subcutaneous injection. After vaccination against ovalbumin twice within two weeks, they were treated with or without depilatory cream to remove hair before receiving a topical application of either the ovalbumin protein or the peptide SIINFEKL. Their draining lymph nodes were collected after 72 hours for staining of different immune cell populations specifically against SIINFEKL. Our goal is to determine if the immune response can be further activated with nelfinavir or novel DDI2 inhibitors.

CHAPTER 5. DISCUSSION AND CONCLUSIONS

This chapter is adapted from the manuscript (in preparation for submission):

Nhu T. Nguyen*, Galen Andrew Collins*, Inbal Rachmin*, Jennifer Allouche*, Sachiko T. Homma, Abdulla Al Emran, Shanivi Srikonda, Max von Franque, Shailbala Singh, Chuan Yan, Kristina Todorova, Tal H. Erlich, Yi Sun, Hongyan Xie, Abigail Scharf, Oriah Jeselsohn, Christopher Ott, Anna Mandinova, Russell Jenkins, David Langenau, F. Stephen Hodi, Cassian Yee, Alfred L. Goldberg# and David E. Fisher# . DDI2 inhibition promotes MHC-I antigen presentation and tumor immunotherapy.

*Contributed equally

#Contributed equally (corresponding authors)

The present finding that DDI2 limits surface MHC-I expression in multiple cancer types implies the existence of a previously unrecognized step in the antigen presentation pathway. DDI2's mechanism is not only of scientific interest but appears to have clinical relevance with potential therapeutic applications since inhibiting DDI2 stimulates cytotoxic T cells responses *in vitro*; while in mice, nelfinavir can enhance the efficacy of immune checkpoint inhibitors.

Most of the present studies involved nelfinavir, which has been widely used in HIV/AIDS treatment, but has also been shown to reduce growth of a variety of tumors, although by unknown mechanisms (Al-Assar et al., 2016; Kawabata et al., 2021; Wilson et al., 2016). Our finding that nelfinavir increases immune activation might help explain these earlier observations. Although nelfinavir has been proposed to affect a variety of cellular processes (T. Chen et al., 2022; Koltai, 2015), DDI2 is its best-documented cellular target (Collins et al., 2022) and is clearly responsible for its effects on antigen presentation, as shown here by genetic and pharmacological approaches. While four other mammalian proteins contain aspartyl protease

domains resembling those in HIV-1 (Puente et al., 2003), DDI2 is the most abundant, most widely expressed, and the best-studied of these enzymes. Interestingly, of the seven HIV protease inhibitors tested, only nelfinavir and tipranavir significantly inhibited the purified DDI2 protease, and they were most effective in increasing MHC-I levels (Figure 2.3B). It is also noteworthy that deleting *DDI2*, inactivating its protease domain (Figure 2.1A-B), or deleting its ubiquitin and proteasome binding domain (Figure 2.1C) all increased B2M and surface MHC-I levels and prevented their elevation by nelfinavir. Because inhibiting DDI2's protease site alters allosterically its ability to bind to proteasomes and ubiquitin (Collins et al., 2022), it remains unclear whether DDI2 limits MHC-I presentation by functioning as a protease or as a shuttling factor.

Recently, chloroquine has been reported to enhance immune recognition of pancreatic cancers by inhibiting surface MHC-I molecule destruction via the endosomal-lysosomal pathway (Yamamoto et al., 2020). Unlike chloroquine, nelfinavir acts before the MHC-I complexes reach the cell surface. Thus, there appear to be at least two distinct pharmacological approaches for increasing surface MHC-I levels, and in most cancers studied here, the increase with nelfinavir was much larger than that with chloroquine. In addition, the stimulation of antigen presentation by nelfinavir differs from that by IFN-γ (Heron et al., 1978) in that it does not increase the expression of MHC-I complex genes (Figure 2.7A). In fact, the effects of nelfinavir do not require any new gene expression, which also rule out the involvement of the UPR.

Nelfinavir stimulates a step after the antigenic peptides are generated by the proteasome and after they are delivered by the TAP transporter into the ER (Figure 2.4F), but before the assembled peptide-MHC-I complex reaches the cell surface (Figure 2.4H). Thus, although DDI2 is in the cytosol, it must normally limit a step in the antigen presentation pathway in the ER (or

perhaps in the *cis*-Golgi). Interestingly, the yeast homolog, Ddi1, binds to SNARE proteins (Lustgarten & Gerst, 1999) and Δ*ddi1* strains secrete more proteins than WT yeast (White et al., 2011). However, human DDI2 lacks a similar SNARE-interacting domain. Thus, it remains unclear how inhibiting a cytosolic enzyme, DDI2, can enhance the delivery of MHC-I-peptide complexes from the ER to the cell surface (Figure 2.4H).

One very attractive mechanism would be that DDI2 plays a critical role in the degradation of some MHC-I molecules through ERAD (Berner et al., 2018; Olzmann et al., 2013), and that by blocking this process, nelfinavir allows more MHC-I complexes to reach the cell surface. DDI2 is, in fact, required for the rapid destruction by ERAD of certain membrane proteins (Leto et al., 2019), and it catalyzes the proteolytic cleavage of the ER-bound proteins, NRF1 and NRF3, enabling them to function as transcription factors (Chowdhury et al., 2017; Koizumi et al., 2016; Sha & Goldberg, 2016). Also, a large fraction of MHC-I heavy chains are degraded by ERAD in cells lacking B2M (Burr et al., 2011), and certain viruses trigger MHC-I degradation by ERAD as a mechanism of immune evasion (van den Boomen & Lehner, 2015). To explain our findings, we propose that a fraction of MHC-I molecules in cancer cells is continuously extracted from the ER membrane and degraded by a DDI2-dependent process, which may check for proper folding and assembly of MHC-I complexes. DDI2 inhibition would thus retard the degradation of MHC-I molecules allowing them more time to bind an appropriate peptide, adopt a proper conformation, and be transported to the cell surface. Although unproven, this mechanism seems more attractive to us than any other in explaining DDI2's role.

These findings have therapeutic potential because DDI2 inhibition increases the activation and the cytotoxicity of $CD8^+$ T lymphocytes against multiple cancers *in vitro* (Figure 3.1). Moreover, the treatment of tumor-bearing mice with nelfinavir enhances the efficacy of

anti-PD-1 therapy in prolonging survival rates (Figure 3.3D-E). Thus, in treating many types of cancer, where immune checkpoint inhibitors are beneficial, the inhibition of DDI2 may be a valuable adjuvant. Inhibitors of DDI2 might also be beneficial in other conditions where stimulating MHC-I presentation is desirable, such as in vaccination or combatting viral infections. In addition, efforts in designing and optimizing novel DDI2 inhibitors other than nelfinavir (and tipranavir) are appreciated to obtain a more potent phenotype.

Although the precise mechanism of DDI2's effects on MHC-I processing remains uncertain, its actions represent a newly recognized step in the antigen presentation pathway that is druggable and offers a new approach to enhancing the efficacy of immunotherapy of multiple cancers. Moreover, the inverse correlation shown here between DDI2 levels and the presence of activated $CD8^+$ T cells in 24 out of the 30 human solid tumor types present in The Cancer Genome Atlas is intriguing (Table 3.4, Table 3.5, Figure 3.6). It suggests that in a large variety of human tumors, DDI2 activity, by limiting antigen presentation, may impair the ability of $CD8^+$ T lymphocytes to mount cytotoxic responses.

CHAPTER 6. MATERIALS AND METHODS

This chapter is adapted from the manuscript (in preparation for submission):

Nhu T. Nguyen*, Galen Andrew Collins*, Inbal Rachmin*, Jennifer Allouche*, Sachiko T. Homma, Abdulla Al Emran, Shanivi Srikonda, Max von Franque, Shailbala Singh, Chuan Yan, Kristina Todorova, Tal H. Erlich, Yi Sun, Hongyan Xie, Abigail Scharf, Oriah Jeselsohn, Christopher Ott, Anna Mandinova, Russell Jenkins, David Langenau, F. Stephen Hodi, Cassian Yee, Alfred L. Goldberg# and David E. Fisher# . DDI2 inhibition promotes MHC-I antigen presentation and tumor immunotherapy.

*Contributed equally

#Contributed equally (corresponding authors)

Cell culture

Human melanoma cell lines A375, SK-MEL-5, SK-MEL-30, M14, UACC62, and UACC257 were obtained from the American Type Culture Collection (ATCC). Human cell lines MEL624, BX-PC-3, gp-100- and Vestigial-like 1- specific $CD8^+$ T cells were provided by Dr. Cassian Yee (MD Anderson). Patient-derived melanoma cell line C415 was provided by Dr. Stephen Hodi (Dana-Farber Cancer Institute). Human cell lines DV-90, PC-14, HC-33, KP4, PaTu-8988T were provided by Dr. Christopher Ott (MGH Cancer Center). Human colon cancer cell line HCT116 was a kind gift from Dr. Shigeo Murata (Koizumi et al., 2016). Human leukemia cell line HAP1 cell line was described in an earlier study (Collins et al., 2022). Human cell line of embryonic kidney 293 expressing the murine class I MHC H-2 K^b (293-K^b) (Wei et al., 2017) was a kind gift from Dr. Jonathan W. Yewdell (National Institutes of Health). Murine pancreatic ductal adenocarcinoma cell line KPC was a kind gift from Dr. Stephanie Dougan

(Dana-Farber Cancer Institute). Murine melanoma cell line UV3 was established from the parental D4M.3A cell line subjected to UVB irradiation *in vitro*, as described (Lo et al., 2021) and is the same cell line previously referred to as D4M.3A-UV3 (Lo et al., 2021). Cells were cultured in the following media: A375, 293-K^b, and UV3 in DMEM supplemented with 10% FBS and 1% penicillin/streptomycin; SK-MEL-5, SK-MEL-30, M14, UACC62, UACC257, HEK293, MEL624, BX-PC-3, DV-90, PC-14, HC-33 in RPMI supplemented with 10% FBS and 1% penicillin/streptomycin; KP4 and PaTu-8988T in DMEM/F12 (1:1) supplemented with 10% FBS and 1% penicillin/streptomycin; HCT116 in McCoy's 5A supplemented with 10% FBS and 1% penicillin/streptomycin; KPC in RPMI supplemented with 10% FBS, 1% penicillin/streptomycin, 1% Glutamax, 1% Nonessential amino acids, 1% sodium pyruvate, and 0.0008% β-mercaptoethanol; HAP1 in Iscove's Modified Dulbecco's Media with 10% FBS and 1% penicillin/streptomycin; gp-100- and VGLL-1- specific $CD8^+$ T cells in RPMI supplemented with 10% FBS, 1% penicillin/streptomycin, 1% Nonessential amino acids, and 1% sodium pyruvate. All cell lines were maintained in a humidified, 37°C, 5% CO_2 incubator.

Cell treatments

Human and murine cancer cell lines (except for 293-Kb cell line) were treated with the following drugs at indicated concentrations in figure legends: nelfinavir (NF, Sigma Aldrich, #PZ0013), chloroquine (CQ, Sigma Aldrich, #C6628), dimethylsulfoxide (DMSO, ATCC, #4-X).

For the CRISPR/Cas9 DDI2 knockout experiments, cancer cell lines were transfected with DDI2 CRISPR/Cas9 KO plasmid (Santa Cruz Biotechnology, # sc-408297) using Lipofectamine 3000 Transfection Reagent (Life Technologies, #L3000008), according to the

manufacturer's instructions. After 72 hours of incubation, GFP+ single cells were sorted into 96-well plates using FACSAria Fusion Cell Sorter (BD Biosciences). Clones were expanded and collected for verification of DDI2 knockout by immunoblotting.

For the DDI2 rescue experiments, HAP1 cells were transfected with pReceiver-FLAG-DDI2 or pReceiver-FLAG-ΔDDI2 plasmid DNA as described in previous study (Collins et al., 2022) by FuGENE 24 hours prior to treatment with NF.

For the short interfering RNA (siRNA) transfection experiments to knock down autophagy genes, the following siRNAs were used: ATG3 siRNA (Santa Cruz Biotechnology, #sc-72582), ATG7 siRNA (Santa Cruz Biotechnology, #sc-41447), NBR1 siRNA (Santa Cruz Biotechnology, #sc- 94187), and siGenome Non-Targeting siRNA pool #2 (Dharmacon Inc, #D-001206-14-05). Cells were transfected with Lipofectamine RNAiMAX (Life Technologies, #13778150), according to the manufacturer's recommendations. After 48 hours of transfection, total protein was harvested for immunoblotting.

Immunoblotting

Whole-cell protein lysates prepared through using RIPA lysis buffer (Sigma-Aldrich, #R0278) with HALT Protease and Phosphatase Inhibitor (ThermoFisher Scientific, #PI78445). Then, protein concentrations were quantified through using Pierce BCA protein assay (ThermoFisher Scientific, #23225). Immunoblotting was subsequently performed through using standard techniques using 4%–15% Criterion TGX Precast Midi Protein gels (Bio-Rad Laboratories, #5671084) and then transferring to 0.2 m nitrocellulose membranes (Bio-Rad Laboratories,

#1620112). Membranes were blocked with 5% non-fat milk (Boston BioProducts, #P-1400) in 0.1% TBS-T and incubated with primary antibody overnight at 4°C, followed by one hour of incubation with secondary antibody at room temperature. Protein bands were visualized using Western Lightning Plus ECL (PerkinElmer, #NEL105001EA) by the Azure c600 Imaging System (Azure Biosystems). Data were quantified using ImageJ software (National Institutes of Health).

Antibody (dilution)	Supplier	Catalog number	Clone
Recombinant Anti-beta 2 Microglobulin Rabbit Monoclonal (1:3000)	Abcam	Cat# ab75853	[EP2978Y]
Anti-human DDI2 Rabbit Polyclonal (1:1000)	Thermo Fisher	Cat# A304-629A	
Anti-rabbit IgG, HRP-linked Goat (1:5000)	Cell Signaling	Cat# 7074S	
Anti-β-actin-peroxidase Mouse Monoclonal (1:10000)	Sigma-Aldrich	Cat# A3854	[AC-15]
Anti-Atg3 Rabbit Polyclonal (1:1000)	Cell Signaling	Cat# 3415	
Anti-Atg7 Rabbit Monoclonal (1:1000)	Cell Signaling	Cat# 8588	[D12B11]
Anti-human LC3B Rabbit Monoclonal (1:1000)	Cell Signaling	Cat# 3868	[D11]
Anti-human NBR1 Mouse Monoclonal (1:500)	Santa Cruz Biotechnology	Cat# sc-130380	[4BR]
Amersham ECL Mouse IgG, HRP-linked $F(ab')_2$ fragment (from sheep)	Cytivia	Cat# NA9310	
Anti-GFP Rabbit Polyclonal (1:1000)	Cell Signaling	Cat# 2555	
Anti-β-Tubulin Rabbit Polyclonal (1:1000)	Cell Signaling	Cat# 2146	
IRDye® 680RD Goat anti-Rabbit IgG Secondary (1:10000)	LI-COR	Cat# 926-68071	

Flow cytometry analysis of surface MHC-I protein expression

After two cold PBS washes, cells were detached with 50 mL of Enzyme Free Cell Dissociation Solution PBS Based (ThermoFisher Scientific, #13151014) and washed with cold FACS buffer (PBS supplemented with 10% FBS) twice. Cells were fixed with 4% paraformaldehyde for 20 min in the dark at room temperature. After three cold FACS buffer washes, paraformaldehyde-fixed cells were incubated with HLA-ABC Monoclonal Antibody (W6/32), APC antibody (ThermoFisher Scientific, #17-9983-41, 1:200 dilution) or APC Mouse IgG2a, κ Isotype Ctrl Monoclonal antibody (ThermoFisher Scientific, #400220, 1:400 dilution) in the dark at 4oC for 45 min. Cells were then washed with cold FACS buffer for three times and analyzed on the Cytek Aurora flow cytometer using SpectroFlo software (Cytek Biosciences). Data quantification was performed using FlowJo software.

Expression of the ovalbumin-derived antigenic peptide SIINFEKL

To express the ovalbumin-derived antigenic peptide SIINFEKL (Addgene vector #11624), which expresses Venus fluorescent protein followed by SIINFEKL (a kind gift from Dr. Jonathan W. *Yewdell*) was used. 293-K^b cells were cultured in 12-well plates to 80% confluency. A transfection mixture of 12 µg DNA and 24 µL ViaFect (Promega, Madison WI, #E4981) was prepared in 100 µL Opti-MEM I Reduced-Serum Medium (Thermo Fisher Scientific, #51985-034) and allowed to mix at room temperature for 20 min and then added to each well containing 1 mL complete medium. After 24 hours, the transfection mixture was replaced with fresh medium. Cells were cultured for another 24 hours before treatments, except for the treatment with Brefeldin A, where cells were treated 36 hours after transfection.

Constructs of Ubiquitin-SIINFEKL (Ub-SIINFEKL) and a signal sequence-SIINFEKL (SS-SIINFEKL) were kind gifts from Dr. Kenneth L. Rock (University of Massachusetts Chan Medical School). Each construct was transfected in 293-K^b cells as the same procedure described above. Twenty-four hours after the transfection, cells were treated with ice-cold citric acid buffer for acid stripping. After 5 hours of recovery, doxycycline was added to the culture media at the concentration of 25 ng/mL for Ub-SIINFEKL and 10 ng/ml for SS-SIINFEKL.

Acid stripping of MHC-I-peptide complexes

To assess newly generated MHC- I antigen presentation, preexisting MHC-I-peptide complexes on the cell surface were removed by acid stripping 5 hours before starting treatments with an inhibitor. Cells were treated with ice-cold citric acid buffer (1:1 mixture of 0.263 M citric acid, and 0.32 M sodium phosphate-NaH_2PO_4) for 90 s, then ice cold culture medium was

added to neutralize the pH. Cells were washed three times with PBS, then incubated in complete media at 37°C.

293-K^b cell treatments

Treatments were started after a 5-hour-recovery from acid stripping. Concentrations and durations of treatment with inhibitors are as follows; nelfinavir (NF, Cayman Chemical, Ann Arbor MI, #15144; concentration:10 μM; duration: indicated in each figure), actinomycin D (ActD, Cayman Chemical, #11421; concentration: 1 μg/ml; duration: 10 hours), bortezomib (BTZ, LC Laboratories, #B-1408; concentration: 0.5 μM; duration: 16 hours), thapsigargin (TG, Cayman Chemical, #10522; concentration: 0.25μM; duration: 16 hours), chloroquine diphosphate salt (CQ, Sigma-Aldrich, #C6628; concentration: 10 μM; duration: 18 hours), Brefeldin A (BFA, Cayman Chemical, #11861; concentration: 5 μg/ml; duration: 9 hours).

Flow cytometry analysis of MHC-I-SIINFEKL presentation

After the treatment with or without inhibitor, cells were washed with PBS, trypsinized, and incubated with 3% (w/v) BSA in PBS for 15 min on ice to block nonspecific staining. After washing with PBS, cells were stained with the APC-conjugated mAb specific for Kb:SIINFEKL complexes (25-D1.16, cat# 141606, BioLegend, San Diego CA, 1:200 dilution) for 30 min on ice. After washing, cells were fixed with 1% PFA in PBS for 15 min. Flow cytometry data were collected on a FACSCalibur using CellQuest software (Becton Dickinson). Data were analyzed from live cell gates using FlowJo software (TreeStar). After gating out the cells expressing Venus fluorescent protein less than untransfected cells, geometric mean fluorescence intensities

(MFIs) were expressed as a percent of MFI of no treatment control condition after subtraction of staining after acid stripping.

Cycloheximide Chase

Forty-eight hours after transfection of Venus-SIINFEKL plasmid, 293K^b cells were treated with 50 μg/mL of the translation inhibitor cycloheximide (Sigma) with and without NF (10 μM). Cells were collected at 0, 14, 24, 48, and 72 hours after initiation of the treatment and lysed for 30 min in ice-cold RIPA buffer and Roche Protease Inhibitor Cocktail Tablet (4693132001). After centrifugation (10,000 ×g for 15 min), the supernatant was used as cleared lysate for Western blotting. Anti-GFP rabbit antibody (Cell Signaling Technologies; catalog no.: 2555; 1:1000 dilution), Anti-tubulin rabbit antibody (Cell Signaling Technologies; catalog no.: 2146; 1:1000 dilution), IRDye 680RD Goat anti-rabbit antibody (LI-COR; catalog no.:926-68071; 1:10000 dilution) were used to detect the signals. Quantification of immunoblots was carried out using ImageStudio Lite Software (LI-COR).

RNA purification and quantitative RT-PCR

Total RNA isolated from cultured melanoma, lung cancer, or pancreatic cancer cells at the indicated time points, through using the RNeasy Plus Mini Kit (QIAGEN, #74136). mRNA expression levels were determined using intron-spanning primers with SYBER FAST qPCR master mix (Kapa Biosystems, #KK4600). Expression values were then calculated using the comparative threshold cycle method (2-ΔΔCt) and normalized to human RPL11 mRNA.

List of primers:

B2M_Forward 5'-GAGGCTATCCAGCGTACTCCA-3'

B2M_Reverse	5’-CGGCAGGCATACTCATCTTTT-3’
HLA-A_Forward	5’-CCGTGGATAGAGCAGGAG-3’
HLA-A Reverse	5’-CGTCGCAGCCATACATTATC-3’
HLA-B_Forward	5’-CAGTTCGTGAGGTTCGACAG-3’
HLA-B_Reverse	5’-CAGCCGTACATGCTCTGGA-3’
RPL11_Forward	5’-TGCCAAAGGATCTGACAGTG-3’
RPL11_Reverse	GTTGGGGAGAGTGGAGACAG-3’

Assay of DDI2 protease activity

150 nM labeled Ub(n)NeD-sfGFP (gift from Tom Rapoport at Harvard Medical School) was incubated with 150 nM DDI2 in 50 mM Hepes (pH 7.4), 150 mM NaCl, 0.5 mM TCEP, and 0.01 mg/ml BSA and incubated 37°C for 1 hour. HIV protease inhibitors were used at 50 μM final concentration. The reaction was stopped with 1× Tricine loading buffer and incubated at 70 °C for 5 min. The samples were run on 16% Tricine Mini Gels (Thermo Fisher Scientific EC66952). The gels were scanned with Typhoon imager at 800 nm (Cytiva).

***In vitro* IFN-γ T cell assay**

Human T cells were cultured as previously described (Bradley et al., 2020). Human cancer cell lines (melanoma or pancreatic cancer) were treated with 10 μM nelfinavir or vehicle DMSO for 72 hours. Media with fresh drugs were changed daily. Cells were detached with Enzyme Free Cell Dissociation Solution PBS Based (ThermoFisher Scientific, #13151014) and incubated with antigen-specific human T cells at 37oC. Melanoma cells MEL624 and A375 were incubated with gp-100-CD8+ cells in a 1:20 ratio for 2 hours. Melanoma cells SK-MEL-5 were

incubated with gp-100-CD8+ cells in a 1:1 ratio for 2 hours. Pancreatic cells BX-PC-3 were incubated with Vestigial-like 1-CD8+ T cells in a 1:10 ratio for 5 hours. The supernatants were collected to measure IFN- γ with the LEGEND MAX™ Human IFN-γ ELISA Kit (BioLegend, #430107), according to the manufacturer's instructions. Signals at 450 nm were measured with Victor microplate reader (PerkinElmer) and signals at 570 nm were measured with EnVision microplate reader (PerkinElmer).

In vitro T cell killing assay

Human T cells were cultured as previously described (Bradley et al., 2020). Human melanoma cell lines were cultured in Lab-Tek II Chamber Slide, 4 Well, Removable, RS Surface (Life Technologies, # 154526PK) and transfected with ZipGFP-Casp3 (Addgene, plasmid #81241) with Lipofectamine 3000 Transfection Reagent (Life Technologies, #L3000008), according to the manufacturer's instructions. After 24 hours, transfected cells were treated with nelfinavir or vehicle DMSO for 72 hours. Media with fresh drugs were changed daily. Cells then were incubated with human melanocytic gp100-specific T cells in a 1:10 ratio and incubated at 37°C. Cells were imaged with Zeiss LSM710 Laser Scanning Confocal (Zeiss) at 0 and 24 hours of incubation with T cells. Data analysis was performed using Imaris software.

In vivo mouse studies

Female 6-week-old C57BL/6 mice used for the transplantation experiments were purchased from Jackson Laboratory and maintained in the animal facility of the Massachusetts General Hospital. All animal procedures were approved by the Massachusetts General Hospital Animal Care and Use Committee (IACUC) under protocol number 2009N000012.

One million cells of mouse pancreatic cancer cell line KPC or melanoma cell line UV3 (generated from the parental D4M.3A cell line subjected to UVB irradiation in vitro) (55) were injected subcutaneously on the flank of each C57BL/6 mouse. For tumor growth and survival studies, on the same day of cell inoculation, mice were injected intraperitoneally with nelfinavir (TCI America, #N0986) diluted in 4% DMSO, 5% PEG, 5% Tween-80, and PBS (50 mg/kg) or the vehicle (4% DMSO, 5% PEG, 5% Tween-80, and PBS) daily for 21 days. Once the tumor engrafted and reached the volume of 50-100 mm3 (calculated as length x width2 / 2), mice were injected with anti-PD-1 antibody (Bio X Cell, #BE0273,10 mg/kg) or matched isotype control (Bio X Cell, #BE0089,10 mg/kg) intraperitoneally every other day for 3 doses. Tumor growth was monitored, and mice were euthanized when the tumor volume reached 500 mm3 or after being evaluated by the Center for Comparative Medicine at Massachusetts General Hospital. For biomarker studies to determine total B2M protein levels and the percentage of infiltrating CD8+ T cells in tumors, once the tumor engrafted and reached the volume of 50-100 mm3 (calculated as length x width2 / 2), mice were injected with nelfinavir (50 mg/kg) or the vehicle daily. KPC tumors were collected after 6 days and UV3 tumors were collected after 2 days for subsequent analyses.

Immunohistrochemistry

For histology, paraffin sections were prepared and stained with hematoxylin and eosin, anti-CD4 antibody, and anti-CD8 antibody using available ihisto service (https://www.ihisto.io). Slides were imaged using the digital slide scanner (Hamamatsu, model S60). $CD4^+$ or $CD8^+$ T cell infiltration was visualized, counted, and quantified using ImageJ (National Institutes of Health).

Clinical data analysis

RNA-seq were downloaded from The Cancer Genome Atlas (TCGA) and fetched from the Tumor-Immune System Interaction Database (TISIDB)(Ru et al., 2019). The original read counts were converted to $\log_2$ CPM using Voom method (Law et al., 2014). Activated $CD8^+$ T-cell-, activated B-cell-, and activated dendritic cell-related gene signatures (Supplemental Table 1) were selected as described previously (Charoentong et al., 2017). Gene set variation analysis (GSVA) package (Hänzelmann et al., 2013) was used to infer the immune signatures using the gene expression profile of patients corresponding to each cancer type. Correlation analyses were performed using the spearman correlation coefficient and p-values were calculated by two-tailed t-tests.

Bibliography

Al-Assar, O., Bittner, M.-I., Lunardi, S., Stratford, M. R., McKenna, W. G., & Brunner, T. B. (2016). The radiosensitizing effects of Nelfinavir on pancreatic cancer with and without pancreatic stellate cells. *Radiotherapy and Oncology: Journal of the European Society for Therapeutic Radiology and Oncology*, *119*(2), 300–305. https://doi.org/10.1016/j.radonc.2016.03.024

Angell, T. E., Lechner, M. G., Jang, J. K., LoPresti, J. S., & Epstein, A. L. (2014). MHC class I loss is a frequent mechanism of immune escape in papillary thyroid cancer that is reversed by interferon and selumetinib treatment in vitro. *Clinical Cancer Research: An Official Journal of the American Association for Cancer Research*, *20*(23), 6034–6044. https://doi.org/10.1158/1078-0432.CCR-14-0879

Barrueto, L., Caminero, F., Cash, L., Makris, C., Lamichhane, P., & Deshmukh, R. R. (2020). Resistance to Checkpoint Inhibition in Cancer Immunotherapy. *Translational Oncology*, *13*(3), 100738. https://doi.org/10.1016/j.tranon.2019.12.010

Baumeister, S. H., Freeman, G. J., Dranoff, G., & Sharpe, A. H. (2016). Coinhibitory Pathways in Immunotherapy for Cancer. *Annual Review of Immunology*, *34*, 539–573. https://doi.org/10.1146/annurev-immunol-032414-112049

Berner, N., Reutter, K.-R., & Wolf, D. H. (2018). Protein Quality Control of the Endoplasmic Reticulum and Ubiquitin-Proteasome-Triggered Degradation of Aberrant Proteins: Yeast Pioneers the Path. *Annual Review of Biochemistry*, *87*, 751–782. https://doi.org/10.1146/annurev-biochem-062917-012749

Birkeland, S. A., Storm, H. H., Lamm, L. U., Barlow, L., Blohmé, I., Forsberg, B., Eklund, B., Fjeldborg, O., Friedberg, M., & Frödin, L. (1995). Cancer risk after renal transplantation

in the Nordic countries, 1964-1986. *International Journal of Cancer*, *60*(2), 183–189. https://doi.org/10.1002/ijc.2910600209

Blank, C., Brown, I., Marks, R., Nishimura, H., Honjo, T., & Gajewski, T. F. (2003). Absence of programmed death receptor 1 alters thymic development and enhances generation of CD4/CD8 double-negative TCR-transgenic T cells. *Journal of Immunology (Baltimore, Md.: 1950)*, *171*(9), 4574–4581. https://doi.org/10.4049/jimmunol.171.9.4574

Blobel, G., & Dobberstein, B. (1975). Transfer of proteins across membranes. I. Presence of proteolytically processed and unprocessed nascent immunoglobulin light chains on membrane-bound ribosomes of murine myeloma. *The Journal of Cell Biology*, *67*(3), 835–851. https://doi.org/10.1083/jcb.67.3.835

Bradley, S. D., Talukder, A. H., Lai, I., Davis, R., Alvarez, H., Tiriac, H., Zhang, M., Chiu, Y., Melendez, B., Jackson, K. R., Katailiha, A., Sonnemann, H. M., Li, F., Kang, Y., Qiao, N., Pan, B.-F., Lorenzi, P. L., Hurd, M., Mittendorf, E. A., … Lizée, G. (2020). Vestigial-like 1 is a shared targetable cancer-placenta antigen expressed by pancreatic and basal-like breast cancers. *Nature Communications*, *11*(1), 5332. https://doi.org/10.1038/s41467-020-19141-w

Brower, E. T., Bacha, U. M., Kawasaki, Y., & Freire, E. (2008). Inhibition of HIV-2 protease by HIV-1 protease inhibitors in clinical use. *Chemical Biology & Drug Design*, *71*(4), 298–305. https://doi.org/10.1111/j.1747-0285.2008.00647.x

Brown, J. A., Dorfman, D. M., Ma, F.-R., Sullivan, E. L., Munoz, O., Wood, C. R., Greenfield, E. A., & Freeman, G. J. (2003). Blockade of programmed death-1 ligands on dendritic cells enhances T cell activation and cytokine production. *Journal of Immunology*

(Baltimore, Md.: 1950), *170*(3), 1257–1266. https://doi.org/10.4049/jimmunol.170.3.1257

Brunet, J. F., Denizot, F., Luciani, M. F., Roux-Dosseto, M., Suzan, M., Mattei, M. G., & Golstein, P. (1987). A new member of the immunoglobulin superfamily—CTLA-4. *Nature*, *328*(6127), 267–270. https://doi.org/10.1038/328267a0

Burnet, M. (1957). Cancer; a biological approach. I. The processes of control. *British Medical Journal*, *1*(5022), 779–786. https://doi.org/10.1136/bmj.1.5022.779

Burr, M. L., Cano, F., Svobodova, S., Boyle, L. H., Boname, J. M., & Lehner, P. J. (2011). HRD1 and UBE2J1 target misfolded MHC class I heavy chains for endoplasmic reticulum-associated degradation. *Proceedings of the National Academy of Sciences of the United States of America*, *108*(5), 2034–2039. https://doi.org/10.1073/pnas.1016229108

Burr, M. L., Sparbier, C. E., Chan, K. L., Chan, Y.-C., Kersbergen, A., Lam, E. Y. N., Azidis-Yates, E., Vassiliadis, D., Bell, C. C., Gilan, O., Jackson, S., Tan, L., Wong, S. Q., Hollizeck, S., Michalak, E. M., Siddle, H. V., McCabe, M. T., Prinjha, R. K., Guerra, G. R., … Dawson, M. A. (2019). An Evolutionarily Conserved Function of Polycomb Silences the MHC Class I Antigen Presentation Pathway and Enables Immune Evasion in Cancer. *Cancer Cell*, *36*(4), 385-401.e8. https://doi.org/10.1016/j.ccell.2019.08.008

Charoentong, P., Finotello, F., Angelova, M., Mayer, C., Efremova, M., Rieder, D., Hackl, H., & Trajanoski, Z. (2017). Pan-cancer Immunogenomic Analyses Reveal Genotype-Immunophenotype Relationships and Predictors of Response to Checkpoint Blockade. *Cell Reports*, *18*(1), 248–262. https://doi.org/10.1016/j.celrep.2016.12.019

Chen, D. S., & Mellman, I. (2013). Oncology Meets Immunology: The Cancer-Immunity Cycle. *Immunity*, *39*(1), 1–10. https://doi.org/10.1016/j.immuni.2013.07.012

Chen, T., Ho, M., Briere, J., Moscvin, M., Czarnecki, P. G., Anderson, K. C., Blackwell, T. K., & Bianchi, G. (2022). Multiple myeloma cells depend on the DDI2/NRF1-mediated proteasome stress response for survival. *Blood Advances*, *6*(2), 429–440. https://doi.org/10.1182/bloodadvances.2020003820

Cho, S. X., Vijayan, S., Yoo, J., Watanabe, T., Ouda, R., An, N., & Kobayashi, K. S. (2021). MHC class I transactivator NLRC5 in host immunity, cancer and beyond. *Immunology*, *162*(3), 252–261. https://doi.org/10.1111/imm.13235

Chowdhury, A. M. M. A., Katoh, H., Hatanaka, A., Iwanari, H., Nakamura, N., Hamakubo, T., Natsume, T., Waku, T., & Kobayashi, A. (2017). Multiple regulatory mechanisms of the biological function of NRF3 (NFE2L3) control cancer cell proliferation. *Scientific Reports*, *7*(1), 12494. https://doi.org/10.1038/s41598-017-12675-y

COLEY, W. B. (1898). THE TREATMENT OF INOPERABLE SARCOMA WITH THE ’MIXED TOXINS OF ERYSIPELAS AND BACILLUS PRODIGIOSUS.: IMMEDIATE AND FINAL RESULTS IN ONE HUNDRED AND FORTY CASES. *Journal of the American Medical Association*, *XXXI*(9), 456–465. https://doi.org/10.1001/jama.1898.92450090022001g

Coley, W. B. (1991). The treatment of malignant tumors by repeated inoculations of erysipelas. With a report of ten original cases. 1893. *Clinical Orthopaedics and Related Research*, *262*, 3–11.

Collins, G. A., & Goldberg, A. L. (2020). Proteins containing ubiquitin-like (Ubl) domains not only bind to 26S proteasomes but also induce their activation. *Proceedings of the*

National Academy of Sciences of the United States of America, *117*(9), 4664–4674. https://doi.org/10.1073/pnas.1915534117

Collins, G. A., Sha, Z., Kuo, C.-L., Erbil, B., & Goldberg, A. L. (2022). Mammalian Ddi2 is a shuttling factor containing a retroviral protease domain that influences binding of ubiquitylated proteins and proteasomal degradation. *The Journal of Biological Chemistry*, *298*(5), 101875. https://doi.org/10.1016/j.jbc.2022.101875

De Clercq, E. (2009). Anti-HIV drugs: 25 compounds approved within 25 years after the discovery of HIV. *International Journal of Antimicrobial Agents*, *33*(4), 307–320. https://doi.org/10.1016/j.ijantimicag.2008.10.010

Dhatchinamoorthy, K., Colbert, J. D., & Rock, K. L. (2021). Cancer Immune Evasion Through Loss of MHC Class I Antigen Presentation. *Frontiers in Immunology*, *12*. https://www.frontiersin.org/articles/10.3389/fimmu.2021.636568

Dighe, A. S., Richards, E., Old, L. J., & Schreiber, R. D. (1994). Enhanced in vivo growth and resistance to rejection of tumor cells expressing dominant negative IFNγ receptors. *Immunity*, *1*(6), 447–456. https://doi.org/10.1016/1074-7613(94)90087-6

Dirac-Svejstrup, A. B., Walker, J., Faull, P., Encheva, V., Akimov, V., Puglia, M., Perkins, D., Kümper, S., Hunjan, S. S., Blagoev, B., Snijders, A. P., Powell, D. J., & Svejstrup, J. Q. (2020). DDI2 Is a Ubiquitin-Directed Endoprotease Responsible for Cleavage of Transcription Factor NRF1. *Molecular Cell*, *79*(2), 332-341.e7. https://doi.org/10.1016/j.molcel.2020.05.035

Dunn, G. P., Bruce, A. T., Ikeda, H., Old, L. J., & Schreiber, R. D. (2002). Cancer immunoediting: From immunosurveillance to tumor escape. *Nature Immunology*, *3*(11), 991–998. https://doi.org/10.1038/ni1102-991

Ehrlich, P. (1909). Über den jetzigen Stand der Karzinomforschung. In *Beiträge zur experimentellen Pathologie und Chemotherapie* (pp. 117–164). Akademische Verlagsgesellschaft.

Eke, A. C., McCormack, S. A., Best, B. M., Stek, A. M., Wang, J., Kreitchmann, R., Shapiro, D., Smith, E., Mofenson, L. M., Capparelli, E. V., Mirochnick, M., & IMPAACT P1026s Protocol Team. (2019). Pharmacokinetics of Increased Nelfinavir Plasma Concentrations in Women During Pregnancy and Postpartum. *Journal of Clinical Pharmacology*, *59*(3), 386–393. https://doi.org/10.1002/jcph.1331

Fassmannová, D., Sedlák, F., Sedláček, J., Špička, I., & Grantz Šašková, K. (2020). Nelfinavir Inhibits the TCF11/Nrf1-Mediated Proteasome Recovery Pathway in Multiple Myeloma. *Cancers*, *12*(5), 1065. https://doi.org/10.3390/cancers12051065

Fruci, D., Lauvau, G., Saveanu, L., Amicosante, M., Butler, R. H., Polack, A., Ginhoux, F., Lemonnier, F., Firat, H., & van Endert, P. M. (2003). Quantifying recruitment of cytosolic peptides for HLA class I presentation: Impact of TAP transport. *Journal of Immunology (Baltimore, Md.: 1950)*, *170*(6), 2977–2984. https://doi.org/10.4049/jimmunol.170.6.2977

Gibbons, R. M., Liu, X., Pulko, V., Harrington, S. M., Krco, C. J., Kwon, E. D., & Dong, H. (2012). B7-H1 limits the entry of effector CD8(+) T cells to the memory pool by upregulating Bim. *Oncoimmunology*, *1*(7), 1061–1073. https://doi.org/10.4161/onci.20850

Gills, J. J., Lopiccolo, J., Tsurutani, J., Shoemaker, R. H., Best, C. J. M., Abu-Asab, M. S., Borojerdi, J., Warfel, N. A., Gardner, E. R., Danish, M., Hollander, M. C., Kawabata, S., Tsokos, M., Figg, W. D., Steeg, P. S., & Dennis, P. A. (2007). Nelfinavir, A lead HIV

protease inhibitor, is a broad-spectrum, anticancer agent that induces endoplasmic reticulum stress, autophagy, and apoptosis in vitro and in vivo. *Clinical Cancer Research: An Official Journal of the American Association for Cancer Research*, *13*(17), 5183–5194. https://doi.org/10.1158/1078-0432.CCR-07-0161

Gu, S. S., Zhang, W., Wang, X., Jiang, P., Traugh, N., Li, Z., Meyer, C., Stewig, B., Xie, Y., Bu, X., Manos, M. P., Font-Tello, A., Gjini, E., Lako, A., Lim, K., Conway, J., Tewari, A. K., Zeng, Z., Sahu, A. D., … Liu, X. S. (2021). Therapeutically increasing MHC-I expression potentiates immune checkpoint blockade. *Cancer Discovery*, *11*(6), 1524–1541. https://doi.org/10.1158/2159-8290.CD-20-0812

Gu, Y., Wang, X., Wang, Y., Wang, Y., Li, J., & Yu, F.-X. (2020). Nelfinavir inhibits human DDI2 and potentiates cytotoxicity of proteasome inhibitors. *Cellular Signalling*, *75*, 109775. https://doi.org/10.1016/j.cellsig.2020.109775

Guntermann, C., & Alexander, D. R. (2002). CTLA-4 suppresses proximal TCR signaling in resting human CD4(+) T cells by inhibiting ZAP-70 Tyr(319) phosphorylation: A potential role for tyrosine phosphatases. *Journal of Immunology (Baltimore, Md.: 1950)*, *168*(9), 4420–4429. https://doi.org/10.4049/jimmunol.168.9.4420

Hamanishi, J., Mandai, M., Iwasaki, M., Okazaki, T., Tanaka, Y., Yamaguchi, K., Higuchi, T., Yagi, H., Takakura, K., Minato, N., Honjo, T., & Fujii, S. (2007). Programmed cell death 1 ligand 1 and tumor-infiltrating CD8+ T lymphocytes are prognostic factors of human ovarian cancer. *Proceedings of the National Academy of Sciences of the United States of America*, *104*(9), 3360–3365. https://doi.org/10.1073/pnas.0611533104

Hanahan, D. (2022). Hallmarks of Cancer: New Dimensions. *Cancer Discovery*, *12*(1), 31–46. https://doi.org/10.1158/2159-8290.CD-21-1059

Hanahan, D., & Weinberg, R. A. (2000). The Hallmarks of Cancer. *Cell*, *100*(1), 57–70. https://doi.org/10.1016/S0092-8674(00)81683-9

Hänzelmann, S., Castelo, R., & Guinney, J. (2013). GSVA: Gene set variation analysis for microarray and RNA-seq data. *BMC Bioinformatics*, *14*, 7. https://doi.org/10.1186/1471-2105-14-7

Harding, F. A., McArthur, J. G., Gross, J. A., Raulet, D. H., & Allison, J. P. (1992). CD28-mediated signalling co-stimulates murine T cells and prevents induction of anergy in T-cell clones. *Nature*, *356*(6370), 607–609. https://doi.org/10.1038/356607a0

Hearn, A., York, I. A., & Rock, K. L. (2009). The specificity of trimming of MHC class I-presented peptides in the endoplasmic reticulum. *Journal of Immunology (Baltimore, Md.: 1950)*, *183*(9), 5526–5536. https://doi.org/10.4049/jimmunol.0803663

Herforth, C., Stone, J. A., Jayewardene, A. L., Blaschke, T. F., Fang, F., Motoya, T., & Aweeka, F. T. (2002). Determination of nelfinavir free drug concentrations in plasma by equilibrium dialysis and liquid chromatography/tandem mass spectrometry: Important factors for method optimization. *European Journal of Pharmaceutical Sciences: Official Journal of the European Federation for Pharmaceutical Sciences*, *15*(2), 185–195. https://doi.org/10.1016/s0928-0987(01)00220-2

Heron, I., Hokland, M., & Berg, K. (1978). Enhanced expression of beta2-microglobulin and HLA antigens on human lymphoid cells by interferon. *Proceedings of the National Academy of Sciences of the United States of America*, *75*(12), 6215–6219. https://doi.org/10.1073/pnas.75.12.6215

Hirano, F., Kaneko, K., Tamura, H., Dong, H., Wang, S., Ichikawa, M., Rietz, C., Flies, D. B., Lau, J. S., Zhu, G., Tamada, K., & Chen, L. (2005). Blockade of B7-H1 and PD-1 by

monoclonal antibodies potentiates cancer therapeutic immunity. *Cancer Research*, *65*(3), 1089–1096.

Hodi, F. S., Mihm, M. C., Soiffer, R. J., Haluska, F. G., Butler, M., Seiden, M. V., Davis, T., Henry-Spires, R., MacRae, S., Willman, A., Padera, R., Jaklitsch, M. T., Shankar, S., Chen, T. C., Korman, A., Allison, J. P., & Dranoff, G. (2003). Biologic activity of cytotoxic T lymphocyte-associated antigen 4 antibody blockade in previously vaccinated metastatic melanoma and ovarian carcinoma patients. *Proceedings of the National Academy of Sciences of the United States of America*, *100*(8), 4712–4717. https://doi.org/10.1073/pnas.0830997100

Hodi, F. S., O'Day, S. J., McDermott, D. F., Weber, R. W., Sosman, J. A., Haanen, J. B., Gonzalez, R., Robert, C., Schadendorf, D., Hassel, J. C., Akerley, W., van den Eertwegh, A. J. M., Lutzky, J., Lorigan, P., Vaubel, J. M., Linette, G. P., Hogg, D., Ottensmeier, C. H., Lebbé, C., … Urba, W. J. (2010). Improved Survival with Ipilimumab in Patients with Metastatic Melanoma. *The New England Journal of Medicine*, *363*(8), 711–723. https://doi.org/10.1056/NEJMoa1003466

Hou, T. Z., Qureshi, O. S., Wang, C. J., Baker, J., Young, S. P., Walker, L. S. K., & Sansom, D. M. (2015). A transendocytosis model of CTLA-4 function predicts its suppressive behavior on regulatory T cells. *Journal of Immunology (Baltimore, Md.: 1950)*, *194*(5), 2148–2159. https://doi.org/10.4049/jimmunol.1401876

Hughes, E. A., Hammond, C., & Cresswell, P. (1997). Misfolded major histocompatibility complex class I heavy chains are translocated into the cytoplasm and degraded by the proteasome. *Proceedings of the National Academy of Sciences of the United States of America*, *94*(5), 1896–1901. https://doi.org/10.1073/pnas.94.5.1896

Inman, B. A., Sebo, T. J., Frigola, X., Dong, H., Bergstralh, E. J., Frank, I., Fradet, Y., Lacombe, L., & Kwon, E. D. (2007). PD-L1 (B7-H1) expression by urothelial carcinoma of the bladder and BCG-induced granulomata: Associations with localized stage progression. *Cancer*, *109*(8), 1499–1505. https://doi.org/10.1002/cncr.22588

Ishida, Y. (2020). PD-1: Its Discovery, Involvement in Cancer Immunotherapy, and Beyond. *Cells*, *9*(6), 1376. https://doi.org/10.3390/cells9061376

Ishida, Y., Agata, Y., Shibahara, K., & Honjo, T. (1992). Induced expression of PD-1, a novel member of the immunoglobulin gene superfamily, upon programmed cell death. *The EMBO Journal*, *11*(11), 3887–3895.

Iwai, Y., Terawaki, S., & Honjo, T. (2005). PD-1 blockade inhibits hematogenous spread of poorly immunogenic tumor cells by enhanced recruitment of effector T cells. *International Immunology*, *17*(2), 133–144. https://doi.org/10.1093/intimm/dxh194

June, C. H., Ledbetter, J. A., Linsley, P. S., & Thompson, C. B. (1990). Role of the CD28 receptor in T-cell activation. *Immunology Today*, *11*(6), 211–216. https://doi.org/10.1016/0167-5699(90)90085-n

Kalbasi, A., & Ribas, A. (2020). Tumour-intrinsic resistance to immune checkpoint blockade. *Nature Reviews. Immunology*, *20*(1), 25–39. https://doi.org/10.1038/s41577-019-0218-4

Kao, C., Oestreich, K. J., Paley, M. A., Crawford, A., Angelosanto, J. M., Ali, M.-A. A., Intlekofer, A. M., Boss, J. M., Reiner, S. L., Weinmann, A. S., & Wherry, E. J. (2011). Transcription factor T-bet represses expression of the inhibitory receptor PD-1 and sustains virus-specific CD8+ T cell responses during chronic infection. *Nature Immunology*, *12*(7), 663–671. https://doi.org/10.1038/ni.2046

Kawabata, S., Connis, N., Gills, J. J., Hann, C. L., & Dennis, P. A. (2021). Nelfinavir Inhibits the Growth of Small-cell Lung Cancer Cells and Patient-derived Xenograft Tumors. *Anticancer Research*, *41*(1), 91–99. https://doi.org/10.21873/anticanres.14754

Keam, S. J. (2023). Tremelimumab: First Approval. *Drugs*, *83*(1), 93–102. https://doi.org/10.1007/s40265-022-01827-8

Keir, M. E., Butte, M. J., Freeman, G. J., & Sharpe, A. H. (2008). PD-1 and Its Ligands in Tolerance and Immunity. *Annual Review of Immunology*, *26*(1), 677–704. https://doi.org/10.1146/annurev.immunol.26.021607.090331

Keir, M. E., Latchman, Y. E., Freeman, G. J., & Sharpe, A. H. (2005). Programmed death-1 (PD-1):PD-ligand 1 interactions inhibit TCR-mediated positive selection of thymocytes. *Journal of Immunology (Baltimore, Md.: 1950)*, *175*(11), 7372–7379. https://doi.org/10.4049/jimmunol.175.11.7372

Kim, S. K., & Cho, S. W. (2022). The Evasion Mechanisms of Cancer Immunity and Drug Intervention in the Tumor Microenvironment. *Frontiers in Pharmacology*, *13*, 868695. https://doi.org/10.3389/fphar.2022.868695

Koizumi, S., Irie, T., Hirayama, S., Sakurai, Y., Yashiroda, H., Naguro, I., Ichijo, H., Hamazaki, J., & Murata, S. (2016). The aspartyl protease DDI2 activates Nrf1 to compensate for proteasome dysfunction. *ELife*, *5*, e18357. https://doi.org/10.7554/eLife.18357

Koltai, T. (2015). Nelfinavir and other protease inhibitors in cancer: Mechanisms involved in anticancer activity. *F1000Research*, *4*, 9. https://doi.org/10.12688/f1000research.5827.2

Kong, K.-F., Fu, G., Zhang, Y., Yokosuka, T., Casas, J., Canonigo-Balancio, A. J., Becart, S., Kim, G., Yates, J. R., Kronenberg, M., Saito, T., Gascoigne, N. R. J., & Altman, A.

(2014). Protein kinase C-η controls CTLA-4-mediated regulatory T cell function. *Nature Immunology*, *15*(5), 465–472. https://doi.org/10.1038/ni.2866

Koopmann, J. O., Albring, J., Hüter, E., Bulbuc, N., Spee, P., Neefjes, J., Hämmerling, G. J., & Momburg, F. (2000). Export of antigenic peptides from the endoplasmic reticulum intersects with retrograde protein translocation through the Sec61p channel. *Immunity*, *13*(1), 117–127. https://doi.org/10.1016/s1074-7613(00)00013-3

Krummel, M. F., & Allison, J. P. (1995). CD28 and CTLA-4 have opposing effects on the response of T cells to stimulation. *The Journal of Experimental Medicine*, *182*(2), 459–465. https://doi.org/10.1084/jem.182.2.459

Latchman, Y. E., Liang, S. C., Wu, Y., Chernova, T., Sobel, R. A., Klemm, M., Kuchroo, V. K., Freeman, G. J., & Sharpe, A. H. (2004). PD-L1-deficient mice show that PD-L1 on T cells, antigen-presenting cells, and host tissues negatively regulates T cells. *Proceedings of the National Academy of Sciences of the United States of America*, *101*(29), 10691–10696. https://doi.org/10.1073/pnas.0307252101

Law, C. W., Chen, Y., Shi, W., & Smyth, G. K. (2014). voom: Precision weights unlock linear model analysis tools for RNA-seq read counts. *Genome Biology*, *15*(2), R29. https://doi.org/10.1186/gb-2014-15-2-r29

Leach, D. R., Krummel, M. F., & Allison, J. P. (1996). Enhancement of antitumor immunity by CTLA-4 blockade. *Science (New York, N.Y.)*, *271*(5256), 1734–1736. https://doi.org/10.1126/science.271.5256.1734

Leto, D. E., Morgens, D. W., Zhang, L., Walczak, C. P., Elias, J. E., Bassik, M. C., & Kopito, R. R. (2019). Genome-wide CRISPR Analysis Identifies Substrate-Specific Conjugation

Modules in ER-Associated Degradation. *Molecular Cell*, *73*(2), 377-389.e11. https://doi.org/10.1016/j.molcel.2018.11.015

Linsley, P. S., Greene, J. L., Brady, W., Bajorath, J., Ledbetter, J. A., & Peach, R. (1994). Human B7-1 (CD80) and B7-2 (CD86) bind with similar avidities but distinct kinetics to CD28 and CTLA-4 receptors. *Immunity*, *1*(9), 793–801. https://doi.org/10.1016/s1074-7613(94)80021-9

Lo, J. A., Kawakubo, M., Juneja, V. R., Su, M. Y., Erlich, T. H., LaFleur, M. W., Kemeny, L. V., Rashid, M., Malehmir, M., Rabi, S. A., Raghavan, R., Allouche, J., Kasumova, G., Frederick, D. T., Pauken, K. E., Weng, Q. Y., Pereira da Silva, M., Xu, Y., van der Sande, A. A. J., … Fisher, D. E. (2021). Epitope spreading toward wild-type melanocyte-lineage antigens rescues suboptimal immune checkpoint blockade responses. *Science Translational Medicine*, *13*(581), eabd8636. https://doi.org/10.1126/scitranslmed.abd8636

Longer, M., Shetty, B., Zamansky, I., & Tyle, P. (1995). Preformulation studies of a novel HIV protease inhibitor, AG1343. *Journal of Pharmaceutical Sciences*, *84*(9), 1090–1093. https://doi.org/10.1002/jps.2600840911

Luo, N., Nixon, M. J., Gonzalez-Ericsson, P. I., Sanchez, V., Opalenik, S. R., Li, H., Zahnow, C. A., Nickels, M. L., Liu, F., Tantawy, M. N., Sanders, M. E., Manning, H. C., & Balko, J. M. (2018). DNA methyltransferase inhibition upregulates MHC-I to potentiate cytotoxic T lymphocyte responses in breast cancer. *Nature Communications*, *9*(1), 248. https://doi.org/10.1038/s41467-017-02630-w

Lupfer, C. R., Stokes, K. L., Kuriakose, T., & Kanneganti, T.-D. (2017). Deficiency of the NOD-Like Receptor NLRC5 Results in Decreased CD8+ T Cell Function and Impaired Viral Clearance. *Journal of Virology*, *91*(17), e00377-17. https://doi.org/10.1128/JVI.00377-17

Lustgarten, V., & Gerst, J. E. (1999). Yeast VSM1 encodes a v-SNARE binding protein that may act as a negative regulator of constitutive exocytosis. *Molecular and Cellular Biology*, *19*(6), 4480–4494. https://doi.org/10.1128/MCB.19.6.4480

Manguso, R. T., Pope, H. W., Zimmer, M. D., Brown, F. D., Yates, K. B., Miller, B. C., Collins, N. B., Bi, K., LaFleur, M. W., Juneja, V. R., Weiss, S. A., Lo, J., Fisher, D. E., Miao, D., Van Allen, E., Root, D. E., Sharpe, A. H., Doench, J. G., & Haining, W. N. (2017). In vivo CRISPR screening identifies Ptpn2 as a cancer immunotherapy target. *Nature*, *547*(7664), 413–418. https://doi.org/10.1038/nature23270

Marzolini, C., Buclin, T., Decosterd, L. A., Biollaz, J., & Telenti, A. (2001). Nelfinavir plasma levels under twice-daily and three-times-daily regimens: High interpatient and low intrapatient variability. *Therapeutic Drug Monitoring*, *23*(4), 394–398. https://doi.org/10.1097/00007691-200108000-00012

McCarthy, E. F. (2006). The Toxins of William B. Coley and the Treatment of Bone and Soft-Tissue Sarcomas. *The Iowa Orthopaedic Journal*, *26*, 154–158.

Meissner, T. B., Li, A., Biswas, A., Lee, K.-H., Liu, Y.-J., Bayir, E., Iliopoulos, D., van den Elsen, P. J., & Kobayashi, K. S. (2010). NLR family member NLRC5 is a transcriptional regulator of MHC class I genes. *Proceedings of the National Academy of Sciences of the United States of America*, *107*(31), 13794–13799. https://doi.org/10.1073/pnas.1008684107

Misumi, Y., Misumi, Y., Miki, K., Takatsuki, A., Tamura, G., & Ikehara, Y. (1986). Novel blockade by brefeldin A of intracellular transport of secretory proteins in cultured rat hepatocytes. *The Journal of Biological Chemistry*, *261*(24), 11398–11403.

Mittal, D., Gubin, M. M., Schreiber, R. D., & Smyth, M. J. (2014). New insights into cancer immunoediting and its three component phases—Elimination, equilibrium and escape. *Current Opinion in Immunology*, *27*, 16–25. https://doi.org/10.1016/j.coi.2014.01.004

Morad, G., Helmink, B. A., Sharma, P., & Wargo, J. A. (2021). Hallmarks of response, resistance, and toxicity to immune checkpoint blockade. *Cell*, *184*(21), 5309–5337. https://doi.org/10.1016/j.cell.2021.09.020

Nakanishi, J., Wada, Y., Matsumoto, K., Azuma, M., Kikuchi, K., & Ueda, S. (2007). Overexpression of B7-H1 (PD-L1) significantly associates with tumor grade and postoperative prognosis in human urothelial cancers. *Cancer Immunology, Immunotherapy: CII*, *56*(8), 1173–1182. https://doi.org/10.1007/s00262-006-0266-z

Naslavsky, N., Weigert, R., & Donaldson, J. G. (2004). Characterization of a nonclathrin endocytic pathway: Membrane cargo and lipid requirements. *Molecular Biology of the Cell*, *15*(8), 3542–3552. https://doi.org/10.1091/mbc.e04-02-0151

Neefjes, J., Jongsma, M. L. M., Paul, P., & Bakke, O. (2011). Towards a systems understanding of MHC class I and MHC class II antigen presentation. *Nature Reviews Immunology*, *11*(12), Article 12. https://doi.org/10.1038/nri3084

Nishimura, H., Agata, Y., Kawasaki, A., Sato, M., Imamura, S., Minato, N., Yagita, H., Nakano, T., & Honjo, T. (1996). Developmentally regulated expression of the PD-1 protein on the surface of double-negative (CD4-CD8-) thymocytes. *International Immunology*, *8*(5), 773–780. https://doi.org/10.1093/intimm/8.5.773

Olzmann, J. A., Kopito, R. R., & Christianson, J. C. (2013). The mammalian endoplasmic reticulum-associated degradation system. *Cold Spring Harbor Perspectives in Biology*, *5*(9), a013185. https://doi.org/10.1101/cshperspect.a013185

Parry, R. V., Chemnitz, J. M., Frauwirth, K. A., Lanfranco, A. R., Braunstein, I., Kobayashi, S. V., Linsley, P. S., Thompson, C. B., & Riley, J. L. (2005). CTLA-4 and PD-1 receptors inhibit T-cell activation by distinct mechanisms. *Molecular and Cellular Biology*, *25*(21), 9543–9553. https://doi.org/10.1128/MCB.25.21.9543-9553.2005

Paterson, A. M., Lovitch, S. B., Sage, P. T., Juneja, V. R., Lee, Y., Trombley, J. D., Arancibia-Cárcamo, C. V., Sobel, R. A., Rudensky, A. Y., Kuchroo, V. K., Freeman, G. J., & Sharpe, A. H. (2015). Deletion of CTLA-4 on regulatory T cells during adulthood leads to resistance to autoimmunity. *The Journal of Experimental Medicine*, *212*(10), 1603–1621. https://doi.org/10.1084/jem.20141030

Pauken, K. E., Torchia, J. A., Chaudhri, A., Sharpe, A. H., & Freeman, G. J. (2021). Emerging concepts in PD-1 checkpoint biology. *Seminars in Immunology*, *52*, 101480. https://doi.org/10.1016/j.smim.2021.101480

Penn, I. (1993). The effect of immunosuppression on pre-existing cancers. *Transplantation*, *55*(4), 742–747. https://doi.org/10.1097/00007890-199304000-00011

Porgador, A., Yewdell, J. W., Deng, Y., Bennink, J. R., & Germain, R. N. (1997). Localization, quantitation, and in situ detection of specific peptide-MHC class I complexes using a monoclonal antibody. *Immunity*, *6*(6), 715–726. https://doi.org/10.1016/s1074-7613(00)80447-1

Puente, X. S., Sánchez, L. M., Overall, C. M., & López-Otín, C. (2003). Human and mouse proteases: A comparative genomic approach. *Nature Reviews. Genetics*, *4*(7), 544–558. https://doi.org/10.1038/nrg1111

Quigley, M., Pereyra, F., Nilsson, B., Porichis, F., Fonseca, C., Eichbaum, Q., Julg, B., Jesneck, J. L., Brosnahan, K., Imam, S., Russell, K., Toth, I., Piechocka-Trocha, A., Dolfi, D., Angelosanto, J., Crawford, A., Shin, H., Kwon, D. S., Zupkosky, J., … Haining, W. N. (2010). Transcriptional analysis of HIV-specific CD8+ T cells shows that PD-1 inhibits T cell function by upregulating BATF. *Nature Medicine*, *16*(10), 1147–1151. https://doi.org/10.1038/nm.2232

Qureshi, O. S., Kaur, S., Hou, T. Z., Jeffery, L. E., Poulter, N. S., Briggs, Z., Kenefeck, R., Willox, A. K., Royle, S. J., Rappoport, J. Z., & Sansom, D. M. (2012). Constitutive clathrin-mediated endocytosis of CTLA-4 persists during T cell activation. *The Journal of Biological Chemistry*, *287*(12), 9429–9440. https://doi.org/10.1074/jbc.M111.304329

Rao, S., Gharib, K., & Han, A. (2019). Cancer Immunosurveillance by T Cells. *International Review of Cell and Molecular Biology*, *342*, 149–173. https://doi.org/10.1016/bs.ircmb.2018.08.001

Raskov, H., Orhan, A., Christensen, J. P., & Gögenur, I. (2021). Cytotoxic CD8+ T cells in cancer and cancer immunotherapy. *British Journal of Cancer*, *124*(2), Article 2. https://doi.org/10.1038/s41416-020-01048-4

Ribas, A., Camacho, L. H., Lopez-Berestein, G., Pavlov, D., Bulanhagui, C. A., Millham, R., Comin-Anduix, B., Reuben, J. M., Seja, E., Parker, C. A., Sharma, A., Glaspy, J. A., & Gomez-Navarro, J. (2005). Antitumor activity in melanoma and anti-self responses in a phase I trial with the anti-cytotoxic T lymphocyte-associated antigen 4 monoclonal

antibody CP-675,206. *Journal of Clinical Oncology: Official Journal of the American Society of Clinical Oncology*, *23*(35), 8968–8977. https://doi.org/10.1200/JCO.2005.01.109

Robert, C., Long, G. V., Brady, B., Dutriaux, C., Maio, M., Mortier, L., Hassel, J. C., Rutkowski, P., McNeil, C., Kalinka-Warzocha, E., Savage, K. J., Hernberg, M. M., Lebbé, C., Charles, J., Mihalcioiu, C., Chiarion-Sileni, V., Mauch, C., Cognetti, F., Arance, A., … Ascierto, P. A. (2015). Nivolumab in previously untreated melanoma without BRAF mutation. *The New England Journal of Medicine*, *372*(4), 320–330. https://doi.org/10.1056/NEJMoa1412082

Robert, C., Thomas, L., Bondarenko, I., O'Day, S., Weber, J., Garbe, C., Lebbe, C., Baurain, J.-F., Testori, A., Grob, J.-J., Davidson, N., Richards, J., Maio, M., Hauschild, A., Miller, W. H., Gascon, P., Lotem, M., Harmankaya, K., Ibrahim, R., … Wolchok, J. D. (2011). Ipilimumab plus dacarbazine for previously untreated metastatic melanoma. *The New England Journal of Medicine*, *364*(26), 2517–2526. https://doi.org/10.1056/NEJMoa1104621

Rock, K. L., Gramm, C., Rothstein, L., Clark, K., Stein, R., Dick, L., Hwang, D., & Goldberg, A. L. (1994). Inhibitors of the proteasome block the degradation of most cell proteins and the generation of peptides presented on MHC class I molecules. *Cell*, *78*(5), 761–771. https://doi.org/10.1016/s0092-8674(94)90462-6

Rodig, S. J., Gusenleitner, D., Jackson, D. G., Gjini, E., Giobbie-Hurder, A., Jin, C., Chang, H., Lovitch, S. B., Horak, C., Weber, J. S., Weirather, J. L., Wolchok, J. D., Postow, M. A., Pavlick, A. C., Chesney, J., & Hodi, F. S. (2018). MHC proteins confer differential

sensitivity to CTLA-4 and PD-1 blockade in untreated metastatic melanoma. *Science Translational Medicine*, *10*(450). https://doi.org/10.1126/scitranslmed.aar3342

Ru, B., Wong, C. N., Tong, Y., Zhong, J. Y., Zhong, S. S. W., Wu, W. C., Chu, K. C., Wong, C. Y., Lau, C. Y., Chen, I., Chan, N. W., & Zhang, J. (2019). TISIDB: An integrated repository portal for tumor-immune system interactions. *Bioinformatics (Oxford, England)*, *35*(20), 4200–4202. https://doi.org/10.1093/bioinformatics/btz210

Sade-Feldman, M., Jiao, Y. J., Chen, J. H., Rooney, M. S., Barzily-Rokni, M., Eliane, J.-P., Bjorgaard, S. L., Hammond, M. R., Vitzthum, H., Blackmon, S. M., Frederick, D. T., Hazar-Rethinam, M., Nadres, B. A., Seventer, E. E. V., Shukla, S. A., Yizhak, K., Ray, J. P., Rosebrock, D., Livitz, D., … Hacohen, N. (2017). Resistance to checkpoint blockade therapy through inactivation of antigen presentation. *Nature Communications*, *8*(1), 1–11. https://doi.org/10.1038/s41467-017-01062-w

Schadendorf, D., Hodi, F. S., Robert, C., Weber, J. S., Margolin, K., Hamid, O., Patt, D., Chen, T.-T., Berman, D. M., & Wolchok, J. D. (2015). Pooled Analysis of Long-Term Survival Data From Phase II and Phase III Trials of Ipilimumab in Unresectable or Metastatic Melanoma. *Journal of Clinical Oncology: Official Journal of the American Society of Clinical Oncology*, *33*(17), 1889–1894. https://doi.org/10.1200/JCO.2014.56.2736

Schreiber, R. D., Old, L. J., & Smyth, M. J. (2011). Cancer immunoediting: Integrating immunity's roles in cancer suppression and promotion. *Science (New York, N.Y.)*, *331*(6024), 1565–1570. https://doi.org/10.1126/science.1203486

Sha, Z., & Goldberg, A. L. (2016). Reply to Vangala et al.: Complete inhibition of the proteasome reduces new proteasome production by causing Nrf1 aggregation. *Current Biology: CB*, *26*(18), R836–R837. https://doi.org/10.1016/j.cub.2016.08.030

Shahinian, A., Pfeffer, K., Lee, K. P., Kündig, T. M., Kishihara, K., Wakeham, A., Kawai, K., Ohashi, P. S., Thompson, C. B., & Mak, T. W. (1993). Differential T cell costimulatory requirements in CD28-deficient mice. *Science (New York, N.Y.)*, *261*(5121), 609–612. https://doi.org/10.1126/science.7688139

Shankaran, V., Ikeda, H., Bruce, A. T., White, J. M., Swanson, P. E., Old, L. J., & Schreiber, R. D. (2001). IFNγ and lymphocytes prevent primary tumour development and shape tumour immunogenicity. *Nature*, *410*(6832), Article 6832. https://doi.org/10.1038/35074122

Sharma, P., Hu-Lieskovan, S., Wargo, J. A., & Ribas, A. (2017). Primary, Adaptive and Acquired Resistance to Cancer Immunotherapy. *Cell*, *168*(4), 707–723. https://doi.org/10.1016/j.cell.2017.01.017

Sharpe, A. H., & Pauken, K. E. (2018). The diverse functions of the PD1 inhibitory pathway. *Nature Reviews. Immunology*, *18*(3), 153–167. https://doi.org/10.1038/nri.2017.108

Smyth, M. J., Thia, K. Y., Street, S. E., MacGregor, D., Godfrey, D. I., & Trapani, J. A. (2000). Perforin-mediated cytotoxicity is critical for surveillance of spontaneous lymphoma. *The Journal of Experimental Medicine*, *192*(5), 755–760. https://doi.org/10.1084/jem.192.5.755

Staehli, F., Ludigs, K., Heinz, L. X., Seguín-Estévez, Q., Ferrero, I., Braun, M., Schroder, K., Rebsamen, M., Tardivel, A., Mattmann, C., MacDonald, H. R., Romero, P., Reith, W., Guarda, G., & Tschopp, J. (2012). NLRC5 deficiency selectively impairs MHC class I-dependent lymphocyte killing by cytotoxic T cells. *Journal of Immunology (Baltimore, Md.: 1950)*, *188*(8), 3820–3828. https://doi.org/10.4049/jimmunol.1102671

Street, S. E. A., Cretney, E., & Smyth, M. J. (2001). Perforin and interferon-γ activities independently control tumor initiation, growth, and metastasis. *Blood*, *97*(1), 192–197. https://doi.org/10.1182/blood.V97.1.192

Strome, S. E., Dong, H., Tamura, H., Voss, S. G., Flies, D. B., Tamada, K., Salomao, D., Cheville, J., Hirano, F., Lin, W., Kasperbauer, J. L., Ballman, K. V., & Chen, L. (2003). B7-H1 blockade augments adoptive T-cell immunotherapy for squamous cell carcinoma. *Cancer Research*, *63*(19), 6501–6505.

Sugawara, S., Abo, T., & Kumagai, K. (1987). A simple method to eliminate the antigenicity of surface class I MHC molecules from the membrane of viable cells by acid treatment at pH 3. *Journal of Immunological Methods*, *100*(1–2), 83–90. https://doi.org/10.1016/0022-1759(87)90175-x

Svane, I. M., Engel, A. M., Thomsen, A. R., & Werdelin, O. (1997). The susceptibility to cytotoxic T lymphocyte mediated lysis of chemically induced sarcomas from immunodeficient and normal mice. *Scandinavian Journal of Immunology*, *45*(1), 28–35. https://doi.org/10.1046/j.1365-3083.1997.d01-369.x

Tanaka, K. (2009). The proteasome: Overview of structure and functions. *Proceedings of the Japan Academy. Series B, Physical and Biological Sciences*, *85*(1), 12–36. https://doi.org/10.2183/pjab.85.12

Thomas, C., & Tampé, R. (2019). MHC I chaperone complexes shaping immunity. *Current Opinion in Immunology*, *58*, 9–15. https://doi.org/10.1016/j.coi.2019.01.001

Tivol, E. A., Borriello, F., Schweitzer, A. N., Lynch, W. P., Bluestone, J. A., & Sharpe, A. H. (1995). Loss of CTLA-4 leads to massive lymphoproliferation and fatal multiorgan tissue

destruction, revealing a critical negative regulatory role of CTLA-4. *Immunity*, *3*(5), 541–547. https://doi.org/10.1016/1074-7613(95)90125-6

Vaddepally, R. K., Kharel, P., Pandey, R., Garje, R., & Chandra, A. B. (2020). Review of Indications of FDA-Approved Immune Checkpoint Inhibitors per NCCN Guidelines with the Level of Evidence. *Cancers*, *12*(3), 738. https://doi.org/10.3390/cancers12030738

van den Boomen, D. J. H., & Lehner, P. J. (2015). Identifying the ERAD ubiquitin E3 ligases for viral and cellular targeting of MHC class I. *Molecular Immunology*, *68*(2 Pt A), 106–111. https://doi.org/10.1016/j.molimm.2015.07.005

Viola, A., & Lanzavecchia, A. (1996). T cell activation determined by T cell receptor number and tunable thresholds. *Science (New York, N.Y.)*, *273*(5271), 104–106. https://doi.org/10.1126/science.273.5271.104

Wearsch, P. A., Peaper, D. R., & Cresswell, P. (2011). Essential glycan-dependent interactions optimize MHC class I peptide loading. *Proceedings of the National Academy of Sciences of the United States of America*, *108*(12), 4950–4955. https://doi.org/10.1073/pnas.1102524108

Wei, J., Zanker, D., Di Carluccio, A. R., Smelkinson, M. G., Takeda, K., Seedhom, M. O., Dersh, D., Gibbs, J. S., Yang, N., Jadhav, A., Chen, W., & Yewdell, J. W. (2017). Varied Role of Ubiquitylation in Generating MHC Class I Peptide Ligands,. *Journal of Immunology (Baltimore, Md. : 1950)*, *198*(10), 3835–3845. https://doi.org/10.4049/jimmunol.1602122

White, R. E., Dickinson, J. R., Semple, C. A. M., Powell, D. J., & Berry, C. (2011). The retroviral proteinase active site and the N-terminus of Ddi1 are required for repression of

protein secretion. *FEBS Letters*, *585*(1), 139–142. https://doi.org/10.1016/j.febslet.2010.11.026

Wilson, J. M., Fokas, E., Dutton, S. J., Patel, N., Hawkins, M. A., Eccles, C., Chu, K.-Y., Durrant, L., Abraham, A. G., Partridge, M., Woodward, M., O'Neill, E., Maughan, T., McKenna, W. G., Mukherjee, S., & Brunner, T. B. (2016). ARCII: A phase II trial of the HIV protease inhibitor Nelfinavir in combination with chemoradiation for locally advanced inoperable pancreatic cancer. *Radiotherapy and Oncology*, *119*(2), 306–311. https://doi.org/10.1016/j.radonc.2016.03.021

Wu, C., Zhu, Y., Jiang, J., Zhao, J., Zhang, X.-G., & Xu, N. (2006). Immunohistochemical localization of programmed death-1 ligand-1 (PD-L1) in gastric carcinoma and its clinical significance. *Acta Histochemica*, *108*(1), 19–24. https://doi.org/10.1016/j.acthis.2006.01.003

Yamamoto, K., Venida, A., Yano, J., Biancur, D. E., Kakiuchi, M., Gupta, S., Sohn, A. S. W., Mukhopadhyay, S., Lin, E. Y., Parker, S. J., Banh, R. S., Paulo, J. A., Wen, K. W., Debnath, J., Kim, G. E., Mancias, J. D., Fearon, D. T., Perera, R. M., & Kimmelman, A. C. (2020). Autophagy promotes immune evasion of pancreatic cancer by degrading MHC-I. *Nature*, *581*(7806), Article 7806. https://doi.org/10.1038/s41586-020-2229-5

Yee, C., Thompson, J. A., Byrd, D., Riddell, S. R., Roche, P., Celis, E., & Greenberg, P. D. (2002). Adoptive T cell therapy using antigen-specific CD8+ T cell clones for the treatment of patients with metastatic melanoma: In vivo persistence, migration, and antitumor effect of transferred T cells. *Proceedings of the National Academy of Sciences*, *99*(25), 16168–16173. https://doi.org/10.1073/pnas.242600099

Yip, M. C. J., Bodnar, N. O., & Rapoport, T. A. (2020). Ddi1 is a ubiquitin-dependent protease. *Proceedings of the National Academy of Sciences of the United States of America*, *117*(14), 7776–7781. https://doi.org/10.1073/pnas.1902298117

Zaretsky, J. M., Garcia-Diaz, A., Shin, D. S., Escuin-Ordinas, H., Hugo, W., Hu-Lieskovan, S., Torrejon, D. Y., Abril-Rodriguez, G., Sandoval, S., Barthly, L., Saco, J., Homet Moreno, B., Mezzadra, R., Chmielowski, B., Ruchalski, K., Shintaku, I. P., Sanchez, P. J., Puig-Saus, C., Cherry, G., … Ribas, A. (2016). Mutations Associated with Acquired Resistance to PD-1 Blockade in Melanoma. *New England Journal of Medicine*, *375*(9), 819–829. https://doi.org/10.1056/NEJMoa1604958